TARGETED NANOMEDICINE PLATFORM FOR CANCER STEM CELLS SPECIFIC THERAPY

BY

VATSAL V. SHAH

A Dissertation submitted to the Graduate School-New Brunswick

Rutgers, the State University of New Jersey

In partial fulfillment of the requirements

For the degree of

Doctor of Philosophy

Graduate Program in Pharmaceutical Sciences

Written under the direction of

Professor Tamara Minko, PhD

And approved by

_____

_____

_____

_____

_____

New Brunswick, New Jersey

January 2013

ABSTRACT OF THE DISSERTATION

TARGETED NANOMEDICINE PLATFORM FOR CANCER STEM CELLS SPECIFIC THERAPY

By VATSAL V. SHAH

Dissertation Director:

Tamara Minko, PhD.

Cancer is one of the most fatal diseases in the world. More than 10 million cases of cancer are reported every year (1). It is responsible for one in 4 deaths in the United States (2).The agents that are currently used for chemotherapy fail to differentiate between the cancerous and normal cells leading to numerous adverse side-effects. Owing to their toxicity, there is limitation to the amount of dose that can be administered. Due to the lack of specificity and restriction of dose, it sometimes becomes very difficult to achieve an effective concentration within the cancer affected tissues (3).

One of the purposes of this proposal is to evaluate various drug delivery systems utilized in cancer therapy or diagnosis for genotoxicity. If a drug delivery system is found to be genotoxic, we propose to modify these genotoxic systems so as to reduce or completely eliminate their genotoxicity. We also propose to test certain raw materials used in cosmetic industry on a regular bases for genotoxicity. The other purpose of this study is to develop a dendrimer based drug delivery system that would specifically knock down

CD44 in cancerous cells. Once CD44 is knocked down, we plan to treat the cancer cells specifically using a chemotherapeutic drug, Paclitaxel attached to PPi dendrimer.

DEDICATION

To the Almighty Lord Krishna;

Whose blessings have always been showered on me.

To my loving Parents;

Who encouraged and made me who I am.

To my advisor, Professor Tamara Minko;

Who has been such a great guiding spirit and an inspiration.

To my fiancée, Nidhi;

Who has been like a wall by my side with her unconditional love.

To my loving Sister, Prachi;

Whose support and affection are so close to my heart.

ACKNOWLEDGEMENTS

I would like to thank God for His presence in all my endeavors.

It has been such an honor to know and work under Dr. Tamara Minko. She has been a constant source of inspiration and a great mentor to me for the past five years. She has always been around when I needed her and guided me selflessly. Her endurance for my ignorance and her patience through my research has made this dissertation possible.

I would like to thank my thesis committee members: Dr. Nava Dayan, Dr. Arash Hatefi, Dr. Bozena Michniak-Kohn and Dr. Guofeng You for their suggestions, time and support. I would like to express my heartfelt gratitude to Dr. Tony Kong for his readiness to help in any situation.

I would like to deeply acknowledge my past and present colleagues from Dr. Minko's laboratory: Dr. Oleh Taratula, Dr. Olga Garbuzenko, Dr. Mahesh Patil, Dr. Min Zhang, John Praskavich, Ronak Savla, Milin Shah, Vera Ivanova and Andriy Kuzmov for their generous help, constructive suggestions and their sense of camaraderie that made the lab a positive lab environment.

I am grateful to the office staff of the Department of Pharmaceutics at Rutgers University: Marianne Shen, Sharana Taylor and Hui Pung for being so helpful and enabling my work at the laboratory.

I also want to thank my friends from the department: Dr. Sujit Nair, Dr.Yashveer Singh, Dr. Manjeet Deskmukh, Dr. Vidya Ganpati, Sujata Sundra Rajan, Sarandeep Boyanpalli, Zahra Diarkhan Karjoo and Vinam Puri for always being there.

I want to thank Department of Life Sciences: Dr. Gary Merrill, Dr. Roselli Golfetti, Dr.Martha Havilland, Jana Curry and Carole Lewandowski for the financial support and great work environment.

I express my deep gratitude for my family members and friends for their good wishes.

Finally I want to express gratitude to all the Professors and staff at Ernest Mario School of Pharmacy, Rutgers, The State University of New Jersey, for providing me with the opportunity to pursue higher education.

TABLE OF CONTENTS

ABSTRACT OF THE DISSERTAION ..... **ii**

DEDICATION ..... **iv**

ACKNOWLEDGEMENTS ..... **v**

Table of contents ..... **vii**

LIST OF FIGURES ..... **x**

1 Introduction **1**

2 BACK GROUND AND SIGNIFICANCE **6**

2.1 Genotoxicity and in vitro Micronucleus test 6

2.1.1 Genotoxicity 6

2.1.2 In vitro Micronucleus test 7

2.2 Drug delivery systems 10

2.2.1 Polyethylene glycol (PEG) 10

2.2.2 Quantum dots (QD) 12

2.2.3 Liposomes 15

2.2.4 Dendrimers 17

2.2.4.1 PAMAM (Poly(amido amino)) Dendrimers 19

2.2.4.2 Polypropylenimine (PPi) Dendrimers 21

2.2.5 Supermagnetic iron oxide 23

2.2.6 Mesoporous silica nanoparticles 25

2.3 Ovarian cancer and Cancer stem cells 27

2.3.1 Ovarian cancer 27

2.3.2 Cancer stem cells and CD44 28

2.3.2.1 Cancer stem cells 28

2.3.2.2 CD44 30

2.4 RNA interference (RNAi) 34

2.5 Luteinizing hormone-releasing hormone (Targeting moiety) 36

2.6 Anticancer agent-Paclitaxel 37

3 SPECIFIC AIMS **55**

4 Evaluation of the cytotoxicity and genotoxicity of various nanocarriers **59**

4.1 Introduction 59

4.2 Materials and Methods 61
4.2.1 Materials 61
4.2.2 Synthesis of the nanocarriers 62
4.2.3 Imaging, particle size and zeta potential of nanocarriers 63
4.2.4 Preparation of chemicals for micronuclei test 64
4.2.5 Cell Line 65
4.2.6 Cell viability 65
4.2.7 Micronuclei test 65
4.2.8 Cellular internalization 66
4.2.9 Statistical analysis 67
4.3 Results 67
4.3.1 Cytotoxicty of different nanocarriers 67
4.3.2 Imaging of nanocarriers by Atomic Force Microscopy (AFM) 68
4.3.3 Zeta potential of nanocarriers 68
4.3.4 Genotoxicity of nanocarriers 68
4.3.5 Correlation between surface charge and genotoxicity 70
4.3.6 Cellular internalization and genotoxicity 70
4.4 Discussion 71
4.5 Conclusions 76

5 Evaluation of the cytotoxicity and genotoxicity of various raw materials utilized in cosmetic industry 84
5.1 Introduction 84
5.2 Materials and Methods 87
5.2.1 Materials 87
5.2.2 Preparation of chemicals 88
5.2.3 Metabolic activation system 89
5.2.4 Cell line 90
5.2.5 Experimental series and condition 90
5.2.6 Cell staining 91
5.2.7 Counting of micronuclei 91
5.2.8 Cellular viability and proliferation 92
5.2.9 Statistical analysis 93
5.3 Results 93
5.3.1 Micronuclei formation 93
5.3.2 Cell viability and proliferation 94
5.4 Discussion 95
5.4.1 Optical brighteners 95

5.4.2 Hydrillien Compounds 96
5.5 Conclusion 99

6 Targeted Nanomedicine for Simultaneous Suppression of CD44 Protein and Cell Death Induction 108
6.1 Introduction 108
6.2 Materials and Methods 109
6.2.1 Materials 109
6.2.2 Synthesis of Paclitaxel - Succinic Acid Conjugate 110
6.2.3 Synthesis of Paclitaxel – PPI Conjugate 111
6.2.4 Modification of Paclitaxel – PPI Conjugate with MAL–PEG–NHS and LHRH 111
6.2.5 Preparation of PPI – siRNA complexes 112
6.2.6 Study of Complex Formation Between siRNA and Dendrimers 113
6.2.7 MALDI TOF Mass Spectroscopy 114
6.2.8 Atomic Force Microscopy 114
6.2.9 Stability of the Complexes in Serum 114
6.2.10 Cancer Cells and Animal Model 115
6.2.11 Cellular Internalization 116
6.2.12 Cell Invasion Assay 117
6.2.13 *In Vitro* Cytotoxicity 118
6.2.14 LHRH Expression 118
6.2.15 CD44 Expression 119
6.2.16 Immunohistochemistry 120
6.2.17 Apoptosis Detection 121
6.2.18 Statistical Analysis 121
6.3 Results 122
6.3.1 Synthesis and Characterization of Cytotoxic Tumor Targeted siRNA Nanocomplexes 122
6.3.2 Expression of CD44 and LHRH in Cancer Cells 123
6.3.3 Cytotoxicity and Cell Invasiveness 124
6.3.4 Cellular Internalization of siRNA 125
6.3.5 *In Vivo* Antitumor Activity 126
6.4 Discussion 128
6.5 Conclusion 130

7 References 139

LIST OF FIGURES

Figure 2.1: Micronuclei formation (shown by arrows) in CHO-K1 cells when exposed to a positive control (Ethyl Methane Sulfonate) (Reproduced from Ref. [17])……..40

Figure 2.2: Various PEG structures: a) linear monomethoxy PEG, b) linear diol PEG, and c) branched PEG (Reproduced from ref. 50,51)……41

Figure 2.3: Cdse quantum dots dispersed in chloroform having different properties based on their size. (A) Fluorescence of quantum dots with diameter of 2.2n, 2.9 nm, 4.1nm and 7.3nm in four vials. (B) Spectra of fluorescence for the four vials (Reproduced from Ref. [68])……..42

Figure 2.4: Basic structure of a liposome. It consists of a phospholipid bilayer shell which is hydrophobic and an aqueous core which is hydrophilic in nature. (Reproduced from Ref. [80])……43

Figure 2.5: A three dimensional structure of dendrimer consisting of an Initiator core, Internal layers (generations) and external surface with functional groups. (Reproduced from Ref. [99])……44

Figure 2.6: Structure of a generation 3 PAMAM dendrimer. Reproduced from Ref. [104])……..45

Figure 2.7: Structure of a 4th generation PPi dendrimer. (Reproduced from Ref. [114])……..46

Figure 2.8: Schematic representation of drug delivery to a specific site using a magnet. A catheter is inserted into an arterial feed to the tumour and a magnetic stand is positioned over the targeted site. (Reproduced from Ref. [122])…… 47

Figure 2.9: Conventional therapy may kill most of the cells in the tumor mass but the CSCs are not affected. As a result, CSC gives rise to the heterogenous tumor and causes a relapse. Targeting cancer stem cells directly can kill them effectively rendering the rest of the tumor unable to maintain or grow eventually leading to a cure. (Reproduced from Ref. [143])……48

Figure 2.10: CD44 interaction with HA and ERBB2 regulate phosphatidylinositol 3-kinase (PI3K) activity. PI3K signaling is responsible for regulating multidrug resistance (MDR) transporter expression and function. It also phosphorylates AKT to p-AKT thus activating cell-survival signaling. (Reproduced from Ref. [170])……49

Figure 2.11: C44 binding with HA enhances the CD44-Nanog binding which increases the transcription activation (step 2a) and expression of its target gene- Rex1 and Sox2. Nanog also complexes with Stat-3 and induces Stat-3-specific transcriptional activation (step 2b) increasing tumor cell growth and MDR-1 gene expression (step 3b) and localization at the plasma membrane (step 4). CD44-HA binding promotes ankyrin-MDR1 (P-gp) association (Step A) which increases the efflux of chemotherapeutic drugs (step B). (Reproduced from Ref. [198])……50

Figure 2.12: A long double-stranded RNA (dsRNA) is cleaved by by the Dicer enzyme into siRNA. The siRNA is incorporated into Argonaute 2 (AGO2) -RNAi-induced silencing complex (RISC). AGO2 cleaves the sense strand and the antisense strand guides the complex to the target mRNA which is cleaved by the catalytic domain of AGO2 and degraded. (Reproduced from Ref. [208])…… ……51

Figure 2.13: Internalization of doxorubicin attached to LHRH peptide by receptor-mediated endocytosis. Once inside the cells, free doxorubicin is released and accumulated in the nucleus where it induces apoptosis. (Reproduced from Ref. [225]……52

Figure 2.14: The chemical structure of Paclitaxel. (Reproduced from Ref. [228])……53

Figure 2.15: Mitotic spindles in a normal cell (left) vs cells treated with Paclitaxel (right). Cells treated with Paclitaxel exhibit malformed mitotic spindle which causes cell arrest and eventually cell death. (Reproduced from Ref. [229])…….54

Figure 4.1: Representative atomic force microscope (AFM) images of different nanocarriers: supermagnetic iron oxide (SPIO) nanoparticles; poly(ethylene glycol) (PEG); quantum dots (QD); poly(propyleneimine) (PPI) dendrimers; poly(amido amine) (PAMAM) dendrimers; polymeric micelles; “neutral” liposomes; cationic liposomes and mesoporous silica (MS) nanoparticles……77

Figure 4.2: Average size of different nanocarriers: 1 – supermagnetic iron oxide (SPIO) nanoparticles; 2 – 2 kDa poly(ethylene glycol) (PEG) polymer; 3 – 10 kDa PEG polymer; 4 – 20 kDa PEG polymer; 5 – quantum dots (QD); 6 – poly(propyleneimine) (PPI) dendrimers; 7 – poly(amido amine) (PAMAM) dendrimers; 8 – polymeric micelles; 9 – “neutral” liposomes (120 nm); 10 – cationic liposomes; 11 – mesoporous silica (MS) nanoparticles; and 12 – “neutral” liposomes (600 nm). Means ± SD are shown……78

Figure 4.3: Zeta potential of different nanocarriers: 1 – 2 kDa poly(ethylene glycol) (PEG) polymer; 2 – 10 kDa PEG polymer; 3 – 20 kDa PEG polymer; 4 – quantum dots (QD); 5 – "neutral" liposomes (120 nm); 6 – "neutral" liposomes (600 nm); 7 – mesoporous silica (MS) nanoparticles; 8 – polymeric micelles; 9 – cationic liposomes; 10 – poly(amido amine) (PAMAM) dendrimers; 11 – modified PAMAM dendrimers; 12 – poly(propyleneimine) (PPI) dendrimers; 13 – modified PPI dendrimers; 14 – supermagnetic iron oxide (SPIO) nanoparticles; and 15 – modified SPIO nanoparticles. Means ± SD are shown. *P < 0.05 when compared with corresponding non-modified nanocarriers……..79

Figure 4.4: Genotoxicity (formation of micronuclei) of different nanocarriers and corresponding controls. Representative fluorescence microscopy images of CHO-K1 cells incubated within 24 hours with different substances: 1 – media (negative control); 2 – ethyl methanesulfonate (EMS, positive control); 3 – 10 kDa poly(ethylene glycol) (PEG) polymer; 4 – quantum dots (QD); 5 – neutral liposomes (120 nm); 6 – mesoporous silica (MS) nanoparticles; 7 – polymeric micelles; 8 – cationic liposomes; 9 – poly(amido amine) (PAMAM) dendrimers; 10 – modified PAMAM dendrimers; 11 – poly(propyleneimine) (PPI) dendrimers; 12 – Modified PPI dendrimers; 13 – supermagnetic iron oxide (SPIO) nanoparticles; and 14 – modified SPIO nanoparticle. The cells were stained with DAPI nuclear dye. For each substance, images on the right panel show magnified cells marked by the square on the left panel……80

Figure 4.5: Genotoxicity of different nanocarriers: 1 – media (negative control); 2 – ethyl methanesulfonate (EMS, positive control); 3 – 2 kDa poly(ethylene glycol) (PEG) polymer; 4 – 10 kDa PEG polymer; 5 – 20 kDa PEG polymer; 6 – quantum dots (QD); 7 – "neutral" liposomes (120 nm); 8 – "neutral" liposomes (600 nm); 9 – mesoporous silica (MS) nanoparticles; 10 – polymeric micelles; 11 – cationic liposomes; 12 – poly(amido amine) (PAMAM) dendrimers; 13 – modified PAMAM dendrimers; 14 – poly(propyleneimine) (PPI) dendrimers; 15 – modified PPI dendrimers; 16 – supermagnetic iron oxide (SPIO) nanoparticles; and 17 – modified SPIO nanoparticles. Means ± SD are shown. *P < 0.05 when compared with media (negative control). †P < 0.05 when compared with a corresponding non-modified carrier……81

Figure 4.6: Correlation between the zeta potential of nanocarriers and their genotoxicity. Shaded area represents the control range of micronuclei formation. Means ± SD are shown……82

Figure 4.7: Cellular internalization of siRNA complexes with different nanocarriers. Representative confocal microscope images of cancer cells incubated within 24 h with fluorescently labeled siRNA delivered by mesoporous silica (MS) nanoparticles, cationic liposomes, modified poly(amido amine) (PAMAM) dendrimers and modified poly(propyleneimine) (PPI) dendrimers……83

Figure 5.1: Treatments used in the study along with the incubation times. A) OB : (1) media only (negative control); (2) DMSO (negative control); (3) cyclophosphamide + S9 mix (10 µg /mL) (positive control); (4) ethyl methanesulfonate (400 µg /ml) (positive

control); (5) OB (0.2 mg/ml); (6) OB (0.3 mg/ml); (7) OB (0.2 mg/ml) + S9 mix; and (8) OB (0.3 mg/ml) + S9 mix. B) Hydrillien 9 compounds (A, B and C): (1) Media only (negative control); (2) media with S9 (negative control); (3) cyclophosphamide + S9 mix (10 µg/mL) (positive control); (4) EMS (400 µg/mL) (positive control); (5) A (0.05%); (6) A (0.05%) + S9 mix; (7) B (0.05%); (8) B (0.05%) + S9 mix; (9) C (0.05%); (10) C (0.05%) + S9 mix. The shaded areas represent the treatments employed. The treatments without S9 activation were incubated for 24 h before harvesting. The treatments with S9 activation were incubated for 3 h. At the end of 3 h, the contents were replaced with media and allowed to incubate for 21 h before harvesting……101

Figure 5.2: Typical light and fluorescent images of CHO-K1 cells incubated for 24 hours with the OB as follows: (1) Media (negative control); (2) DMSO (negative control); (3) Cyclosphosphamide + S9 mix (positive control); (4) Ethyl methyl sulfonate (positive control); (5) OB, 0.2 mg/ml in DMSO; (6) OB, 0.3 mg/ml in DMSO; (7) OB, 0.2 mg/ml in DMSO + S9 mix; and (8) OB, 0.3 mg/ml in DMSO + S9 mix. The cells were stained with DAPI nuclear dye……102

Figure 5.3: Number of micronuclei per 1000 cells for OB. CHO-K1 cells were incubated for 24 hours with the following substances: (1) Media (negative control); (2) DMSO (negative control); (3) Cyclosphosphamide + S9 mix (positive control); (4) Ethyl methanesulfonate (positive control); (5) OB, 0.2 mg/ml in DMSO; (6) OB, 0.3 mg/ml in DMSO; (7) OB, 0.2 mg/ml in DMSO + S9 mix; and (8) OB, 0.3 mg/ml in DMSO + S9 mix. Means ± S.D. are shown. *P<0.05 when compared with negative control……103

Figure 5.4: Typical light and fluorescent images of Chinese Hamster Ovary-K1 cells incubated for 24 h with Hydrillien 9 compounds as follows: 1 – media (negative control); 2 – media (negative control) + S9 mix; 3 – cyclophosphamide + S9 mix (positive control); 4 – ethyl methanesulfonate (positive control); 5 – compound A (0.05%); 6 -compound A (0.05%) + S9 mix; 7 – compound B (0.05%); 8 – compound B (0.05%) + S9 mix; 9 – compound C (0.05%); 10 – compound C (0.05%) + S9 mix. The cells were stained with 6-diamidino-2-phenylindole dihydrochloride nuclear dye……104

Figure 5.5: Number of micronuclei per 1000 cells for Hydrillien compounds. Chinese Hamster Ovary-K1 cells were incubated for 24 h with the following substances: 1 – media (negative control); 2 – cyclophosphamide + S9 mix (positive control); 3 – ethyl methanesulfonate (positive control); 4 – compound A (0.05%); 5 – compound A (0.05%) + S9 mix; 6 – compound B (0.05%); 7 – compound B (0.05%) + S9 mix; 8 – compound C (0.05%); 9 – compound C (0.05%) + S9 mix. Means ± SD are shown. *P < 0.05 when compared with negative control……105

Figure 5.6: (A) Cellular viability. CHO-K1 cells were incubated for 24 hours with the following substances: (1) DMSO (negative control); (2) Cyclophosphamide + S9 mix (positive control); (3) Ethyl methanesulfonate (positive control); (4) OB, 0.2 mg/ml in DMSO; (5) OB, 0.3 mg/ml in DMSO; (6) OB, 0.2 mg/ml in DMSO + S9 mix; and (7) OB, 0.3 mg/ml in DMSO + S9 mix. Means ± S.D. are shown. (B) Influence of test substances on cellular proliferation. The same number of cells (3 × 104) were seeded in the flask and incubated with media (1) and a test substance in two concentrations: 0.2 mg/ml (2) and

0.3 mg/ml (3). Cells were counted 48 h after the addition of the test substances. Means ± S.D. are shown from four independent measurements……106

Figure 5.7: Cellular viability (A) and proliferation (B). Chinese Hamster Ovary-K1 cells were incubated for 24 h with the following substances: 1 – media (negative control); 2 – cyclophosphamide + S9 mix (positive control); 3 – ethyl methanesulfonate (positive control); 4 – compound A (0.05%); 5 - compound A (0.05%) + S9 mix; 6 – compound B (0.05%); 7 – compound B (0.05%) + S9 mix; 8 – compound C (0.05%); 9 – compound C (0.05%) + S9 mix. For (B), cellular proliferation was calculated as the ratio of the cell count 48 h after incubation to the initial cell count seeded on the plate. Means ± SD are shown……107

Fig.6.1: Complex cancer targeted drug delivery system. A, Schema of the delivery system containing poly(propylenimine) (PPI) dendrimer as a carrier; paclitaxel (TAX) as an anticancer drug, conjugated to the dendrimer via succinic acid (SA) spacer; luteinizing-hormone-releasing hormone (LHRH) as a cancer targeting moiety, conjugated to the dendrimer via poly(ethylene glycol) (PEG) spacer; siRNA targeted to CD44 mRNA. B, Representative gel electrophoresis image of siRNA complexated with PPI dendrimer at different nitrogen to phosphate (N/P) ratios from 0 (no PPI dendrimer) to 3.00. C, representative image of matrix-assisted laser desorption/ionisation-time of flight (MALDI-TOF) mass spectrometry analysis of PPI-TAX complex. The most abundant peak [M+Na] was observed at mass M=8122 indicating that paclitaxel was conjugated with the PPI G5 dendrimer (M=8099). D, Quantitative analysis of ethidium bromide displacement assay for PPi dendrimer-siRNA complexes. The complexes were

synthesized with 0.4 µM siRNA and 126 µM ethidium bromide. The concentration of PPi dendrimer was increased to obtain N/P ratios from 0 (no PPI dendrimer) to 3. A decrease in fluorescence indicates binding of siRNA to PPi dendrimer. E, AFM images of nanoparticles resulted from the complex formation between the carrier and siRNA……131

Fig.6.2: Expression of CD44 and LHRHR mRNA. A, Expression of CD44 mRNA in tissues isolated from primary tumor and metastases in same patients with different types of gynecological cancers. Means ± SD are shown. *P < 0.05 when compared with primary tumor. B, Expression of CD44 mRNA in cancer cells isolated from malignant ascites obtained from patients with advanced ovarian carcinoma. Cells were incubated with substances indicated. Means ± SD are shown. *P < 0.05 when compared with control (cells incubated with fresh media); †P < 0.05 when compared with non-targeted complexes. C, Expression of LHRH receptors in gynecological tumors and healthy tissues……132

Fig.6.3: Expression of CD44 protein (immunocytochemistry) in human cancer cells isolated from malignant ascites from patient with advanced ovarian carcinoma. Cells were treated with PPi-siRNA-LHRH nanocomplex. Untreated cells received media alone. Representative light and fluorescence microscope images. CD44 protein was stained using primary anti-CD44 antibody and secondary antibody conjugated with Cy3® fluorofor. Nuclei were stained with DAPI nuclear dye. Red color represents CD44 protein; blue color represents cell nuclei……133

Fig. 6.4: Invasion and viability of cancer cells isolated from malignant ascites obtained from patients with advanced ovarian carcinoma. A, Cell invasion was measured in the cells growing with media alone or media containing 15% fetal bovine serum (FBS, chemoattractant) and treated with LHRH-PPI-CD44 siRNA. B, Influence of different substances on cellular viability. Cells were incubated with substances indicated. Means ± SD are shown. *P < 0.05 when compared with control (cells incubated with fresh media); †P < 0.05 when compared with non-targeted complexes; ‡P < 0.05 when compared with free non-bound TAX……134

Fig.6.5: Cellular internalization of naked siRNA and siRNA delivered by cancer targeted delivery system. A, representative images of naked fluorophore-labeled siRNA (siGLO Red, red fluorescence) incubated with ovarian cancer cells. B, representative images of ovarian cancer cells incubated with fluorescently labeled siRNA (siGLO Red, red fluorescence) conjugated to cancer targeted PPI dendrimer labeled with FITC (green fluorescence). Superimposition of red (siRNA) and green (dendrimer) fluorescence images gives yellow color. C, Representative confocal microscopy images of ovarian cancer cells incubated with LHRH-PPI-siRNA (z-series, from the top of the cell to the bottom). Red color represents siRNA. Scale bar – 15 µm……135

Fig.6.6: Expression of CD44 protein (immunohistochemistry) in tumor tissues form mice bearing xenografts of human cancer cells isolated from malignant ascites from patient with advanced ovarian carcinoma. Mice were treated seven times twice per week within four weeks starting from the day 0 with the indicated formulations. Representative fluorescence images are shown……136

Fig.6.7: Apoptosis induction in tumor and other organs at the end of the experiments (day 28 of the treatment) of mice bearing xenografts of human cancer cells isolated from malignant ascites from patient with advanced ovarian carcinoma. Mice were treated seven times twice per week within four weeks starting from the day 0 with the indicated formulations. A, Representative fluorescence microscopy images of tumor tissue slides labeled by TUNEL. B, The enrichment of histone-associated DNA fragments (mono- and oligonucleosomes) per gram tissue in the tumor and different organs. Values in control animals were set to unit 1, and the degree of apoptosis was expressed in relative units. Means ± SD are shown. *P < 0.05 when compared with control……137

Fig.6.8: Tumor volume in mice bearing xenografts of human cancer cells isolated from malignant ascites from patient with advanced ovarian carcinoma. Mice were treated seven times twice per week within four weeks starting from the day 0 with the indicated formulations. Means ± SD are shown……138

1 INTRODUCTION

Cancer is one of the most fatal diseases in the world. More than 10 million cases of cancer are reported every year (1). It is responsible for one in 4 deaths in the United States (2).The agents that are currently used for chemotherapy fail to differentiate between the cancerous and normal cells leading to numerous adverse side-effects. Owing to their toxicity, there is limitation to the amount of dose that can be administered. Due to the lack of specificity and restriction of dose, it sometimes becomes very difficult to achieve an effective concentration within the cancer affected tissues (3).

Nanoparticles utilized as drug delivery systems are submicron sized particles (3-200 nm), devices or systems synthesized using diverse materials like polymers, lipids, viruses or oraganometallic compound (4). Nanoparticles have the ability to specifically substantiate the concentration of drugs within cancerous cells while sparing the normal cells. They do so by using passive and active targeting strategies. (5). They can bind to receptors specifically expressed on cancerous cells (active targeting) and get enveloped into endosomes via receptor mediated endocytosis. Enclosure within endosomes prevents the nanoparticles to be recognized by P-glycoprotein, thereby avoiding one of the main multi-drug resistance mechanisms (6). For these reasons nanoparticles have been able to grasp a lot of attention not only in the field of cancer therapeutics but also cancer diagnostics. Their utility in the field of cancer therapeutics has increased greatly

in recent times. In spite of all the benefits, nanoparticles also have the limitation of toxicity.

There has been a growing concern regarding the health and safety of nanoparticles in the last 4 years. In 2004, the Royal Society and Royal Academy of Engineering published a report accentuating a dearth of information on the impact of nanoparticles on human health (7). As a result of increase in number of toxicity issues related to nanoparticles, two novel branches of bionanosciences have evolved: nanotoxicology and most recently nanogenotoxicology (8-12) . Nanotoxicology is associated with the studying mechanisms of cytotoxicity of nanoparticles whereas nanogenotoxicology concentrates on the analysis of the ability of the nanoparticles to induce DNA damage.

A lot of studies investigating cytotoxicity of different nanoparticles have been reported but only a handful of them also analyze genotoxicity (8, 9, 11, 13-16). Identifying genotoxicity becomes very essential when nanoparticles are utilized for chronic treatment. Genotoxicity can be induced at very low non-cytotoxic concentrations (10). Even if the healthy cells are exposed to a very low concentration of the nanoparticles, they can inflict DNA damage. Such DNA damage in the long run can lead to adverse genetic effects. So it is very important to identify the nanoparticles that are genotoxic and propose modifications to render them non-toxic.

Experimenting on animals was banned in the cosmetic and personal care industry after the emergence of the 7th amendment to the EU Directive. Hence a variety of *in vitro* and *ex vivo* protocols has been utilized for the testing and validation of various raw materials in the cosmetic industry. After the implementation of the 7th amendment, the safety criteria in the cosmetic industry have been broadened form acute adverse effects such as irritation to the determination of long-terms accumulating effects which can induce chronic and lethal diseases like inflammation and cancer (17). One of these studies is the genotoxic evaluation of raw materials. Similar to nanoparticles as discussed previously, compounds used for the manufacturing of cosmetic have genotoxic potential they can induce DNA damage even if they can induce DNA damage to healthy cells at non-cytotoxic concentrations. Hence testing the cytotoxicity is not sufficient to declare the compounds safe.

The fifth leading cause of cancer related diseases is ovarian cancer. It is the most lethal of all the types of gynecological cancer in United States (18). Ovarian cancer responds very well to the initial chemotherapy but the five year survival rates are only 30% owing to the invasiveness, insidious progression and resistance to treatment (19, 20). Ovarian cancer can spread into abdominal cavity through intraperitoneal metastases and lead to the formation of ascites (19-22). This ascites fluid consists of ovarian cancer, lymphoid and mesothelial cells. It also consists of growth factors (23, 24), bioactive lipids such as lysophosphatidic acid (25), cytokines (26, 27) and extracellular matrix constituents (28).

These aforementioned factors can individually promote cell growth, invasion and tumor survival.

Paclitaxel is an FDA approved drug that is widely used for the treatment of patients with breast, ovarian, lung, head and neck cancers, and Kaposi's sarcoma (29). It is a hydrophobic drug with a very poor water solubility (<0.1 µg/mL). To overcome this limitation, it is frequently administered with Cremophor EL or other co-solvent formulations. These may however cause severe allergic reactions in certain patients (30). Hence great efforts have been made to synthesize a solvent free polymer bound drug delivery system which not only improves the solubility of the drug but also potentiates the efficacy and safety of the drug.

RNA interference (RNAi) is a technique of suppressing the gene expression by preventing gene transcription by utilizing a long double-stranded RNA (dsRNA) that targets and degrades a homologous target mRNA (31). Small-interfering RNAs (siRNAs) are short double stranded RNAs which also function by the technique of RNA interference. siRNA can knock down a gene in cancer cells that may be responsible for tumor resistance or metastasis. When such siRNA are used in adjunct with a chemotherapeutic drug like Paclitaxel, it can enhance the effectiveness of the therapy.

CD44 is a cell surface glycoprotein involved in cell-cell interactions, cell adhesion and migration (32). It has been shown to be responsible for activating pathways like

transcriptional activation, tumor cell growth, and multidrug resistance in ovarian and breast cancer which confers tumor stem cell specific behavior (33). CD44 can be knocked down by delivering siRNA against CD44 inside the cancer cells using dendrimers like Polyamidoamine (PAMAM) or polypropylenimine (PPi). A specific delivery of siRNA into the cancer cells can be achieved by attaching a targeting moiety like luteinizing hormone-releasing peptide (LHRH) on the distal ends of the dendrimers. Attachment of LHRH prevents the delivery of siRNA to healthy cells thereby reducing the adverse side-effects (34).

One of the purposes of this proposal is to evaluate various drug delivery systems utilized in cancer therapy or diagnosis for genotoxicity. If a drug delivery system is found to be genotoxic, we propose to modify these genotoxic systems so as to reduce or completely eliminate their genotoxicity. We also propose to test certain raw materials used in cosmetic industry on a regular bases for genotoxicity. The other purpose of this study is to develop a dendrimer based drug delivery system that would specifically knock down CD44 in cancerous cells. Once CD44 is knocked down, we plan to treat the cancer cells specifically using a chemotherapeutic drug, Paclitaxel attached to PPi dendrimer.

2 BACK GROUND AND SIGNIFICANCE

2.1 Genotoxicity and in vitro Micronucleus test

2.1.1 Genotoxicity

Certain agents can induce changes in the structure or the number of genes by chemically interacting with DNA and/or non-DNA targets (35). These agents are defined as genotoxins (35). The phenomenon of inducing DNA damage by genotoxins is known as genotoxicity. Genotoxicity of materials can be tested by various *in vivo* tests including mammalian spermatogonial chromosome aberration test, the spermatid micronucleus assay, the mammalian oocyte chromosome aberration/aneuploidy test, and unscheduled DNA synthesis test in testicular cells, the mammalian erythrocyte micronucleus test, the mammalian bone marrow chromosome aberration test, the liver unscheduled DNA synthesis and the mouse spot test. Genotoxicity can also be evaluated by various *in vitro* tests like the bacterial reverse mutation test (Ames test), the *E. coli* reverse mutation assay, *in vitro* mammalian chromosome aberration test, *in vitro* mammalian cell gene mutation test and *in vitro* micronucleus test (36). These tests facilitate to identify the hazards based on DNA damage and its fixation. Gene mutations, chromosomal damage and recombination are certain factors that are considered imperative to cause heritable changes and lead to malignancy in the long run. Change in the number of chromosomes is also known to causes tumorigenesis. Agents that are tested positive by such genotoxicity tests can be potential human carcinogens and/or mutagens. Although relationship between carcinogenesis and exposure to certain chemicals has already been established for humans, a similar kind of relation as not

been established between the latter and heritable diseases. Hence genotoxicity tests have been deemed valuable for interpretation of carcinogenicity of various agents (37).

2.1.2 In vitro Micronucleus test

In vitro tests are gaining precedence over *in vivo* tests in cosmetic industries because of the emergence of the 7th amendment to the EU directive which bans the cosmetic industries from experimenting on animals (17). The *in vitro* chromosomal aberration assay and *in vitro* micronucleus test have always been used by industries, academics and contract laboratories. A high correlation has been found between the two tests (>85%) in each of the studies done. The ECVAM (European Centre for the Validation of Alternative Methods) Scientific Advisory Committee (ESAC) endorsed that *in-vitro* micronucleus test was reliable and reproducible method and could be used as an alternative to the in-vitro chromosomal aberration test based on a weight-of-evidence retrospective validation (36, 38). In order to decrease the variability of protocols between different labs, a standard protocol was drafted by Organization for Economic Co-operation and Development (OECD). These guidelines are known as the OECD testing guidelines. The issues of variability that were taken into consideration were test exposure protocol, use of cell lines and studies with absence and presence of cytochalasin B (39).

The *in vitro* micronucleus test determines genotoxicity by detection of micronuclei in the cytoplasm of interphase cells. Acentric chromosome fragments (chromosomes

lacking centromere) or whole chromosomes can fail to migrate to the poles during anaphase of cell division. A nuclear envelope forms around these unmigrated fragments and whole chromosomes during the telophase. This gives them the morphology of a nucleus. But this nucleus is smaller than the main nucleus and hence it is known as "micronucleus" (40). The *in vitro* micronucleus test can detect both aneugenic (compounds that induce loss or gain of whole chromosomes) and clastogenic damage (compound that cause disruption or breakages of chromosomes) (41, 42) in those cells that have undergone cell division after being exposed to the test substance. This can be done my using cytokinesis block, immunochemical labeling of kinetochores, or hybridization with centromeric/telomeric probes (fluorescence *in situ* hybridization; FISH) (43-47) .

In order to conduct the test, the cells are allowed to grown for a period that is sufficient to all the chromosome or spindle damage after or during the exposure to test substance. Such damage leads to the formation of micronuclei in interphase cells. To test a substance for aneuploidy, the substance should be present during mitosis. The interphase cells are harvested and stained and analyzed for the presence of micronuclei thereafter. The scoring of micronuclei is done those cells that have completed mitosis during exposure to the test substance. Only binucleate cells are scored in cell cultures that are treated with a cytokinesis blocker. If the cell cultures are not treated with a cytokinesis blocker, it is important to show that cells that are being analyzed are likely to have undergone cell division during or after the exposure to the test substance. This is

done by demonstrating that the cells undergo cell proliferation in both control and treated cultures.

Micronuclei represent the transmittance of chromosomal damage to daughter cells. Micronuclei formed in a CHO-K1 cell line on exposure to a positive control (Ethyl Methane Sulfonate) has been demonstrated in **Fig. 2.1** (17). Chromosomal aberrations in metaphase may not be transmitted. Hence assessing micronuclei in interphase cells is much easier than chromosomal aberrations in metaphase cells. The only requirement for this test is the presence or absence of micronuclei in the cell. This makes the process much faster and easier when compared with chromosomal aberration test. Thousands of cells can be scored per treatment which increases the reliability of the test (39). Since micronuclei can arise from lagging chromosomes; the micronucleus test has the potential to detect aneuploidy-inducing agents that are arduous to recognize using chromosomal aberration test. However, as described earlier, special techniques such as FISH have to be employed to differentiate chemicals inducing polyploidy and clastogenicity.

According to the OECD guidelines, it is required to utilize an exogenous source of metabolic activation when conducting an *in vitro* micronuclei test. It is only exempt when the cells are metabolically competent with respect to the substances being tested. The exogenous metabolic system mimics an in vivo condition up to certain extent. Co-

factor-supplemented post-mitochondrial fraction (S9) prepared from the livers of rodents treated with enzyme-inducing agents such as Aroclor 1254 is the most commonly used metabolic activating system (48, 49). Certain factors such as marked changes in pH or osmolality can lead to false positives which do not reflect intrinsic mutagenicity. Such conditions should be avoided by buffering the stock solution and using equal volumes for the test and controls.

2.2 Drug delivery systems

Research on drug delivery systems have become an interesting and fast growing aspect which pharmaceutical industries are looking at to improve their products. The main aim of utilizing drug delivery systems is to improve pharmacokinetic and pharmacodynamic parameters of a drug entity. Some of the popular approaches include drug-polymer conjugation, incorporating drug into nanoparticles, polymeric matrices, liposomes and micelles. As mentioned previously, these drug delivery systems can assist in controlled drug release, reduced body clearance, increased stability, decrease in toxicity and increasing the specificity and efficacy (50). Several drug delivery systems used in cancer research are discussed as follows.

2.2.1 Polyethylene glycol (PEG)

PEG is a polymer synthesized by ring-opening polymerization of ethylene oxide. The initiation of the reaction is done by methanol or water which leads to the formation of

polymers with one or two end-chain hydroxyl groups respectively (mPEG–OH or HO – PEG – OH). The polymers can be linear or branched shaped bearing different molecular weights as shown in **Fig. 2.2** (50, 51). The PEG structures can be attached chemically to several drug entities by pegylation. Pegylation was first demonstrated by Frank Davis et.al when they protected proteins from enzymatic degradation during drug delivery by attaching PEG (52). Studies have shown that the ethylene glycol subunit of PEG is tightly associated with two or three molecules if water in a solution. Pegylated compounds behave as being five to ten times larger than a protein of similar molecular mass because of the binding of water molecules as confirmed by size exclusion chromatography and gel electrophoresis (53). This association of water molecules with PEG polymer acts as a shield to protect the entire drug delivery system from enzyme degradation, excretion by the kidneys, reticuloendothelial (RES) clearance, cell surface protein interactions and thereby eliminating adverse allergic reactions (51, 52, 54). Pegylated drug delivery systems tend to have a higher stability over a range of pH and temperature changes as compared to the unpegylated entities (55). PEG's chemical degradation is limited and its excretion dependent on its molecular weight. PEGs with molecular weight lower than 20kD are predominantly secreted in the urine where as higher molecular weight PEGs are cleared more slowly through liver. Thus attaching a high molecular PEG to small drug can yield an improved bio-distribution, selective cellular uptake to specific targeting to certain cells or organs (56-58). Owing to the above mentioned properties, PEG has been approved by FDA for human use.

PEG conjugates are generally referred as first or second generation. PEG conjugates with a molecular wt less than 12 kD and monomethoxy PEG are considered as first generation. The monomethoxy PEG have relevant percentage of diol chains as an impurity which often leads to side reaction products or to weak and reversible linkages (59). Although the first generation conjugates had limitation, a few products like PEG-adenosine deaminase (Adagen®) (60) for the treatment of severe combined immunodeficiency disease (SCID) and PEG-asparaginase (Oncaspar®) (61) for the treatment of leukemia made it to the market and are still used. The second generation conjugates have higher purity of PEG as compared to the first generation with a reduction in polydispersivity and diol content. Among these, the branched PEG conjugates have much wider applications due to their enhanced sized as compared to the linear PEG conjugates. A few among many second generation PEG products that are currently used include linear PEG-interferon α2b (PEG-Intron®) (62) and branched PEG-interferon α2a (Pegasys®) (63, 64) for the treatment of Hepatitis C; PEG-growth hormone receptor antagonist (Pegvisomant, Somavert®) (65) for the treatment of Acromegaly and pegylated liposomal formulation of doxorubicin (Doxil) for the treatment of Kaposi's sarcoma and breast cancer (66, 67).

2.2.2 Quantum dots (QD)

Quantum dots are semiconductor particles of nearly spherical shape with a diameter ranging from 2-10 nanometers (68). Quantum dots were first synthesized in 1982 by

Efros and Ekimov. They grew nanoparticles and microcrystals of semiconductor in glass matrices (69, 70). Bawendi and coworkers were the first to synthesize quantum dots from from cadmium sulfide (CdS), cadmium selenide (CdSe), or cadmium telluride (CdTe) which proved to be a major breakthrough (71). The Cdse quantum dots gained much popularity in the field of biological sciences. The presence of cadmium raises the issue of toxicity. Hence efforts are being made to replace cadmium with other materials. One such example is the synthesis of gallium phosphide quantum dots (72). However properties of these quantum dots do not match up to those of Cdse quantum dots.

The Cdse quantum dots are generally composed of Cdse core surrounded by a shell of semiconductor metals such as zinc sulfide. Owing to the semiconductor nature and size dependent fluorescence of quantum dots, they have been used in optoelectronic devices, biological detection and for the study of colloids and size-dependent properties of nanoparticles (68). The functioning of quantum dots can be explained by band gap energy. Band gap energy is the minimum energy required for an electron to excite to an energy level higher to its grounds state. An electron in the semiconductor absorbs a photon of energy higher than the band gap energy and emits fluorescence while returning back to the ground state. The characteristics of small quantum dots used in biological field are dependent on size. Adjusting the size of the particles can yield quantum dots with different optical properties as shown in **Fig. 2.3**.

Conventional fluorophores like organic and fluorescent proteins have several limitations which are overcome by quantum dots. Quantum dots are 10-1000 times brighter as compared to the conventional fluorophores. They have a higher stability against photo bleaching. Conventional fluorophores have the limitation of unwanted excitations and overlapping spectra due to narrow excitation wavelength range and broad emission peaks. Quantum dots on the other hand have narrower and symmetric emission spectra (68). Quantum dots can be excited utilizing a single light source while emitting different wavelengths ranging from ultraviolet (73), visible, near infrared (74) to mid infrared (75). Owing to the above mentioned advantages, quantum dots have gained much popularity in fluorescence imaging.

Quantum dots also have a great potential as a drug delivery agent. But quantum dots have a limitation of hydrophobicity. In order to render them useful in biological field they need to disperse in aqueous solutions. One of the strategies to overcome this limitation is to coat the quantum dots with amphiphilic polymer. The biological and physical properties of quantum dots may alter by surface coating them. The hydrophilic coating of quantum dots can be modified with biomolecules such as antibodies, small molecules, peptides, and aptamers (68, 76). Owing to these properties, quantum dots can be utilized as an imaging as well as delivery agent for therapeutic entities. One such example is the targeted delivery for imaging and treatment of ovarian cancer conjugating quantum dots with doxorubicin and muc-1 aptamer (77). Quantum dots have also been reported to be utilized in photodynamic and radiation therapy (78).

2.2.3 Liposomes

Liposomes are spherical vesicles consisting of one or more concentric lipid bi-layers enclosing an aqueous core (79) as shown in **Fig. 2.4** (80). Liposomes were first developed in 1980 by A D Bangham (81). Ever since their discovery, liposomes have become an important tool in biological and medicinal sciences. Early liposomes were utilized to deliver many compounds by packing them in the aqueous compartment (82). Today hydrophobic drugs are packed in the lipid bilayer for delivering them in the cells. The potential of liposomes as a vehicle for drug delivery was realized when they were utilized for replacement therapy in genetic deficiencies of liposomal enzymes in 1970s (83, 84). Today many anti-tumor and antifungal liposomal formulations are commercially available.

There are several mechanisms by which liposomes function. Liposomes can attach to the cell membrane and fuse with it thereby releasing its content in the cell. They can be taken by cell and the phospholipids get incorporated in the cell membrane releasing the drug trapped within. The liposomes can also be taken up by a cell and the therapeutic entities can be releases by the digestion of liposomes by lysosomes present within the cell (82).

The surface properties of liposomes can be modified by using different lipids for the synthesis. When zwitterionic lipids such as phosphatidylcholines are utilized for the synthesis, neutral liposomes are generated. Use of negatively charged lipids such as

phosphatidylserines can yield liposomes with a negative surface charge (85). Similarly, using cationic lipids will yield positively charged liposomes. Liposomes can be used for targeted drug delivery to specific cells by covalently attaching antibodies on liposomal surface. Liposomes have the limitation of low blood circulation time since they are rapidly cleared from the circulation by the reticuloendothelial system (RES). This limitation can be overcome by modifying the surface of liposomes so as to escape recognition by phagocytes. Surface coating of liposomes with polyethylene glycol (PEG) has been widely utilized to escape recognition (86, 87). Cationic or anionic liposomes are rapidly removed from circulation due to their binding with proteins (88, 89). Synthesis of liposomes with a mixture of saturated phosphatidylcholines increases steric stabilization and reduce protein binding. This will result in liposomes having higher half-life and longer circulation time (90, 91).

Liposomes have been widely used for pulmonary delivery of drugs. Liposomal aerosols have several advantages such as sustained release, prevention of local irritation, reduced toxicity and higher stability (82). Liposome had a great impact in the field of cancer drug delivery. Chronic use of anticancer drugs leads to many toxic side effects. Liposomal drug formulations have the least side effects. Doxil is a liposomal preparation of doxorubicin used for the treatment of Kaposi's sarcoma. They have a long circulation time owing to its characteristic of being stealth. Caelyx and Myocet are other doxorubicin liposomal preparations recommended for the treatment of metastatic ovarian cancer and metastatic breast cancer respectively (90). Most of the liposomes

are passively targeted. Studies done by Zhang and co workers show that the doxorubicin liposomal preparations can be modified for specifically targeting cancer cells. They also showed that the drug resistant proteins in cancer cells can be knocked down by simultaneously co-delivery anti-sense oligonucleotides thereby increasing the efficacy of the formulation (92).

2.2.4 Dendrimers

Dendrimers are structurally-perfect synthetic molecules with highly branched molecular structure synthesized in a repeating algorithmic fashion (93). The name 'dendrimer' is derived from two Greek words: Dendron meaning a tree and meros meaning part. A fully controlled synthesis of dendrimer was carried out for the first time by Vögtle and co-workers in 1978 (94). Dendrimers started receiving a lot of attention in early 1990s (95). They had a lot of applications owing to their unique structure (96). Dendrimers comprise of three distinguishing areas: An initiator core, interior layers (generations) and the exterior surface with functional groups (97, 98) as shown in **Fig. 2.5** (99).

The core consists of the starting molecule used for the synthesis of dendrimer which is repeated as the synthesis progresses. Various types of dendrimers are obtained depending on the type of initial molecule utilized. Poly(amido amino) PAMAM dendrimers have ethelene diamine as the repeating structure. As the sequence of reactions is repeated, the branching units that are radically attached to the core increase. These repeated branching units give rise to the interior layers or generations. Generation number indicates the number of focal points emerging from the core and

progressing towards the surface. A dendrimer with 4 focal points from the core to the periphery is referred as a 4^{th} generation dendrimer or G4-dendrimer. The dendrimer core is sometimes referred as G0 since the core does not have any focal points. The homo-structural spatial portions between focal points are known as dendrimer shells. The space between the last outer branching point and the surface is called the outer shell while the inner shell comprises of the dendrimer interior. Before reaching the dendrimer surface, the last focal point creates a number of pincers in the outer shell. In dendrimers like PAMAM, the number of pincer are half the number of surface groups since each focal point gives rise to two chains or branches. The groups that are present on the surface are known as end or terminal group. Amino-terminated dendrimers have amine functional group on their surface (97-99).

Dendrimers can be synthesized using two techniques: a) Divergent method 2) Convergent method. In the divergent method, the synthesis starts from the central core and augments towards the periphery via a series of reactions mostly Michael reactions (100). If each step of the reaction is not allowed to finish completely, trailing generations (branches of unequal length may arise). The divergent method is a successful technique and is commonly used for large scale synthesis of dendrimers like PAMAM, PPi, Tecto and Micellar dendrimers (99). In contrast to the divergent method, the synthesis of a dendrimer in convergent method starts from the end groups and advances inwards towards the core (101). When the branched polymeric arms (dendrons) reach the required size, they are attached to the core molecule. Dendrimers

with high shells cannot be synthesized using the convergent method because of steric interactions during the reaction between denrons and the core molecule. Dendrimers that are commonly synthesized using convergent methods include Chiral, Multiple antigen peptide and metallo dendrimers.

Dendrimers have several advantages over linear polymers. Dendrimers are monodisperse while linear polymers are polydisperse. The polymerization technique that is classically used results linear polymers with different sizes. Dendrimer synthesis is much controlled and it yields dendrimers with specific size and mass. Dendrimers have much improved physical and chemical properties as compared to linear polymers owing to their molecular architecture. Dendrimers exist as tightly packed ball in solution which confers them favorable rheological properties (101). The viscosity of dendrimers is lower than that of linear polymer solutions (102). Dendrimers are highly reactive owing to the many chain ends. Functional groups on the periphery strongly influence the solubility of dendrimers. Dendrimers with hydrophilic terminal groups are soluble in polar solvents whereas dendrimers terminating in hydrophobic groups are soluble in non polar solvents. It is possible to encapsulate therapeutic entities in the interior cavity or attach them with the functional group present on the surface via covalent or electrostatic interactions.

2.2.4.1 PAMAM (Poly(amido amino)) Dendrimers

PAMAM was the first dendrimer synthesized. They were developed by Tomalia and co-workers in 1984 (103). They are also known as starbust dendrimers. The core molecule in PAMAM is ammonia. A structure of generation 3 PAMAM dendrimer is shown in **Fig. 2.6** (104). PAMAM dendrimers are cationic in nature because of the positive charge on their surface and hence can bind to DNA (negatively charged) at physiological pH. As a result PAMAM dendrimers have received maximum attention as a transfecting agent for gene delivery (93). A successful DNA transfection *in vitro* by PAMAM dendrimers was demonstrated by Haensler and coworkers (105). Charge ratios of 5-20 are required for successful transfection by PAMAM. Charge ratio (N/P) is defined as the number of terminal positive charge amine groups (N) in PAMAM to the number of negatively charged phosphates (P) in DNA.

PAMAM dendrimers have been widely used for drug delivery. As discussed previously, PAMAM has been successfully used as a transfecting agent. They have been used as vectors for gene delivery (106). Patil and co-workers showed that PAMAM dendrimers can be used for delivery of siRNA for genes like BCL2 and knock it down successfully (107). Zhou and co-workers demonstrated that PAMAM can be used as carriers for anti-tumor drugs like 5-Fluorouracil (5FU) (108). 5FU is an excellent anti-tumor agent with high toxic side effects. They conjugated PAMAM dendrimer with 5FU by acetylation to yield dendrimer-5FU conjugates. These conjugates were water soluble and slowly released 5FU on hydrolysis. The slow release of 5FU reduces its toxicity to normal

tissues. PAMAM dendrimer have also been utilized in magnetic resonance imaging by chelating them with polygadolinium as demonstrated by Wiener and co-workers (109).

PAMAM dendrimers are highly hemolytic and cytotoxic. The cytotoxicity is highly dependent on the number of terminal amine groups and the generation of the dendrimer (110). Toxicity of dendrimers is strongly influenced by the surface. Chen and coworkers showed that cationic dendrimers exhibit more toxicity than their anionic counterparts (111). Lee el al. and Patil et al. showed that quaternized PAMAM-OH dendrimers were less cytotoxic as compared to PAMAM-NH2 because of the shielding of cationic groups by hydroxyl groups (112, 113). PEG has been used widely to mask the cationic groups on PAMAM and reduce their toxicity (107).

2.2.4.2 Polypropylenimine (PPi) Dendrimers

Polypropylenimine (PPi) dendrimers were first developed by de Brabander-van-den Berg and Meijer in 1993 (114). They are also known as Astramol dendrimers. PPi dendrimers have butylenediamine as the core molecule. A fourth generation PPi structure is shown in **Fig. 2.7**. PPi dendrimers have similar properties like PAMAM dendrimers. They have positive charge on the surface owing to the amine groups on the surface. This allows them to bind to negatively charged DNA via electrostatic interactions. Studies have shown that PPi dendrimers can be used for nucleotide delivery (115, 116).

PPi dendrimers and quaternized PPi dendrimers have been utilized for gene delivery by various groups. Schatzlein and co-workers demonstrated that quaternized PPI dendrimers can be used as vectors for gene delivery in-vivo targeted towards liver (117). Zinselmeyer and coworkers compared various generation of PPI dendrimer for gene delivery and concluded that lower generation PPI dendrimers (specifically PPI G2) presented improved biocompatibility and in vitro transfection capability (118). Lim etl al. demonstrated that PPi dendrimers self assembled with DNA and curcubituril and were able to transfect mammalian cells successfully. They demonstrated that PPi dendrimers can be used as non-covalent gene delivery systems (119). Chen and co-workers demonstrated that generation 4 PPi dendrimers can enhance the uptake of oligodeoxynucleotides in MDA-MB-231 breast cancer cells as compared to oligodeoxynucleotides (115).

Due to the presence of terminal amine groups and multiple cationic charges on PPi dendrimers, they also exhibit cytotoxicity like PAMAM dendrimers do. They also exhibit hemolytic toxicity due to the interaction of free cationic terminal groups with RBCs (120). In order to reduce the toxicity related to PPi dendrimer, many authors have utilized modified PPi dendrimers for drug delivery. Taratula and co-workers modified the surface of generation 5 dendrimers with PEG for delivering siRNA in A2780 ovarian cancer cells and observed a decrease in toxicity and enhanced delivery in to the cells (121). Agashe et al. synthesized two different functionalized PPI dendrimers: t-BOC-protected amino-acid-coated PPI dendrimers and carbohydrate-coated PPI dendrimers.

The functionalized PPi dendrimer had reduced cytotoxicity and improved biocompatibility as compared to non functionalized PPi (120).

2.2.5 Supermagnetic iron oxide

Magnetic nanoparticles exhibit a unique feature of super magnetism. The super magnetism property of these particles is highly dependent on the size of the nanoparticles which should be below a critical value. The critical value is dependent on the type of material but if generally ranges from 10 to 20 nm. When the temperature is above the blocking temperature, each nanoparticle becomes a single magnetic domain (state of uniform magnetization at any field) and exhibits superparamagnetic behavior. Each nanoparticle possesses a large constant magnetic moment. They behave like a giant paramagnet atom and respond quickly when a magnetic field is applied without any remanence (residual magnetism) or coercivity (the field required to bring the magnetization to zero) (122). Frenkel and Dorfman were the first to demonstrate that a ferromagnetic particle below a critical size consists of a single magnetic domain (123).

Particles prepared from magnetite (Fe_3O_4) or its oxidized form maghemite (Fe_2O_3) are commonly known as iron oxide particles. Movement of particles having mass and electric charges is responsible for the magnetic effects. A magnetic dipole called magneton is created by a spinning electric-charged particle. In materials made from iron (ferromagnetic), magnetons are associated in groups. When all magnetons are aligned in the same direction by exchange forces, it leads to the formation of magnetic domain. Ferromagnetism is distinguished from paramagnetism by the concept of domains. The

size dependence of magnetic behavior is determined by the domain structure in a ferromagnetic material. When the size of such particles is smaller than a critical size, it becomes a single domain. Coercivity is a property of importance for such small particles. When the particle size is very small, their coercivity becomes zero i.e. they lose their magnetic properties and become superparamagnetic. Super paramagnetism is caused by thermal effects. The temperature fluctuations have enough strength to spontaneously demagnetize the particle. These particles become magnetic in presence of an external magnet but revert to a non magnetic state when the external magnet is removed. So an 'active' mode of particles can be achieved as and when required (124). This gives the particles a unique advantage when working in biological environment.

Supermagnetic iron oxide nanoparticles have been utilized in hyperthermia therapeutic procedure in cancer treatment (125). The rationale for the hyperthermia therapy is based on a directly killing the cancer cells at temperatures above 41–42˚C. The loss processes that occur during the reorientation of the magnetization of magnetic particles are responsible for generating the heat. Use of iron oxide nanoparticles allows the heating in restricted tumor area and can absorb more power at tolerable AC magnetic fields owing to their smaller size. Iron oxide nanoparticles have also been utilized for targeted drug delivery as shown in **Fig. 2.8** (122). Kwon and co-workers demonstrated that the particles can be specifically delivered to a desired target area, fix them and allow the medication to be released slowly by using an external magnetic field (126). The iron oxide particles have also been utilized for NMR imaging. They can enhance the

between the normal and affected tissue or determine the status of organ function and blood flow. Endorem and Resovit are commercially available iron oxide nanoparticles of maghemite that are used in NMR imaging for the location and diagnosis of brain and cardiac infarcts, liver lesions or tumors.

2.2.6 Mesoporous silica nanoparticles

Mesoporous silica nanoparticles (MSP) have many unique characteristics such as being chemically and thermally stable, having large surface areas, tunable pore sizes and well-defined surface properties. These characteristics make ideal for hosting various molecules (127). MSPs possess three distinct domains which can be functionalized independently: a) The silica frame work; b) Nanochannels or pores; c) The outermost surface of nanoparticles (128). Submicrometer-scaled MSP called MCM-41 were first synthesized by Grun et al. in 1968 by using modified Stober synthesis. Cai et al. synthesized MSP in the range of 100nm using dilute surfactant (129). MSP with size lower than 50nm were obtained by Imai and co-workers using a double surfactant system (130). Dialysis was employed by Urata and co-workers to eliminate surfactants and prevent aggregation. They were able to obtain MSNs with diameters less than 20 nm (131).

MSPs have very high versatility since it is easy to introduce various functional groups by covalent bonding or electrostatic interactions. Functional groups can be covalently attached by introducing organic structures in the form of silanes using co-condensation

(the hydrolysis of the functional silanes while the particles are forming) or post-synthetic grafting (introducing functional groups to the exposed silica surface after MSP are formed) techniques (132). The property to encapsulate different molecules inside the pore channels makes MSP an excellent choice for drug delivery. Encapsulation can prevent the therapeutic entities from enzymatic degradation. The cargo molecules are loaded on the particle through adsorption via hydrogen bonding or electrostatic interactions (133).

Based on the properties discussed above, MSPs have been utilized to deliver hydrophobic drugs by taking advantage of the large pore capacity. Studies have shown that MSPs can successfully deliver drugs like camptothecin and paclitaxel into human cancer cells (134, 135). By attaching targeting moieties to the surface of MSP, the specificity of drug delivery can be increased. Several research groups functionalized MSPs with folate groups to target human cancer cell lines that over express α-folate receptors (134, 136, 137). Ferris and co-workers demonstrated that attaching transferring and cyclic-RGD peptides as targeting moieties on MSP surface can help in differentiating between normal and cancer cells, and between primary and metastatic cancer cells respectively (138). Meng et al. showed that MSPs can be used for dual delivery of siRNA and anticancer drug. They modified the particle surface with a phosphonate group which allowed electrostatic binding of the anti-cancer drug doxorubicin to the porous interior. Phosphonate modification also allowed exterior coating with the cationic polymer, polyethylenimine so that it can electrostatically bind

with P-glycoprotein siRNA. This dual drug delivery system was capable of increasing the intracellular drug concentration to levels exceeding that of free Dox or the drug being delivered by MSP in the absence of siRNA co-delivery (139).

2.3 Ovarian cancer and Cancer stem cells

2.3.1 Ovarian cancer

Ovarian cancer is defined as the cancer that starts in the ovaries (female reproductive organ that produces eggs) (140). It is the ninth most common cancer among women and the fifth leading cause of cancer related death among women. However ovarian cancer is the most lethal of all gynecologic cancers (18). According to the American Cancer Society, in 2012 an estimated 22,280 cases will be diagnosed with ovarian cancer out of which 15,500 will die in United States. Several factors are considered responsible for developing ovarian cancer. Women with more children and births in earlier life have a low risk of ovarian cancer. A small number of cases are affected by certain gene defects (BRCA1 and BRCA2). Women with a family history of ovarian or breast cancer are more prone to be affected by the ovarian cancer (18). The ovaries contain 3 types of cells: a) Epithelial cells (cover the ovary); b) Germ cells (Cells that develop into eggs); c) Stromal cells (Structural tissue holding ovary). Each of these cell types can develop into different types of tumor namely epithelial, germ cell and stromal tumors. The malignant forms of epithelial ovarian cancer are referred as carcinomas. Epithelial ovarian carcinomas account for 85 to 90 % of the ovarian cancers. These tumors are generally considered as “ovarian cancer”. Ovarian cancer is categorized into stages based on the severity of

condition. Stage I: The cancer is contained within the ovaries and has not spread. Stage II: The cancer is present in one or both ovaries and has spread to parts of pelvis like uterus, fallopian tubes, bladder, the sigmoid colon or the rectum. Stage III: Cancer has spread beyond the pelvis into the lining of the abdomen and/or spread to lymph nodes. Stage IV: This is the most advance stage where the cancer has spread to various organs located outside like lungs or liver (141). Invasiveness, insidious progression and quick development of resistance to chemotherapy are the main reasons for the invasiveness of ovarian cancer. In 75% of the cases, the disease is already in late III or IV stage at the time of diagnosis. Ovarian cancer responds very well to the initial chemotherapy but the five year survival with the later stages are extremely low at 30% (19). When the cancer crosses the lining of abdomen and into peritoneum, the fluid produced is referred to as ascites which comprises of ovarian cancer, lymphoid and mesothelial cells. It also consists of growth factors (23, 24), bioactive lipids such as lysophosphatidic acid (25), cytokines (26, 27) and extracellular matrix constituents (28). These aforementioned factors can individually promote cell growth, invasion and tumor survival. Depending upon the type of tumor, 45 to 75% of women present the incidence of ascites (142).

2.3.2 Cancer stem cells and CD44

2.3.2.1 Cancer stem cells

Stem cells are defined as cells that can conserve themselves through self renewal and possess the ability to differentiate into mature cells of a particular tissue (143). The properties of normal stem cells were first established from the studies of

hematopoiesis by Weissman (144). He showed that the hematopoietic stem cells (HSCs) could not only self renew but also generate differentiated blood cells. Similar adult stem cells were later found in a number of tissues and organs like muscle, intestine, heart, lungs and mammary glands (145-147). In physiology, normal stem cells play the role of maintaining tissue homeostasis and tissue regeneration after damage. Stem cells are usually in a prolonged state of quiescence under normal conditions which is governed by p21CIP1 and p18INK4C regulators (148). Based on the intrinsic or extrinsic stimulatory signals, stem cells exit from the quiescent state and either self renew or differentiate to generate progenies (144, 149). Various factors of the Wnt, Notch and hedgehog signaling pathway promote stem cell self renewal (150-153).

Applying the principles of stem cell as discussed above, a cancer stem cell model for tumors have been proposed. Cancer stem cells (CSC) can be defined as a small subset of cancer cells having the capacity to regenerate cancer through the process of self renewal. The purified CSC can differentiate and produce heterogeneous phenotypes of parental cancer from which they were derived (154). These observations point to the fact that CSCs can initiate and sustain tumor growth. The heterogeneous nontumorigenic cell types usually constitute the bulk of cancer cells in a tumor. CSCs have the inherent property of pumping out drug from the cell by utilizing ABC family of drug transporters (155). This property makes the CSCs relative refractive to the current cancer therapies. Such conventional therapies would only eradicate rapidly dividing

non-stem cell components of the tumor but not the CSCS resulting in a relapse of the tumor (156) as shown in **Fig. 2.9** (143).

Development of a cancer therapy that targets and eliminates CSC is very important to achieve successful results. Before that the CSCs have to be identified. Several studies have been done to identify the CSCs by identifying the cell markers that are specific to CSCs. Different types of tumors have CSCs that exhibit unique cell markers. In 1997, Bonnet and co-workers identified CSCs possessing the cell surface antigenic phenotype CD34+CD38- which could reproduce the complete leukemic hierarchy when xenografted (157).Similarly Al-Hajj and co-workers isolated CSCs form breast cancer with a CD44+ CD24- phenotype. As few as 100 cells with this phenotype were able to form tumors in mice, whereas tens of thousands of cells with alternate phenotypes failed to form tumors. When these tumorigenic cells were serially passaged, they generated new tumors containing additional CD44+ CD24- cells as well as phenotypically diverse mixed populations of non-tumorigenic cells present in the initial tumor (158). Several other studies have identified CSCs in brain, lung, skin and prostrate cancers which possess CD133+, Sca-1+ CD34+ Lin-, CD20+ and CD44+ CD133+ as their cell markers respectively (146, 159-161).

2.3.2.2 CD44

CD44 is considered as a stem cell marker in many cancers such as breast, intestinal and prostate. It is considered as a useful marker for progression and metastasis certain

cancers (162). CD44 is used as a stem cell marker for ovarian cancer (163). Cd44 is single chain glycoprotein with an ectodomain, a transmembrane domain and a cytoplasmic domain. It is encoded by single gene located on the short arm of chromosome 11 in humans (164).It can have a molecular weight ranging from 80 to 200 kDa. This broad range of molecular wt is due to the variable N- and O- linked glysocsylation and alternative splicing in the extracellular domain (165, 166). The CD44 glycoprotein is acidic in nature because of the sialic acid. CD44 is an adhesion molecule present on the cell surface as a receptor through which cells interact with other cells or components of extracellular matrix as well as movement on various tissues (167). The extracellular N-terminal exons having the binding domain residues give rise to a globular structure. This globular structure acts a binding site for hyaluronic acid (HA) (168), fibroblast growth factors, osteopontin and matrix metalloproteinases (MMPs). All these ligands are very important in relation to cancer (169). HA however is the main ligand for CD44.

Cancer cells have the ability to survive under conditions that lead to growth arrest or apoptosis in normal cells. One such condition is anchorage-independent growth where the cancer cells can grow in soft agar or suspension which usually lead to apoptosis in normal cells (170). Several studies have shown that the interaction of CD44 and HA endows the cancer cells with resistance to growth arrest and apoptosis under anchorage-independent conditions (171-175). Studies have also shown that CD44-HA interaction activates the phosphatidylinositol 3-kinase (PI3K) dependent AKT signaling pathway which is responsible for the cell survival and multi-drug resistance in cancer

cells (173, 176-178). PI3K signaling regulates multidrug resistance (MDR), mainly MDR1 transporter expression and function (179). It also phosphorylates AKT which is responsible for cell-survival signaling. CD44 interacts with ERBB2 and HA to activate the PI3K which in-turn activates the AKT pathways thus encouraging multi-drug resistance and cell survival as shown in **Fig 2.10** (170).

CD44 is also known to be involved in cell invasion and metastasis. Extracellular matrix (ECM) barriers prevent the cells penetrating the normal tissue architecture and blood vessel walls. Pericellular proteolysis of these ECM barriers is essential for the invasiveness of the cancer cells. MMPs play a crucial role in cancer cell invasion which includes facilitating tumor growth at the secondary site (180, 181). CD44 interaction with HA stimulates the production of MMP9 and MMP2 in glioma and lung carcinoma cells respectively (182, 183). This interaction also encourages the binding of MMP9 to the ectodomain of CD44 which promotes increased invasiveness, processing of tumor growth factor (TGF) and angiogenesis (184, 185). Another MMP and MT1-MMp are targeted by CD44 to lamellipodia which increased CD44 shedding and cancer-cell migration (186, 187). CD44 interacts with Na+-H+ exchanger NHE1 leading to the acidification of the cancer cell milieu which leads to an increase in invasiveness (188). Direct interaction of CD44 with ankyrin (189) and the members of ezrin/radixin/moesin (ERM) family are also known to be involved in tumorigenesis (190). Absence of CD44 prevents the metastasis of sarcoma in mice (191).

CD44 is known to be closely associated with the Nanog family of proteins for induction of transcription that is correlated with stem cell function and chemoresistance. Nanog is one of the important factors for maintaining pluripotency and self-renewal of embryonic stem cells (192). The genes required for pluripotency are controlled by the interaction of Nanog with stem cell regulators like Rex1, Sox2 and Oct3/4 (193, 194). Stem cell differentiation is inhibited by the constitutive expression of Nanog (192). Stress signal down regulated Nanog expression due to DNA damage (195). These results point towards the important role of Nanog in stem cell differentiation. Signal transducer and activator of transcription protein 3 (Stat-3) is another factor that has been known to an essential factor in cell growth regulation, differentiation and survival (196). Studies have shown that Nanog and Stat-3 function closely to maintain stem cells properties (197). Bourguignon and coworkers demonstrated that CD44 and HA binding stimulates CD44-Nanog complex formation thus activating Nanog and stem cell marker expression (198). This also activated the Nanog interaction with Stat-3 leading to Stat-3 dependent transcriptional activation of MDR1 gene expression and tumor cell growth. CD44-HA interaction also promoted ankyrin (member of membrane skeleton family expressed in epithelial cells and tissues) (199) association with MDR1 and multi drug fluxes as shown in **Fig. 2.11** (198).

Based on all the discussion, CD44 can be considered as a major protein in endowing the cancer cells stem-cell like properties. Targeting CD44 with siRNA and knocking it down can thwart the progression of the cancer.

2.4 RNA interference (RNAi)

RNA interference (RNAi) is a technique by which a particular gene of interest can be prevented from expressing by utilizing a long double-stranded RNA (dsRNA) (typically, > 200 base pairs) that targets and degrades a homologous target mRNA (31). RNAi was first demonstrated by Fire and co-workers in 1998 (200). They specifically silenced homologous genes by injecting dsRNA into the nematode *Caenorhabditis elegans*. Montgomery and coworkers showed that the endogenous mRNA was the target for dsRNA and the targeted mRNA degraded before translation could occur (201). After the discovery of RNAi, many research groups used it for studying invertebrates like fruit flies (202), trypanosomes (203), planaria (204), and hydra (205). Hamilton and co-workers indicated that RNAi can also be also achieved in plants (206). Elbashir and coworkers in 2001 were the first to provide evidence that small interfering siRNA can be successfully used in mammalian cells. They showed that siRNA can bypass the conversion step of dsRNA into short RNA fragments (207). This discovery of siRNA initiated a lot of research to discover new pathways of gene silencing thereby revolutionizing the understating of various pathways of gene regulation and providing new approaches for drug discovery. Since then, RNAi therapy has been employed for treating disease by addressing targets that were once considered unreachable.

The mechanism by which RNAi works is shown in **Fig 2.12** (208). RNAi is a two step process. The first step involves the delivery of dsRNA inside the cells. In the cytoplasm,

the dsRNA get cleaved into a 22 nucleotide RNA known as small interfering (siRNA) by a highly conserved RNAase III family nuclease, Dicer (209). The siRNA has a sequence homologous to the target gene. dsRNA longer than 30 base pairs can activate the interferon response which results in non-specific suppression of genes (210).Thus the use of siRNA instead of dsRNA was encouraged to prevent the interferon response and to skip the first dicing step (207). The next step is the incorporation of the siRNA into multi-enzyme complex which includes RNA induced silencing complex (RISC) and Argonaute 2 (AGO2). This complex discards and cleaves the sense or passenger strand and retains the antisense strand (211). Since the antisense strand is homologous to the target gene it guides the activated AGO2-RISC complex to the target mRNA which bears the complementary sequence (212). The catalytic domain of AGO2 then cleaves the mRNA strand between 10 and 11 nucleotides of the guide strand relative to the 5' end. The cleaved mRNA fragments undergo rapid nucleolytic degradation. This frees the AGO2-RISC complex to degrade another target mRNA (31, 213).

However there are certain limitations to RNAi therapy when using siRNA alone. As mentioned earlier, the first step of RNAi is the delivery of siRNA inside the cells. This is a major barrier for siRNA as it has limitation of poor ability to penetrate the cell membrane (214). The negative charges on the surface of the cell membrane repel the negatively charged siRNA thereby restricting its entry into the cell. siRNAs have a short half-life as they are rapidly digested by nucleases in human plasma (215, 216). Even if the siRNA remain stable without being degraded in plasma, they are rapidly excreted

through urine owing to their small size (217). Studies have also shown that siRNA with base pairs less than 21 have less effectiveness (218).

In order to achieve a successful therapy, it is essential to deliver the siRNA into the cytoplasm by utilizing a drug delivery system which does not elicit an immune response and releases the siRNA once inside the cell. Many drug delivery systems have been studied which can improve the cellular internalization of siRNA. Once such system is PPi based dendrimers. As discussed earlier, PPi is a cationic molecule. siRNAs can easily form complexes with PPi because of the electrostatic interaction between the negatively charged phosphate groups and positively charged amine groups. This interaction between positive and negative charges can increase the cell uptake thereby elevating the efficiency of transfection (219).

2.5 Luteinizing hormone-releasing hormone (Targeting moiety)

Luteinizing hormone-releasing hormone (LHRH) is a hypothalamic decapeptide that plays an important role in the controlling mammalian reproduction (220). Hypothalamus secretes LHRH in a pulsatile manner stimulating the production and release of luteinizing hormone and follicle-stimulating hormone. LHRH receptors are expressed by 80 % of human ovarian cancer (221). Many study groups have demonstrated that LHRH receptors are not expressed on other organs or hemotopoietic stem cells (222-224). Hence LHRH receptor can be employed as a target for specifically delivering anticancer drugs to the tumors by tagging them with LHRH peptide. There are many advantages of

utilizing LHRH peptide. LHRH peptide aids in the internalization of the drug delivery system. Free anti-cancer agents are usually taken up by cells by simple diffusion. They can be subjected to efflux form the cells by drug transporters like MDR-1. The mechanism of internalization of a LHRH tagged drug delivery system is receptor mediated endocytosis. The LHRH peptide attached to the drug delivery system binds to the LHRH receptor on the cancer cells. After the receptor binding, the drug delivery receptor complex is internalized via coated vesicles. Once inside the cell, the anticancer drugs can be released and confer its effect. Emons and co-workers demonstrated this by attaching LHRH peptide to an anti-cancer drug doxorubicin as shown in **Fig 2.13** (225). LHRH peptide assists in the internalization of the doxorubicin. Once inside the cells, free doxorubicin is released and accumulated in the nucleus where it induces apoptosis. Such receptor-mediated endocytosis can also bypass MDR-1. The other advantage of targeted drug delivery system is a reduction in toxicity. Zhang and co-workers utilized liposomal formulations of doxorubicin and cisplatin with LHRH peptide as the targeting moiety for the treatment of ovarian cancer (226). The non-targeted drug delivery system accumulates almost equally in tumor and other organs like liver and kidney. The targeted formulation was prominently accumulated in the tumors and not the other organs. Thus targeting with LHRH peptide can help reduce the toxicity associated with anticancer drugs.

2.6 Anticancer agent-Paclitaxel

Paclitaxel is an anti-tumor agent that has been successfully used for the treatment of many forms of human cancer. It was isolated from the crude bark extract of Pacific yew tree, Taxus *brevifolia* in 1971 by Wani and coworkers (227). The structure of Paclitaxel is as shown in **Fig 2.14**. The chemical name of paclitaxel is 5β, 20-epoxy-1,2α,4, 7β,10β,13α-hexahydroxytax-11-en-9-one4, 10-diacetate 2-benzoate 13-ester with (2R,3S)-N-benzoyl-3-phenylisoserine. It is very lipophilic and insoluble in water (228). It acts by inhibiting mitosis. Microtubules play a crucial role in mitosis. Paclitaxel attaches to the B subunit of tubulin in a selective and reversible manner. This polymerizes the tubulin and leads to the formation of unusually stable microtubules which resist depolymerization by calcium and cold temperature. The conversion of microtubules to tubulin dimers is important for the formation of spindle during cell division. Hence cells subjected to Paclitaxel exhibit disorganized microtubules (**Fig 2.15**)(229) and lead to cell cycle arrest in G2/M phase. This cell cycle arrest eventually causes apoptosis (230, 231).

Paclitaxel is the first choice of drug for ovarian cancer in combination with platinum compounds (232, 233). However Paclitaxel has certain limitations. Since it is very hydrophobic, it has very poor water solubility. Hence it is co-administered with Cremophor EL or other co-solvents which can cause severe allergic reactions. Cremophor EL also exhibits neuro and nephrotoxcity. (30). Various formulation strategies have been studied to overcome this problem. One of them includes the encapsulation of Paclitaxel in various polymers. Such encapsulation techniques are non-covalent and straight forward but there is a limitation to the drug loading capacity and

the release rates are less controlled. Paclitaxel can be covalently attached to carriers like PPi dendrimers by linkers which can be cleaved enzymatically once inside the cell and release the free drug. Such covalent binding offers higher drug loading. The surface of the dendrimer can be modified to specifically target tumor cells.

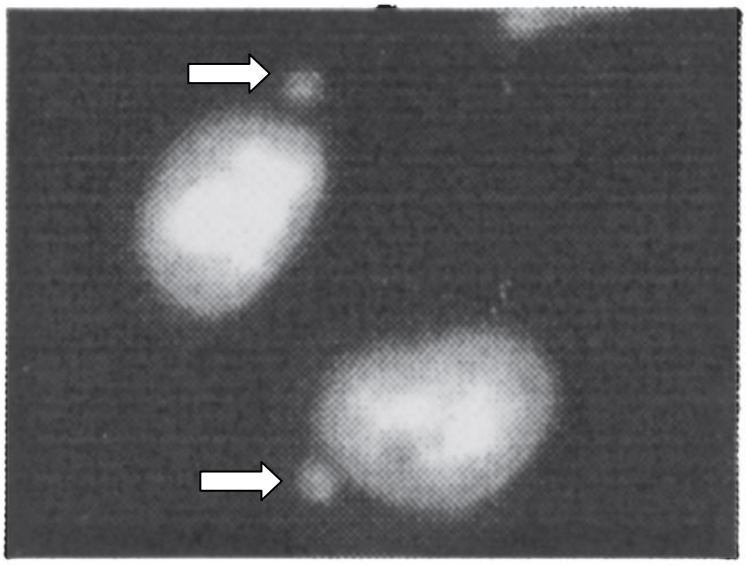

Figure 2.1: Micronuclei formation (shown by arrows) in CHO-K1 cells when exposed to a positive control (Ethyl Methane Sulfonate) (Reproduced from Ref. [17])

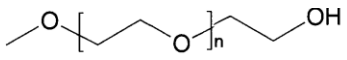

a) mPEG-OH

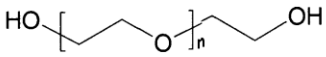

b) HO-PEG-OH

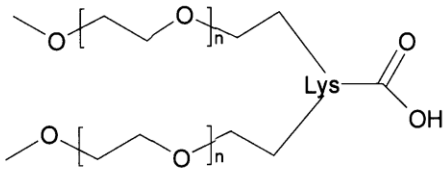

c) mPEG2-COOH

Figure 2.2: Various PEG structures: a) linear monomethoxy PEG, b) linear diol PEG, and c) branched PEG (Reproduced from ref. 50,51)

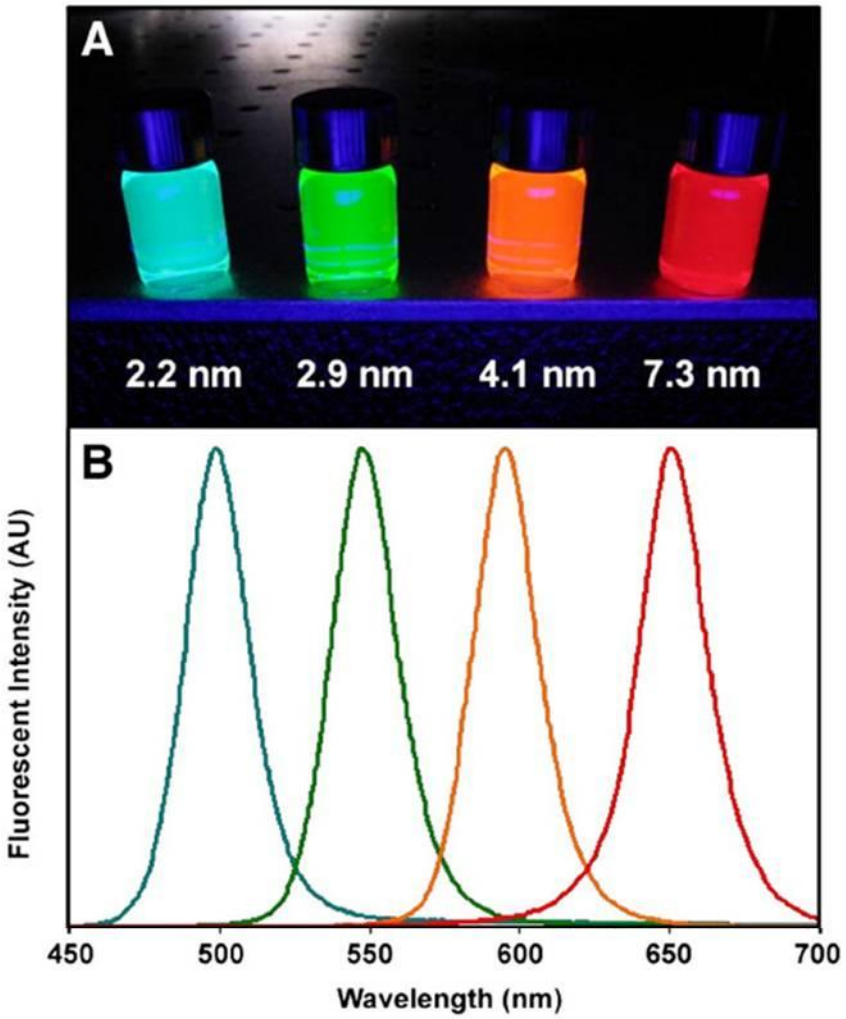

Figure 2.3: Cdse quantum dots dispersed in chloroform having different properties based on their size. (A) Fluorescence of quantum dots with diameter of 2.2n, 2.9 nm, 4.1nm and 7.3nm in four vials. (B) Spectra of fluorescence for the four vials (Reproduced from Ref. [68]) .

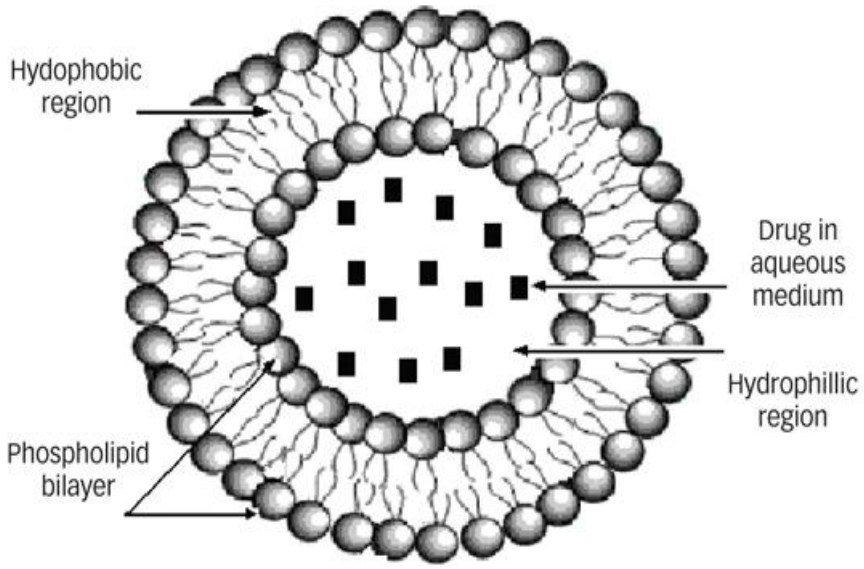

Figure 2.4: Basic structure of a liposome. It consists of a phospholipid bilayer shell which is hydrophobic and an aqueous core which is hydrophilic in nature. (Reproduced from Ref. [80])

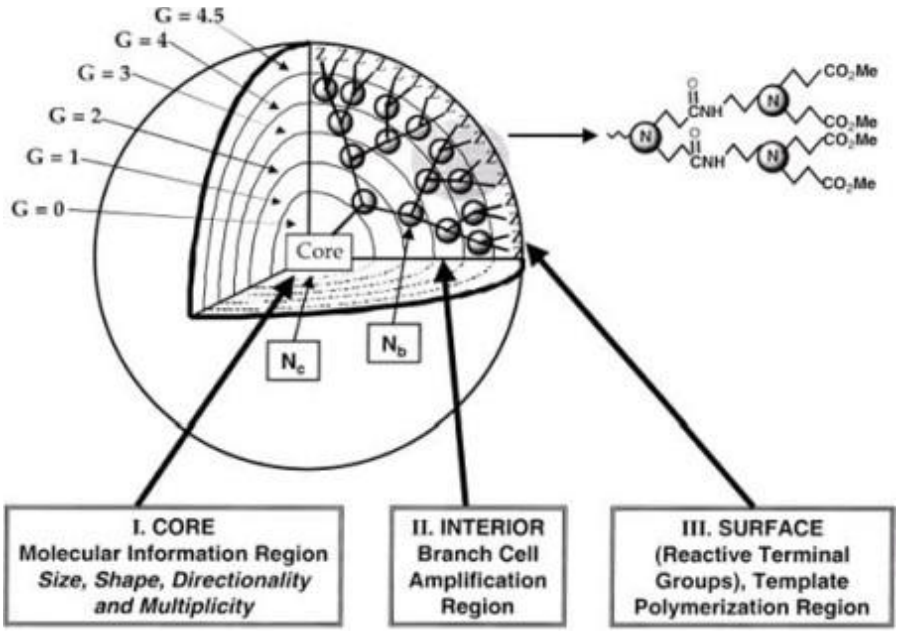

Figure 2.5: A three dimensional structure of dendrimer consisting of an Initiator core, Internal layers (generations) and external surface with functional groups. (Reproduced from Ref. [99])

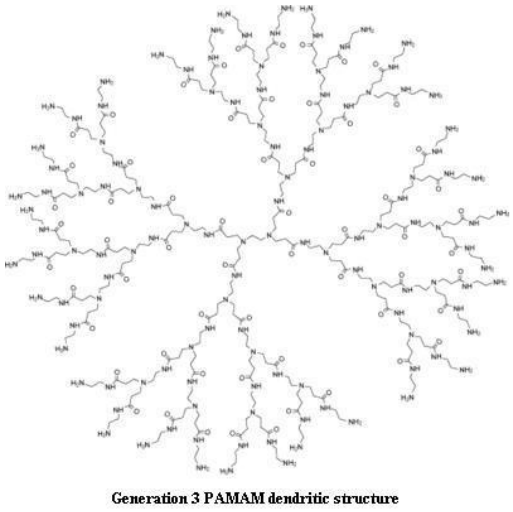

Figure 2.6: Structure of a generation 3 PAMAM dendrimer. Reproduced from Ref. [104])

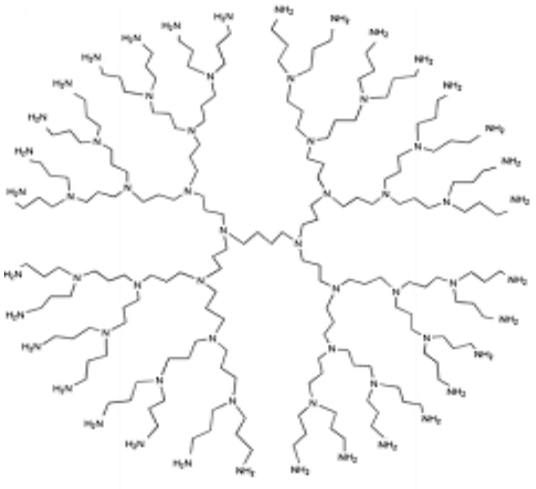

Figure 2.7: Structure of a 4th generation PPi dendrimer. (Reproduced from Ref. [114])

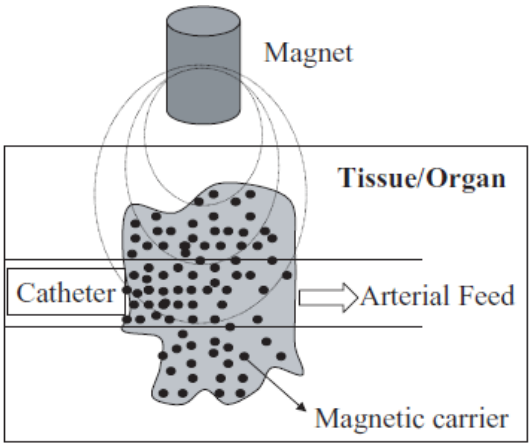

Figure 2.8: Schematic representation of drug delivery to a specific site using a magnet. A catheter is inserted into an arterial feed to the tumour and a magnetic stand is positioned over the targeted site. (Reproduced from Ref. [122])

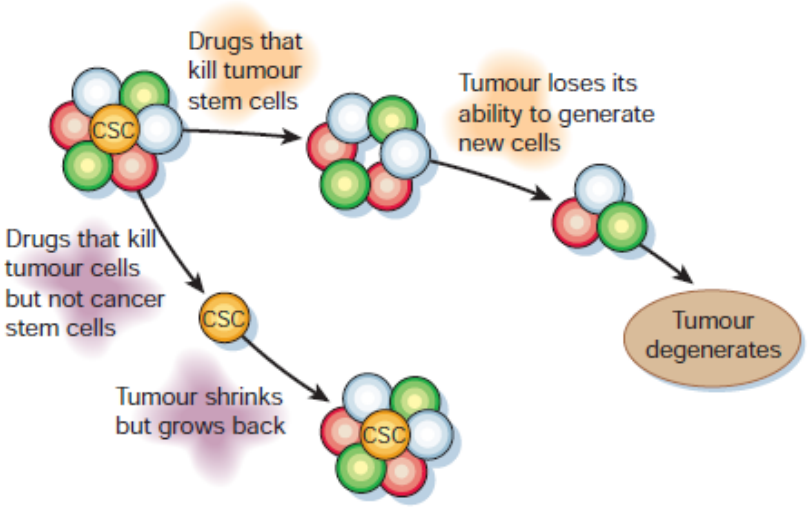

Figure 2.9: Conventional therapy may kill most of the cells in the tumor mass mass but the CSCs are not affected. As a result, CSC gives rise to the heterogenous tumor and causes a relapse. Targeting cancer stem cells directly can kill them effectively rendering the rest of the tumor unable to maintain or grow eventually leading to a cure. (Reproduced from Ref. [143])

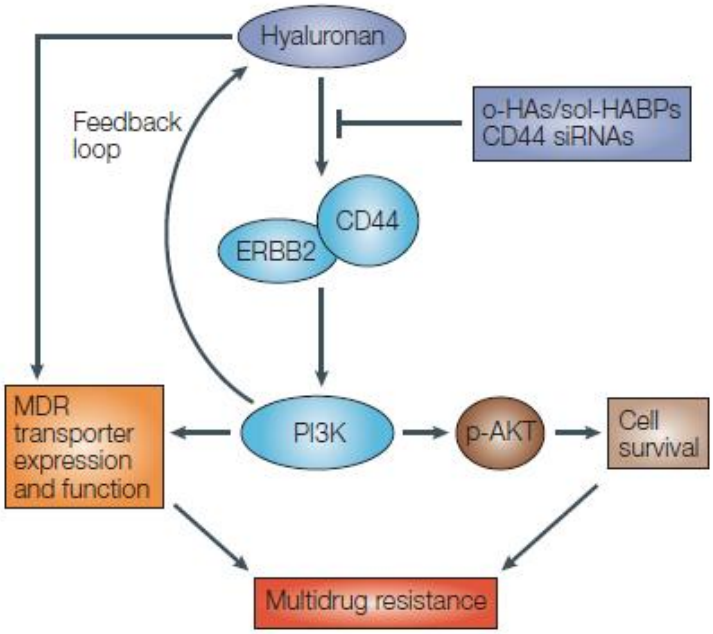

Figure 2.10: CD44 interaction with HA and ERBB2 regulate phosphatidylinositol 3-kinase (PI3K) activity. PI3K signaling is responsible for regulating multidrug resistance (MDR) transporter expression and function. It also phosphorylates AKT to p-AKT thus activating cell-survival signaling. (Reproduced from Ref. [170])

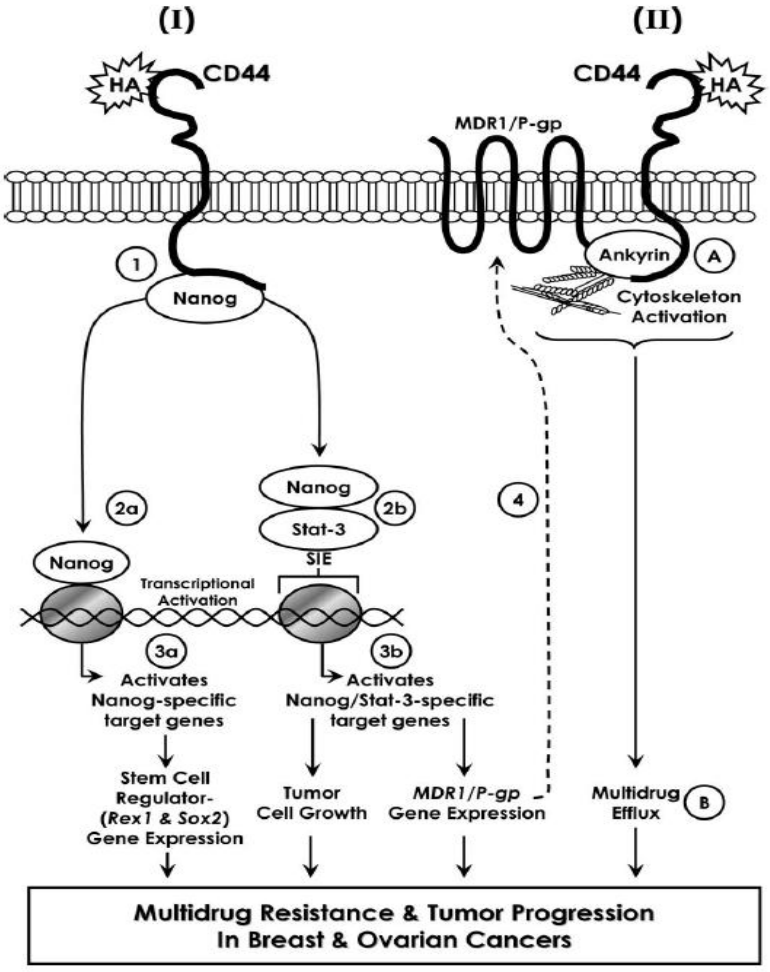

Figure 2.11: CD44 binding with HA enhances the CD44-Nanog binding which increases the transcription activation (step 2a) and expression of its target gene- Rex1 and Sox2. Nanog also complexes with Stat-3 and induces Stat-3-specific transcriptional activation (step 2b) increasing tumor cell growth and MDR-1 gene expression (step 3b) and localization at the plasma membrane (step 4). CD44-HA binding promotes ankyrin-MDR1 (P-gp) association (Step A) which increases the efflux of chemotherapeutic drugs (step B). (Reproduced from Ref. [198])

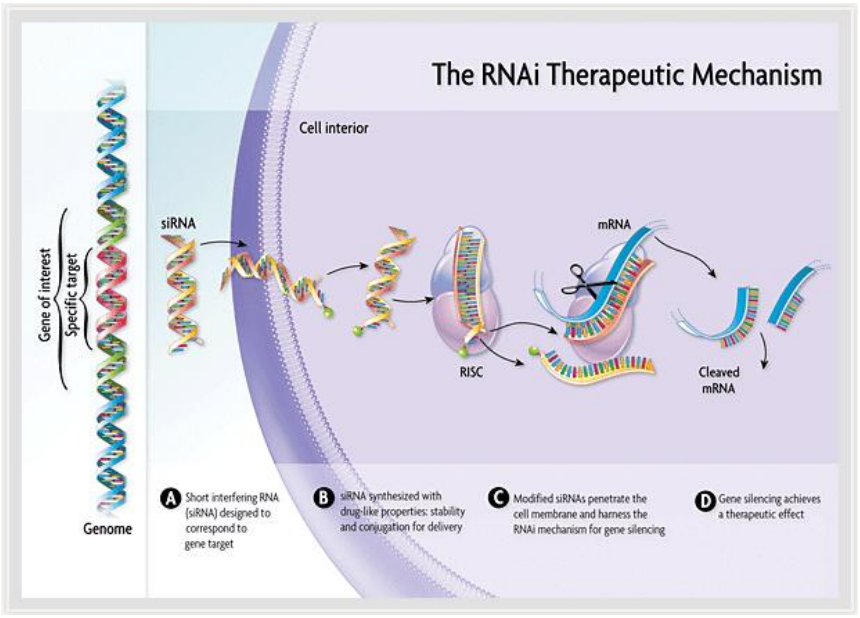

Figure 2.12: A long double-stranded RNA (dsRNA) is cleaved by by the Dicer enzyme into siRNA. The siRNA is incorporated into Argonaute 2 (AGO2) -RNAi-induced silencing complex (RISC). AGO2 cleaves the sense strand and the antisense strand guides the complex to the target mRNA which is cleaved by the catalytic domain of AGO2 and degraded. (Reproduced from Ref. [208])

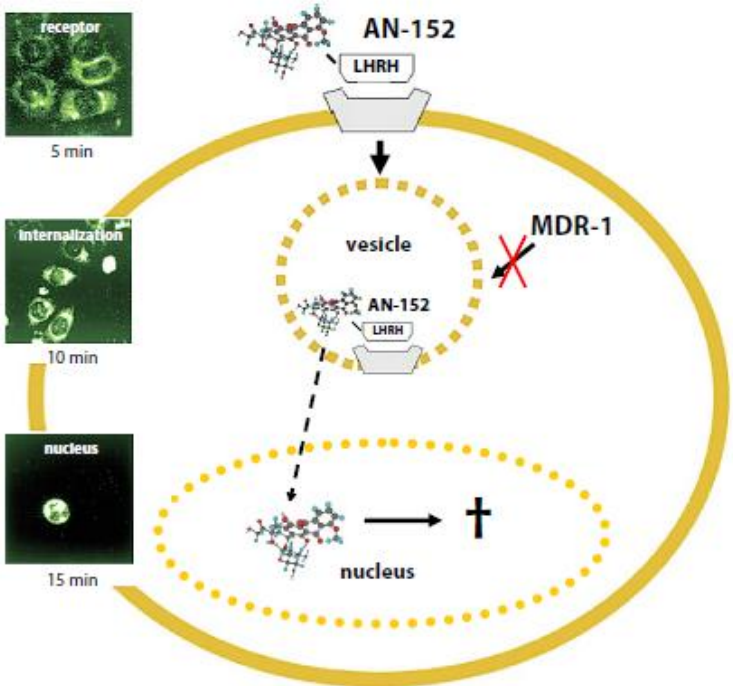

Figure 2.13: Internalization of doxorubicin attached to LHRH peptide by receptor-mediated endocytosis. Once inside the cells, free doxorubicin is released and accumulated in the nucleus where it induces apoptosis. (Reproduced from Ref. [225])

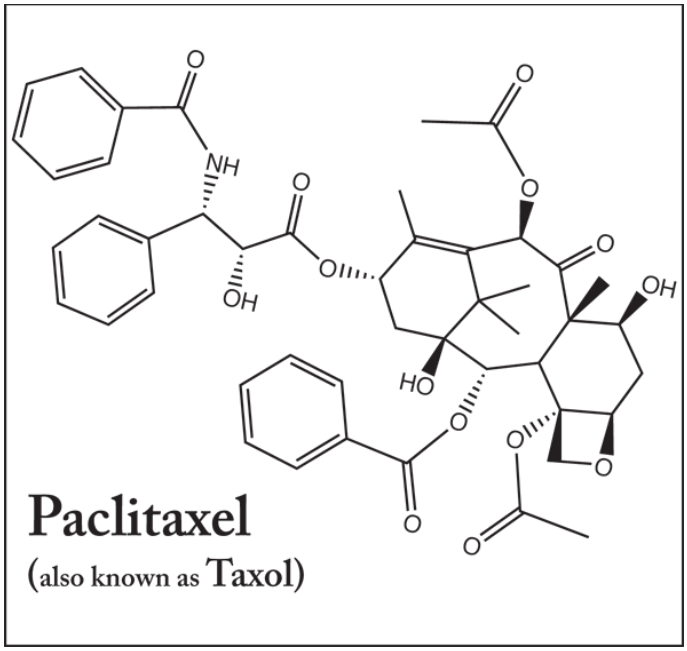

Figure 2.14: The chemical structure of Paclitaxel. (Reproduced from Ref. [228])

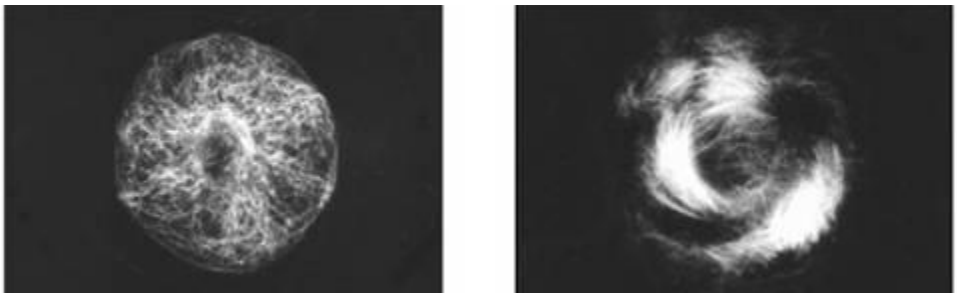

Figure 2.15: Mitotic spindles in a normal cell (left) vs cells treated with Paclitaxel (right). Cells treated with Paclitaxel exhibit malformed mitotic spindle which causes cell arrest and eventually cell death. (Reproduced from Ref. [229])

3 SPECIFIC AIMS

Specific Aim 1: To evaluate the cytotoxicity and genotoxicity of nanocarriers used in cancer drug delivery and propose modifications to limit the adverse effects.

Concerns regarding the health and safety of nanocarriers used in various fields have been continuously growing. The Royal Society and Royal Academy of Engineering reported that there is a lack of information on how nanoparticles affect human health in 2004 (7). This resulted in the evolution of one of the novel branches for the evaluation of impact nanocarriers have on human health: Nanogenotoxicology (8-12). Nanogenotoxicology is the analysis of the ability of the nanoparticles to induce DNA damage. Many studies have reported the cytotoxicity of various nanocarriers used in cancer treatment but studies reporting genotoxicity are rare (8, 9, 11). Thus it is vital to recognize nanoparticles that have the ability to impart genotoxicity. It has been found that even non-cytotoxic concentrations can induce genotoxicity. This can be of great concern when DNA of healthy cells can be damaged when subjected to non-cytotoxic concentration of nanocarriers. Hence it is of great importance to identify such nanocarriers for genotoxicity using tests like micronuclei test. Micronuclei test detects the formation of small membrane bound DNA fragments (micronuclei) induced by certain compounds. The number of micronuclei produced can be analyzed to conclude whether a nanocarrier is genotoxic. This study will evaluate various nanocarriers with different composition, size, molecular weight and electric charge for cytotoxicity and

genotoxicity. If a nanocarrier is found to be genotoxic, we also plan to modify such nanocarriers to reduce or completely eliminate their genotoxic potential.

Specific Aim 2: To evaluate the cytotoxicity and genotoxicity of various raw materials used in the cosmetic industry.

With the emergence of the 7th amendment to the EU Directive, the cosmetic and personal care industry is banned from experimenting on animals. It is therefore utilizing, studying, and validating a variety of *in vitro* and *ex vivo* protocols. One of the more important end points in the evaluation of safety is the potential of a compound to become genotoxic. While the cosmetic industry is known to produce relatively safe products, with the 7th amendment the perspective of safety has been broadened from acute, clearly perceivable, adverse effects such as irritation to the inclusion of the evaluation of long-term accumulating effects that can lead to a variety of chronic and deadly diseases such as inflammation and cancer. Moreover, the focus on *in vitro* methodologies is expanding our knowledge in understanding biochemical pathways rather than focusing on clinical evaluation. Consequently, the cosmetic product manufacturers are focusing on *in vitro* studies to ensure safety and on studying their effects. Compounds that can change the genetic information of a living cell may lead to mutations. These can result in different type of toxic effects, ranging from cell death to the development of malignant tumors. While a variety of assays are currently in use in the area of regulatory genotoxicity, substantial *in vivo* testing is still required for the confirmation of genotoxic predictions. A mutagenic (from Latin word for *change*)

compound can change the genetic information of the cell and thus increase the frequency of mutations. The term “genotoxicity” is used broadly and refers to potentially harmful effects on genetic material that are not necessarily associated with mutagenicity. The purpose of this study was to evaluate the cytotoxicity and genotoxicity of optical brightener and hydrophilic poly with different preservatives that are commonly utilized in cosmetic industry.

Specific Aim 3: Targeted Nanomedicine for Simultaneous Suppression of CD44 Protein and Cell Death Induction

The CD44 antigen, a cell-surface glycoprotein involved in cell-cell interactions, cell adhesion and migration, is considered as a major cell surface marker for cancer stem cells (CSC). It is generally believed that the overexpression of this protein results in tumor initiation, growth, development of metastases, and drug resistance. We hypothesize that simultaneous delivery of CD44 siRNA and paclitaxel will not only effectively induce cell death but also prevent tumor recurrence and metastases. We synthesized, characterized, and tested nanoscale-based drug delivery system (NDDS) containing modified Polypropylenimine (PPI) dendrimer as a carrier; anticancer drug paclitaxel as a cell death inducer; a synthetic analog of luteinizing hormone-releasing hormone (LHRH) peptide as a tumor targeting moiety, and siRNA targeted to CD44 mRNA. The proposed NDDS was tested in vitro and in vivo using metastatic cancer cells isolated from malignant intraperitoneal ascites from patients with advanced ovarian carcinoma. These cells were used to initiate subcutaneous tumor xenografts in nude

mice. We found that in contrast to cells isolated from primary tumors, CD44 was highly overexpressed in these cells. Treatment with NDDS containing siRNA targeted to CD44 mRNA, anticancer drug and tumor-specific targeting agent led to the suppression of CD44 mRNA and protein, efficient induction of cell death in CSC cells, effective tumor shrinkage and prevention of adverse side effects of the treatment on healthy organs. Therefore, we were able to verify our hypothesis and show high therapeutic potential for combinatorial treatment of ovarian carcinoma with anticancer drug and cancer stem cells suppressor.

4 EVALUATION OF THE CYTOTOXICITY AND GENOTOXICITY OF VARIOUS NANOCARRIERS

4.1 Introduction

Different nanocarriers are currently being used for the delivery of various drugs and nucleic acids. The advantages of nanocarriers as drug vehicles include but are not limited to improving solubility and stability of the delivered agents as well as enhancing their uptake by targeted cells. A rapid expansion of nanotechnology raises several environmental, health, and safety issues that should be understood, investigated, and regulated (234, 235). The study of possible threats of nanocarriers led to the emergence of two novel branches of bionanoscience: nanotoxicology and most recently nanogenotoxicology (8, 12, 236, 237). Nanotoxicology studies mechanisms of cytotoxicity of nanomaterials while nanogenotoxicology is focused on analyzing the potential of engineered nanomaterials on damaging DNA. While cytotoxicity of nanocarriers is relatively widely analyzed for different nanomaterials, genotoxicity of nanocarriers were investigated only in limited number of recent publications (8, 13-16, 236-240). Meanwhile, genotoxicity of drug carriers should be avoided especially for prolonged chronic treatment. If nanocarriers are used for the delivery of cytotoxic drugs (e.g. for chemotherapy of cancer) and are delivered specifically for the targeted site of action (e.g. tumor), then their own cyto- and genotoxicity is less important when compared with other factors (delivery efficiency, profile of drug release, cost, etc.).

However, when the carriers are used for the delivery of non-cytotoxic agents and may be accumulated in healthy tissues, then it is critically important to prevent cytotoxicity of nanocarriers and their adverse genetic effects.

Genotoxicity can be determined by many different tests. One of the tests is micronuclei test. Micronuclei test detects the formation of small membrane bound DNA fragments (micronuclei) induced by chemicals. Damage by certain chemicals lead to the formation of acentric fragments (chromosome fragments lacking a centromere) and prevent these acentric fragments or whole chromosomes to migrate with other chromosomes during the anaphase of cell division. A nuclear envelope then forms around these fragments and whole chromosomes during the telophase. This process imparts the unmigrated fragments or whole chromosomes the morphology of a nucleus. However the newly formed nucleus is smaller than the main nucleus and hence it is known as "micronucleus" (40). Aneugenic (compounds that induce loss or gain of whole chromosomes) as well as clastogenic damage (compound that cause disruption or breakages of chromosomes) (41, 42) can be detected by the micronucleus test in the cells that have experienced cell division after the exposure to a genotoxic compound.

In the present study, we selected one representative nanocarrier from the most widely used types of drugs and nucleic acid delivery vehicles and analyzed nanoparticles with different composition, size, molecular weight, and electrical charge: (1) supermagnetic iron oxide (SPIO) nanoparticles; (2) – 2, 10 and 20 kDa poly(ethylene glycol) (PEG)

polymer; (3) – quantum dots (QD); (4) – poly(propyleneimine) (PPI) dendrimers and poly(amido amine) (PAMAM) dendrimers; (5) – polymeric micelles; (6) – "neutral" liposomes (120 nm and 600 nm); (7) – cationic liposomes; and (8) – mesoporous silica (MS) nanoparticles. The size of studied nanocarriers varied from 10 to 600 nm while surface charge values covered a region from -10 to +90 mV. Here we tried to answer two questions. First, which type of nanoparticles can cause genetic aberrations under non-cytotoxic concentrations by inducing the formation of micronuclei during cell division? Second, how one can limit genotoxicity of nanocarriers by their modifications suitable for the delivery of siRNA? Consequently, the present study was aimed at evaluating and comparing the genotoxicity of different nanocarriers and developing possible modifications of genotoxic nanoparticles in order to limit their adverse effects on DNA and to use for intracellular delivery of siRNA.

4.2 Materials and Methods

4.2.1 Materials

Chinese Hamster Ovary (CHO-K1) cells were employed in all *in vitro* experiments. The cells were purchased from the American Type Culture Collection (ATCC, Manassas, VA 20108) and cultured in F-12K medium supplemented with 10% fetal bovine serum (Invitrogen, Carlsbad, CA) and penicillin-streptomycin (100 UI/ml-100ug/ml, Sigma, St. Louis, Mo). Poly(ethylene glycol) (PEG) polymer, neutral and cationic liposomes, polymeric micelles, poly(amido amine) (PAMAM) and poly(propyleneimine) (PPI) dendrimers, quantum dots (QD), mesoporous silica (MS) and supermagnetic iron oxide (SPIO) nanoparticles were investigated. PEG polymers (2, 10 and 20 kDa) were

purchased from Rapp Polymere GmbH (Tubingen, Germany). Carboxyl terminated Quantum Dots (QD-COOH) with an emission peak at 490 nm were purchased from eBioscience, Inc. (San Diego, CA). The chemicals for positive controls were purchased from Sigma Chemical Co. (St. Louis, MO). These include cyclophosphamide (CAS no. 50-18-0), ethyl methanesulfonate (CAS no. 62-50-0) and dimethyl sulfoxide (DMSO). Nicotinamide adenine dinucleotide phosphate (NADP) was purchased from Fisher Scientific Co (Suwannee, GA). Sodium phosphate buffer was obtained from Moltox (Boone, NC). Glucose 6 phosphate and Tween 20 were received from Sigma Aldrich (St Louis, MO), 4', 6- diamidino-2-phenylindole dihydrochloride (DAPI) (Sigma, St.Louise. MO).

4.2.2 Synthesis of the nanocarriers

Liposomes were prepared as previously described (13, 241). Briefly, neutral PEGylated liposomes were formulated from egg phosphatidylcholine: cholesterol:1,2,-distearoyl-sn-glycero-3-phosphoethanolamine-N-aminopolyethelenglycol (DSPE-PEG) in mole ratio 51:44:5, respectively, using the ethanol injection method with final concentration 10 mM. Cationic liposomes were prepared from positively charged dioleoyl-2-trimethylammonium propane (DOTAP, Avanti Polar Lipids, Alabaster, AL) in concentration 10 mM. DSPE-PEG 2000 micelles were prepared as previously described (242). Briefly, DSPE-PEG powder was dissolved in tert-butanol, lyophilized overnight followed by rehydration in 0.9% NaCl to a final concentration above the lipopolymer critical micelle concentration (10 mM). PAMAM generation 4.0 (ethylenediamine core) and PPI tetrahexacontaamine generation 5 dendrimers were obtained from Sigma-

Aldrich (Milwaukee, WI). Amine terminated quantum dots were prepared as previously described (77). Mobile Crystaline Material-41 (MCM-41) type MS nanoparticles were synthesized using a surfactant-templated, base-catalyzed condensation method as previously reported [19]. SPIO nanoparticles were synthesized as previously described (243). Briefly, iron oxide nanocrystals of 5 nm in diameter were synthesized in organic solvents at high temperature. For solubilization of iron oxide nanoparticles in water, micelles were formed with amphiphilic polymers by transferring iron oxide nanocrystals from organic solvents into water.

4.2.3 Imaging, particle size and zeta potential of nanocarriers

The samples of nanocarriers were imaged with a tapping mode atomic force microscope (Nanoscope III A, Veeco Digital Instruments, Chadds Ford, PA) as previously described (244). Breifly, a , a 125 µm long rectangular silicon cantilever/tip assembly with a spring constant of 40 N/m,resonance frequency of 315-352 kHz, and tip radius of 5-10 nm was used. The images were generated by the change in amplitude of the free oscillation of the cantilever as it interacts with the sample. The height differences on the surface are indicated by the color code: lighter regions indicate higher heights. Particle size was measured by dynamic light scattering using 90 Plus Particle Sizer Analyzer (Brookhaven Instruments Corp., New York, NY). To characterize a surface charge of nanoparticles, zeta potential was measured on PALS Zeta Potential Analyzer (Brookhaven Instruments Corp., Holtsville, NY).

4.2.4 Preparation of chemicals for micronuclei test

Ethyl methanesulfonate (EMS) was used as a positive control to analyze the formation of micronuclei. An amount of 0.1 ml of EMS (density 1.15 g/ cm^3) was diluted to 1.0 ml with dimethyl sulfoxide (DMSO). A measured 10.5 μl of this solution was added to a 3 ml of media to give a final concentration of 400 μg/ml in each well (245).

The stock solution for cell staining was prepared as previously described (17). Briefly, 5 mg of DAPI were dissolved in 1 ml dimethylformamide and allowed to stand until the dissolution was complete. For the working solution, 4 μl of the stock solution were added to 50 ml of phosphate buffer solution (PBS) and stored at 4^0 C protected from light before the use.

Inclusion of a metabolic activation system in the genotoxicity assay enables the detection of mutagenic activity for carcinogens and/or mutagens which require such metabolic activation (*i.e.* cyclophosphamide). The metabolic activation system was prepared according to the previously described procedure (246). Aroclor-1254 induced rat liver S9 fraction was purchased from Moltox (Boone, NC). The following chemicals were added in the order listed to get a total volume of 3 ml of S9 mix: sterile double distilled H_2O (840 μl), 0.1 M sodium phosphate buffer, pH 7.4 (1.5 ml**),** 4 mM NADP (150 μl), 120 mM glucose-6-phosphate (22 μl), 8 mM/33 mM potassium/magnesium salt solution (60 μl), rat liver fraction 300 μl to give a final concentration of 10 % (v/v). The final concentration of the metabolic activator used for each well was 1% (v/v). EMS does

not require metabolic activation and therefore the metabolic activation system was not used in the experiments involving EMS.

4.2.5 Cell Line

Chinese Hamster Ovary (CHO-K1) cells were used as recommended in the OECD protocol (39). Cells were cultured in ATCC-formulated F-12K medium supplemented with 10% fetal bovine serum (Fisher Chemicals, Fairlawn, NJ) and penicillin-streptomycin (100 UI/ml,100ug/ml). Cells were grown at 37°C in a humidified atmosphere of 5% CO2 (v/v) in air. All experiments were performed on cells in the exponential growth phase.

4.2.6 Cell viability

A modified MTT (3-(4, 5-dimethylthiazol-2-yl)-2, 5-diphenyltetrazolium bromide) assay was used to assess the cytotoxicity of the studied substances as previously described (247). To measure cytotoxicity, cells were separately incubated in a 96-well microtiter plate with different concentrations of each studied substance. Control cells received an equivalent volume of fresh medium. The duration of incubation was 24 h. On the basis of these measurements, cellular viability and was calculated for each substance. A decrease in the cellular viability and decrease in the IC_{50} dose indicated an increase in toxicity.

4.2.7 Micronuclei test

Genotoxicity of the studied carriers were evaluated using the *in vitro* micronucleus assay on CHO-K1 cells as previously described (17). Briefly, about 300,000 cells were cultured with the media in 25 cm^2 flasks and held 24 hours before treatment. They were then

incubated with tested nanocarriers for 24 h using non toxic concentrations determined by the cellular viability assay. Negative control cells were incubated with fresh media, while positive control cells were treated with ethyl methane sulfonate (400 µg/ml). . For the series with metabolic activation, the cells were treated for 3 hours after which the media was replaced with fresh media and the cells were incubated for additional 21 hours. For the series without S9 activation, the cells were incubated for 24 hours. The methanol was removed and the cells were washed with phosphate buffer and the cells' nuclei were then stained with 600 nM of 4, 6 diamidino-2-phenylindole (DAPI) for 8 minutes. This solution was removed and all the flasks were washed with PBS containing 0.05 % Tween 20 (Sigma Aldrich, St Louis, MO). After staining, the formation of micronuclei was detected by a fluorescent microscope (Olympus, New York, NY) and documented by counting the number of micronuclei per 1000 cells.

4.2.8 Cellular internalization

Cellular internalization of 6-FAM labeled siRNA-nanoparticle complexes was analyzed by laser scanning spectral confocal (Leica Microsystems Inc., Bannockburn, IL) microscopes. Prior the visualization cells were plated (20,000 cells/well) in 6-well tissue culture plates and treated with analyzed drug carrier-siRNA complexes for 24 h. The concentration of siRNA was 0.25 µM. After 24 h of treatment, cells were washed three times with DPBS, 1 mL of fresh medium was added to each well and photographed by a confocal microscope.

4.2.9 Statistical analysis

Statistical analysis was performed as a one-way analysis of variants (ANOVA) and comparisons among groups were performed by independent sample *t*-tests. The results are expressed as mean value ± SD. The difference between variants was considered significant if $P<0.05$.

4.3 Results

4.3.1 Cytotoxicty of different nanocarriers

Cytotoxicity of all studied nanocarriers was studied. It was found that QD, PEG polymers (2, 10 and 20 kDa) and "neutral" liposomes (120 and 600 nm) were not toxic at all available concentrations. PPI dendrimers at highest available concentrations demonstrated low cytotoxicity (cellular viability was 30% lower when compared with the control level). In contrast, MS nanoparticles, PAMAM dendrimers and SPIO nanoparticles showed substantial cytotoxicity when their concentrations exceeded 0.1 mg/mL, 0.8 mg/mL and 80 μg/mL, respectively. Based on these measurements, maximal non-toxic concentrations of each nanocarrier were selected for the further studies. These working concentrations were equal to: 0.078 mg/mL (PEG Polymers), 2.50 mM ("neutral" liposomes), 0.117 mM (cationic liposomes), 0.0195 mM (polymeric micelles), 0.391 μg/mL (PAMAM dendrimer), 0.0978 μM (PPI dendrimer), 7.03 nM (QD), 3.91 μg/mL (MS nanoparticles), and 1.526 μg/mL (SPIO nanoparticles).

4.3.2 Imaging of nanocarriers by Atomic Force Microscopy (AFM)

All used carriers were characterized by atomic force microscope imaging and measurements of their size and surface charge. Atomic force microscope analysis showed that all studied vehicles formed well-defined nanoparticle-like structures (**Fig. 4.1**). These results allowed us to designate all studied carriers as true compact "particles." The measurements of particle size showed that the size of the particles varied from 10 to 600 nm (**Fig. 4.2**). Therefore, carriers employed covered almost the entire range of carrier sizes designated for nanocarriers. Consequently, carriers used can be referred as "nanoparticles".

4.3.3 Zeta potential of nanocarriers

Zeta potential of all nanocarriers is presented in **Fig. 4.3**. It ranged from approximately -10 mV for micelles and "neutral" liposomes to more than + 90 mV for SPIO nanoparticles. Therefore, these parameters of the selected nanocarriers covered almost entire region of nanocarrier charges that are currently used in nanomedicine for intracellular delivery of drugs, siRNA and other bioactive materials or are employed for bioimaging.

4.3.4 Genotoxicity of nanocarriers

Representative images of stained cells incubated with different nanocarriers and corresponding negative and positive controls are shown in Fig. 4. Quantitative analysis of genotoxicity is presented in **Fig. 4.4**. It was found that PEG polymer, QD, "neutral"

liposomes, MS nanoparticles, and micelles in non-cytotoxic concentrations did not induce measurable genotoxic effects in terms of formation of micronuclei (please see Fig. 4.4, images 3-7 and Fig. 4.5, bars 3-10). In contrast, cationic liposomes, PAMAM and PPI dendrimers, and SPIO nanoparticles significantly increased the formation of micronuclei in tested cells (please see Fig. 4.4, images 8, 9, 11, 13 and Fig. 4.5, bars 11, 12, 14, 16).

In order to decrease genotoxicity of nanocarriers, we performed the following modifications. PAMAM dendrimers were internally quaternized and surface acetylated as previously described [22]. The modified dendrimers also did not demonstrate any signs of cytotoxicity for all available concentrations. Analysis of genotoxicity showed that the modification of PAMAM dendrimers prevented not only cytotoxic effects but also limited the formation of micronuclei (please compare images 9 and 10 in Fig. 4.4 and bars 12 and 13 in Fig. 4.5). For the purpose of decreasing genotoxicity of PPI dendrimers and use them for the delivery of nucleic acids, PPI dendrimers were condensed with siRNA and the formed siRNA nanoparticles were caged with a dithiol containing cross-linker molecules followed by coating them with PEG polymer as described [32]. As can be seen from the present experimental data, the modification substantially limited genotoxicity of the carriers. In fact, such modification almost completely prevented the formation of micronuclei during the incubation with cells (please compare images 11 and 12 in Fig. 4.4 and bars 14 and 15 in Fig. 4.5). To decrease the toxicity of SPIO nanoparticles and make them suitable for siRNA delivery, the following approach was used. Complexes were formed by cooperative condensation of

siRNA with 5 nm SPIO nanoparticles and PPI generation 5 dendrimers, then the resulted complexes were coated with PEG polymer as previously described [20]. Experimental data obtained show that the modification also significantly limited genotoxicity of nanoparticles preventing the formation of micronuclei in the cells (please compare images 13 and 14 in Fig. 4.4 and bars 16 and 17 in Fig.4.5).

4.3.5 Correlation between surface charge and genotoxicity

To reveal an influence of surface charge on genotoxicity of nanoparticles, we analyzed the correlation between zeta potential of nanocarriers and their genotoxicity (Fig. 4.6). It was found that negatively charged and neutral nanocarriers did not induce the formation of additional micronuclei when compared with spontaneous micronucleus formation in control (cells incubated with media). A strong positive linear correlation (r = 0.987) was found between the value of zeta potential and genotoxicity of positively charged nanocarriers.

4.3.6 Cellular internalization and genotoxicity

To analyze the relationship between the cellular internalization of siRNA and genotoxicity of nanocarriers, we studied the internalization of fluorescently labeled siRNA delivered by nanocarriers with different genotoxicity: mesoporous silica nanoparticles, cationic liposomes, modified poly(amido amine) and poly(propyleneimine) dendrimers (Fig. 4.7). It was found that all studied nanocarrier-siRNA complexes successfully penetrated the cells and siRNA was efficiently released from the complexes into the cellular cytoplasm. We did not found substantial

differences between all studied nanocarriers with different genotoxicity in the efficiency of siRNA delivery inside the cells.

4.4 Discussion

Our ultimate goal was to select a single representative of each of the most frequently used classes of nanocarriers in order to cover a wide range of sizes, molecular weights, compositions, and electrical charges. Such a selection is based upon the following considerations. First, we tried to select a typical representative from each of nanocarriers that have been developed, well characterized, and widely used in various nanomedical applications. Secondly, we intended to cover a wide range of carrier composition, architecture, size, and electrical charge. Consequently, the following nanocarriers have been selected for the analysis: supermagnetic iron oxide nanoparticles, poly(ethylene glycol) polymers with different molecular weight, quantum dots, poly(propyleneimine) and poly(amido amine) dendrimers, polymeric micelles, “neutral” and cationic liposomes, and mesoporous silica nanoparticles. Such a selection allowed us to analyze the influence of architecture, molecular weight, size, and surface charge on genotoxicity of nanocarriers. It is understandable that in most cases nanocarriers are used in concentrations that do not induce significant cytotoxic effects *in vitro* or in doses that do not exceed the maximal tolerated doses *in vivo*. It is generally assumed that such concentrations are safe and will not induce severe side effects, including undesirable genotoxic effects. We also used all nanocarriers in concentrations that did not induce substantial cell death *in vitro*. The viability of cells incubated with working concentrations of nanoparticles employed in the present study was 90% or

higher when compared with untreated cells incubated with fresh media. However, some nanocarriers demonstrated marked genotoxicity even under non-toxic concentrations. We found that PEG polymer, QD, “neutral” liposomes, MS nanoparticles, and micelles did not demonstrate signs of genotoxicity in non-cytotoxic concentrations. In contrast, cationic liposomes, PAMAM and PPI dendrimers, and SPIO nanoparticles being applied in non-cytotoxic concentrations did induce micronuclei formation in tested cells. These results are in good agreement with the literature data reporting that different dendrimers can induce not only cell death but also moderate genotoxic effects (238). Genotoxicity of iron oxide nanoparticles has also been recently reported (240). However, it should be stressed that in the available literature we did not find a comparison of different nanocarriers in terms of their genotoxicity analyzed in the similar conditions in one experimental study. In this sense, the present work fills the gap and allows us to select genotoxic carriers for further modifications.

PAMAM dendrimers were modified in order to eliminate surface charges and protect siRNA conjugated with dendrimers from the harsh action of the environment during its voyage in the blood stream towards the targets (244). This modification included acetylation of surface branches and internal quaternization. The modified dendrimers have neutral surfaces and cationic charges inside the dendrimers (not on the outer surface). Our previous data showed that these modified dendrimers formed well-condensed, spherical particles (polyplexes) with siRNA, protected nucleic acids from degradation, and provided their effective cellular internalization (244). In summary, the proposed modification of PAMAM dendrimers decreased their surface charges creating

internal sites with positive charges for conjugation with negatively charged siRNA molecules. Consequently, one or several dendrimers can cover a siRNA molecule forming well-defined spherical nanocomplexes and protecting the payload from the degradation during the journey in the systemic circulation to the site of the action. We found (244) that such complexes efficiently penetrate inside the cells and release siRNA in the cytoplasm probably as a result of pH decreasing and braking the electrostatic bonds between the dendrimers and nucleic acids. In contrast, the conjugation of siRNA with externally charged dendrimers led to the formation of nanotubes that were unable to efficiently deliver siRNA inside the cells. Present experimental data also show that such a modification substantially limits the genotoxicity of these types of dendrimers.

PPI dendrimers were condensed with siRNA and the formed siRNA nanoparticles were caged with a dithiol containing cross-linker molecule followed by coating them with PEG polymer as described (248). Previously, we found that, this layer-by-layer modification of dendrimers increased the siRNA stability in plasma and intracellular bioavailability, provided for their efficient cellular uptake, accumulation of siRNA inside the cells, and efficient gene silencing (248). Present experimental data support this finding. In addition, it was found in the present experimental work, that this modification decreased genotoxicity of formed dendrimer-siRNA complexes.

The modification of SPIO nanoparticles included two steps. First, complexes were formed by cooperative condensation of siRNA with SPIO nanoparticles and PPI dendrimers. Secondly, the resulted complexes were coated with PEG polymer as

previously described (243). Previously, we found that such a modification decreased the cytotoxicity of the nanoparticles, protected the payload in the blood stream, enhanced the efficiency of cellular internalization of siRNA and increased the efficiency of targeted gene suppression (243). In addition, as was shown in the present study, these modifications of SPIO nanoparticles decreased their genotoxicity. In summary, the proposed modifications of nanoparticles eliminated their positive surface charge, allowed for stable complexes with siRNA, provided for an efficient intracellular delivery of nucleic acids, and limited cytotoxicity and genotoxicity of nanocarriers.

The exact mechanisms of genotoxic effects of nanoparticles are still unknown. One can suggest that the following factors can potentially affect genotoxicity of nanocarriers: composition, size, molecular weight, particle geometry, and surface charge. In the present study, all of these parameters varied substantially in the investigated nanoparticles. Recently, it was suggested based on the results of the comparative analysis that particle composition probably played a primary role in the cytotoxic effects of different nanoparticles while the potential genotoxicity might be mostly attributed to particle shape (16). However, based on the results obtained in the present study, it is most probable that the surface charge of nanocarriers plays a central role in genotoxic effects. Three major sets of data support this assumption. First, the degree of genotoxicity of nanocarriers does not correlate with their size or molecular weight. In fact, comparable genotoxicity was found in nanocarriers with huge differences in size (from ~20 nm in PEG polymers to ~600 nm in large “neutral” liposomes). At the same time, nanocarriers with comparable size demonstrated dramatically different

genotoxicity. For instance, PEG polymers (~20 nm), QD (~40 nm), polymeric micelles (~30 nm) did not induce genotoxicity, but SPIO nanoparticles (~10 nm), PAMAM and PPI dendrimers (~20 nm) were genotoxic; larger carriers like "neutral" liposomes (~120 nm) and MS nanoparticles (~180 nm) did not lead to the formation of micronuclei, but cationic liposomes (~190 nm) were genotoxic (Fig. 2-5). The increase in molecular weight of PEG-based nanocarriers from 2 to 20 kDa also did not influence its genotoxicity. Secondly, some nanocarriers of similar size, molecular weight, and shape possessed substantially different genotoxicity. Examples from the present study include "neutral" (non-genotoxic) and cationic (highly genotoxic) liposomes. It seems that the presence of positive charge substantially increases the genotoxicity of nanoparticles. Thirdly, modifications of nanocarriers that eliminate their surface charge (*e.g.* PAMAM, PPI dendrimers and SPIO nanoparticles) reduced their genotoxicity. A strong positive correlation between micronuclei formation and surface charge of nanoparticles revealed in the present study support this conclusion. The results also agreed with the literature data showing that toxic effects of different nanocarriers correlates with positive charge of their surface (249-252).

Theoretically, differences in the internalization of siRNA inside the cells could potentially influence genotoxicity of complexes of siRNA with nanocarriers. To examine this probability, we studied cellular internalization and release of siRNA delivered by nanocarriers with substantially different genotoxicity. We did not found substantial differences between all studied nanocarriers with different genotoxicity in the efficiency

of siRNA delivery inside the cells. Therefore, it is unlikely that genotoxicity of nanocarriers depend on efficiency of cellular internalization of the siRNA.

Additional investigations are planned in our laboratory in order to elucidate possible mechanisms of genotoxicity of nanocarriers. It should be stressed again that nanocarriers were used in the present study for the genotoxic study in non-cytotoxic concentrations that did not decrease cellular viability. However, some carriers did demonstrate substantial genotoxicity, which confirms the importance of testing genotoxicity together with cytotoxicity in order to assess the safety of nanocarriers.

4.5 Conclusions

In summary, the present experimental data clearly showed the importance of genotoxicity testing during the characterization of nanocarriers. In fact, even in non-cytotoxic concentrations, nanocarriers with positive surface charges induced formation of micronuclei after incubation with cells. Genotoxicity of nanocarriers correlated well with their surface charges. We also proposed several modifications of genotoxic dendrimers and SPIO nanoparticles in order to limit their genotoxicity. These modifications prevented the formation of micronuclei in cells incubated with nanocarriers, limited their cytotoxicity, and increased the stability and efficiency of cellular internalization of complexated siRNA, making such modified nanocarriers attractive for the delivery of nucleic acid for clinical applications.

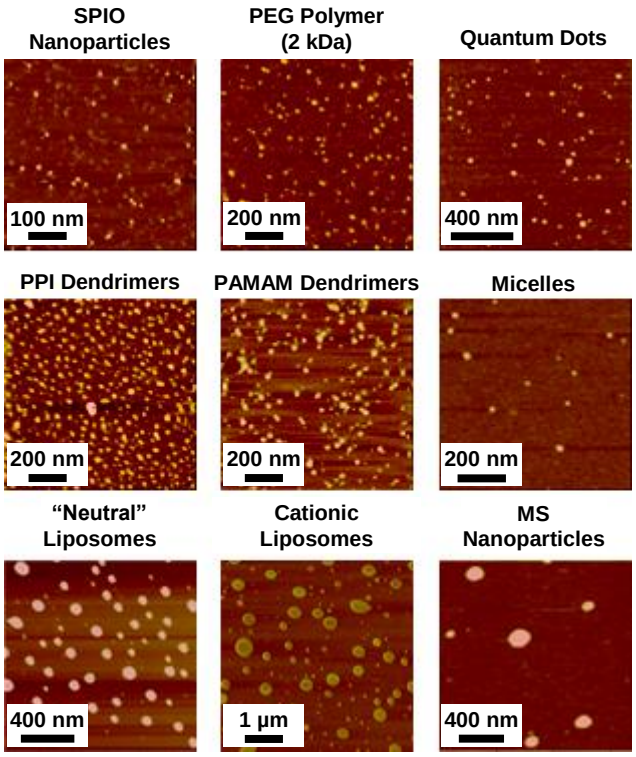

Figure 4.1: Representative atomic force microscope (AFM) images of different nanocarriers: supermagnetic iron oxide (SPIO) nanoparticles; poly(ethylene glycol) (PEG); quantum dots (QD); poly(propyleneimine) (PPI) dendrimers; poly(amido amine) (PAMAM) dendrimers; polymeric micelles; "neutral" liposomes; cationic liposomes and mesoporous silica (MS) nanoparticles.

.

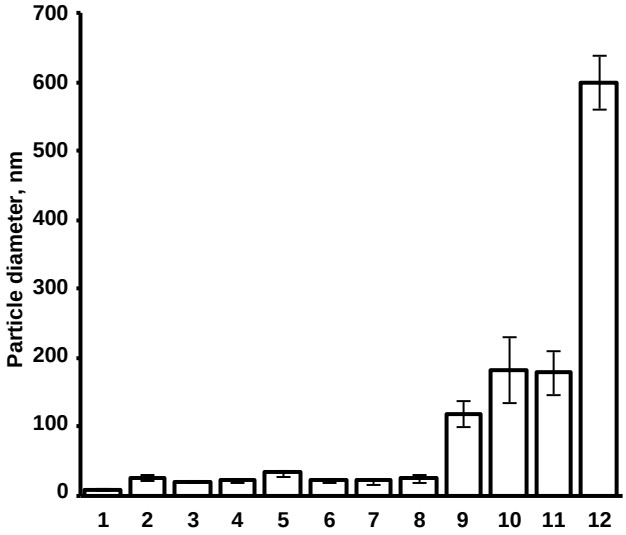

Figure 4.2: Average size of different nanocarriers: 1 – supermagnetic iron oxide (SPIO) nanoparticles; 2 – 2 kDa poly(ethylene glycol) (PEG) polymer; 3 – 10 kDa PEG polymer; 4 – 20 kDa PEG polymer; 5 – quantum dots (QD); 6 – poly(propyleneimine) (PPI) dendrimers; 7 – poly(amido amine) (PAMAM) dendrimers; 8 – polymeric micelles; 9 – "neutral" liposomes (120 nm); 10 – cationic liposomes; 11 – mesoporous silica (MS) nanoparticles; and 12 – "neutral" liposomes (600 nm). Means ± SD are shown

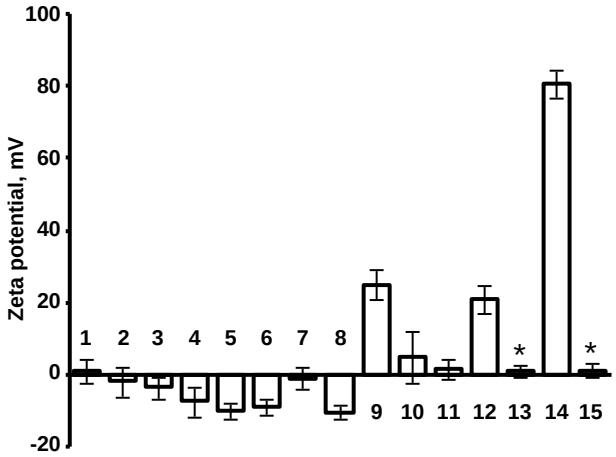

Figure 4.3: Zeta potential of different nanocarriers: 1 – 2 kDa poly(ethylene glycol) (PEG) polymer; 2 – 10 kDa PEG polymer; 3 – 20 kDa PEG polymer; 4 – quantum dots (QD); 5 – "neutral" liposomes (120 nm); 6 – "neutral" liposomes (600 nm); 7 – mesoporous silica (MS) nanoparticles; 8 – polymeric micelles; 9 – cationic liposomes; 10 – poly(amido amine) (PAMAM) dendrimers; 11 – modified PAMAM dendrimers; 12 – poly(propyleneimine) (PPI) dendrimers; 13 – modified PPI dendrimers; 14 – supermagnetic iron oxide (SPIO) nanoparticles; and 15 – modified SPIO nanoparticles. Means ± SD are shown. *P < 0.05 when compared with corresponding non-modified nanocarrier.

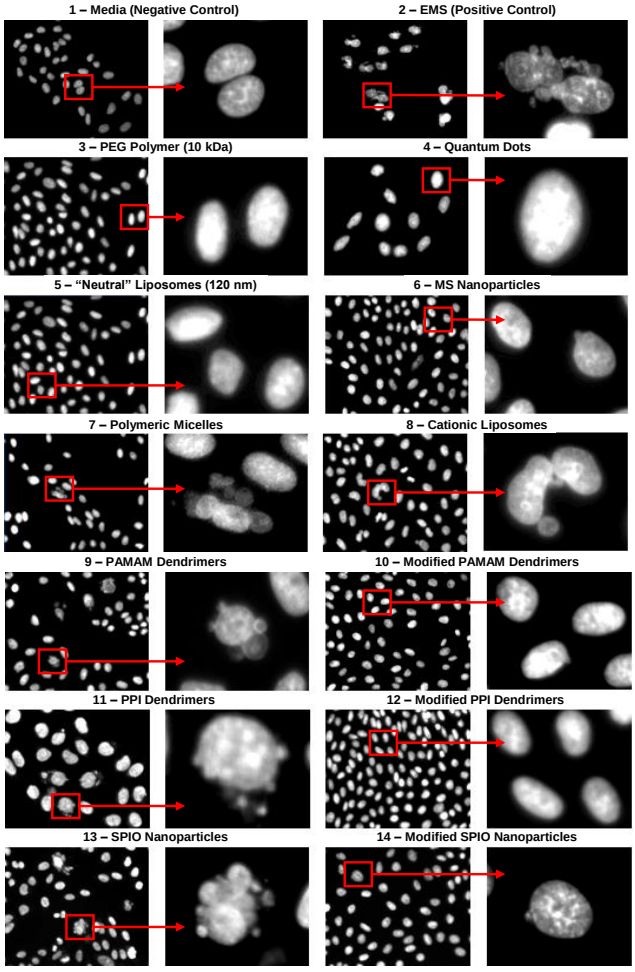

Figure 4.4: Genotoxicity (formation of micronuclei) of different nanocarriers and corresponding controls. Representative fluorescence microscopy images of CHO-K1 cells incubated within 24 hours with different substances: 1 – media (negative control); 2 – ethyl methanesulfonate (EMS, positive control); 3 – 10 kDa poly(ethylene glycol) (PEG) polymer; 4 – quantum dots (QD); 5 – neutral liposomes (120 nm); 6 – mesoporous silica (MS) nanoparticles; 7 – polymeric micelles; 8 – cationic liposomes; 9 – poly(amido amine) (PAMAM) dendrimers; 10 – modified PAMAM dendrimers; 11 – poly(propyleneimine) (PPI) dendrimers; 12 – Modified PPI dendrimers; 13 – supermagnetic iron oxide (SPIO) nanoparticles; and 14 – modified SPIO nanoparticle. The cells were stained with DAPI nuclear dye. For each substance, images on the right panel show magnified cells marked by the square on the left panel.

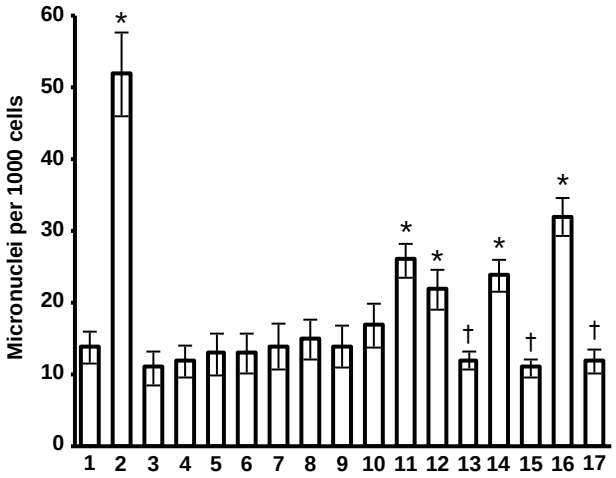

Figure 4.5: Genotoxicity of different nanocarriers: 1 – media (negative control); 2 – ethyl methanesulfonate (EMS, positive control); 3 – 2 kDa poly(ethylene glycol) (PEG) polymer; 4 – 10 kDa PEG polymer; 5 – 20 kDa PEG polymer; 6 – quantum dots (QD); 7 – "neutral" liposomes (120 nm); 8 – "neutral" liposomes (600 nm); 9 – mesoporous silica (MS) nanoparticles; 10 – polymeric micelles; 11 – cationic liposomes; 12 – poly(amido amine) (PAMAM) dendrimers; 13 – modified PAMAM dendrimers; 14 – poly(propyleneimine) (PPI) dendrimers; 15 – modified PPI dendrimers; 16 – supermagnetic iron oxide (SPIO) nanoparticles; and 17 – modified SPIO nanoparticles. Means ± SD are shown. *$P < 0.05$ when compared with media (negative control). †$P < 0.05$ when compared with a corresponding non-modified carrier.

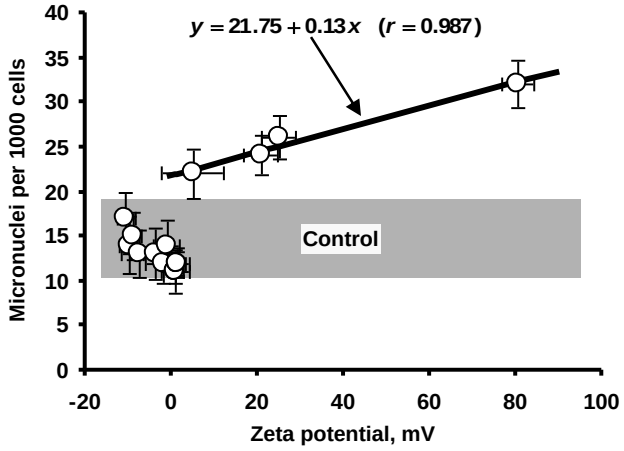

Figure 4.6: Correlation between the zeta potential of nanocarriers and their genotoxicity. Shaded area represents the control range of micronuclei formation. Means ± SD are shown.

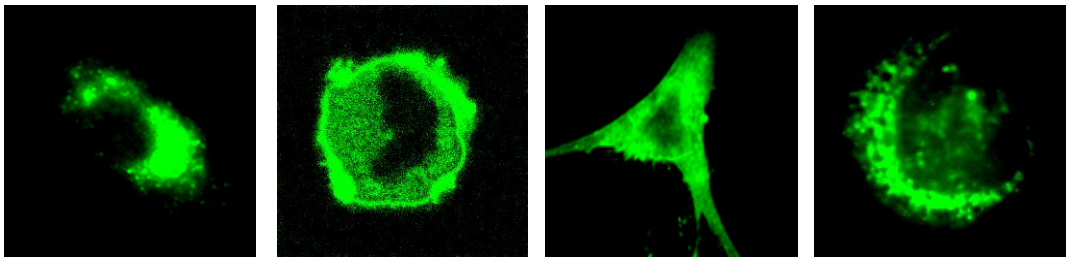

Figure 4.7: Cellular internalization of siRNA complexes with different nanocarriers. Representative confocal microscope images of cancer cells incubated within 24 h with fluorescently labeled siRNA delivered by mesoporous silica (MS) nanoparticles, cationic liposomes, modified poly(amido amine) (PAMAM) dendrimers and modified poly(propyleneimine) (PPI) dendrimers.

5 EVALUATION OF THE CYTOTOXICITY AND GENOTOXICITY OF VARIOUS RAW MATERIALS UTILIZED IN COSMETIC INDUSTRY

5.1 Introduction

Optical brighteners (OB) are defined as dyes that are capable of absorbing light in violet and ultraviolet region and then re-emit it in the blue region. Optical brighteners are used in shampoos and conditioners for grey or blonde hair. In addition to increasing the luminance and sparkle of the hair, it can also correct dull and yellowish discoloration without darkening the hair. Optical brightener microspheres are also utilized in some face and eye powder which can clear up shadowed areas of the skin such as “tired eyes” (253).

Every cosmetic or personal care product that contains water requires the inclusion of preservatives to prevent microbial growth. Although these products are not produced under completely sterile conditions and therefore are not germ free, their manufacturing conditions and equipment should be clean. The preservation system acts not to battle contamination in production, but as a protective measure to prevent further contamination when used by the consumer. The preservation system prolongs the shelf life of the product from a few days (without preservatives) to a few years (with the appropriate preservation system). When choosing a preservative system, a few concepts should be considered. The system should be tested and challenged with the typical microorganisms, but also mimic the duration of application on skin (leave on or

wash off product) and the expected number of times the consumer will potentially contaminate the formulation.

The amount of preservatives used in a given cosmetic formulation is relatively low when compared with the other components. We are all exposed to preservatives with almost every application or use of any product as most do contain water. Moreover, these compounds are designed to be toxic to the living microorganisms and therefore may pose risk to other biological entities. In terms of safety, the longer the duration of exposure to such optical brighteners and preservatives, the higher the potential risk for skin absorption and possible toxic effects. In addition, possible contact with mucus membrane such as the eye requires special attention with the choice of preservatives and their efficacy. Although exposure to these compounds at their low use level may not present an acute, immediate reaction, a late onset effect can occur from chronic exposure and bio-accumulation. Consequently, it has become a priority to test these compounds for safety. One of the more important end points in the evaluation of safety is the potential of a compound to become genotoxic.

The 7th amendment to the EU Directive banned the cosmetic industry to from experimenting on experimenting on animals (17). Hence the cosmetic industry is utilizing, studying, and validating a variety of in vitro and ex vivo protocols to test the compounds. One test method recommended for the estimation of genotoxicity is known as the micronuclei assay. The objective of the micronucleus test is to detect and quantify the formation of micronuclei in the cytoplasm of interphase cells. A

micronucleus is a small nucleus that forms whenever a chromosome or a fragment of a chromosome is not incorporated into one of the daughter nuclei during cell division. Normally, in vivo, micronuclei will be removed by the spleen. However, with extensive continuous exposure, the spleen might not have the capacity for complete removal. This can lead to mutations as the next cell generation forms. The micronucleus assay detects both clastogenic (disruption or breakage of chromosomes) and aneugenic (loss or gain of a whole chromosome) activity. The micronucleus assay identifies cell damage that is transmitted to daughter cells by microscopic observation and counting the number of cells that, after division, contain a micronucleus. This assay is considered as one of the most successful and reliable assays for estimating genetic damage induced by a test substances. The major advantages of this procedure include simultaneous detection of chromosome and genome mutations, applicable to many cell types, rapidity, relatively low cost, simplicity, potential for automation and statistical power. Additional possible tests may include the microbial mutagenicity test (Ames test) and cytogenetic tests in vivo [e.g. the bone marrow micronucleus test or the liver unscheduled DNA syntheses (UDS) test]. The Ames test is suitable for the initial detection of genetic toxicity; however, DNA damage considered relevant for mammalian cells cannot be adequately measured in bacteria and should be evaluated in mammalian cells.

In this study we tested the genotoxic potential of an optical brightener (OB) powder (INCI: sodium silicoaluminate (and) glycidoxypropyl trimethyloxysilane/ PEI-250 cross fluorescent brightener 230 salt (and) polyvinylalcohol crosspolymer) that is used in

cosmetic facial products. It is a solid dry powder with an average size of 5 microns that is insoluble but dispersible in water. We also tested a hydrophilic polymer, Hydrillien 9 (International Nomenclature of Cosmetic Ingredients name: Sodium Acrylates/Acrylonitrogens Copolymer), preserved with three different preservation systems for genotoxicity. It is a soft, pale yellow to yellow granular gel used as a thickener and stabilizer in emulsions. It contains 70–90% water and therefore requires preservation at the time of manufacturing. Its recommended use level in emulsions is 0.2–5%; therefore, the preservation system will be further diluted when incorporated into the finished product. Both the studies were conducted in accordance with the OECD Guidelines number 487: in vitro Mammalian Cell Micronucleus Assay that was revised on December, 2009 (39).

5.2 Materials and Methods

5.2.1 Materials

The chemicals for the control group were purchased from Sigma Chemical Co. (St. Louis, MO). These include cyclophosphamide (CAS no. 50-18-0), ethyl methanesulfonate (CAS no. 62-50-0), and dimethyl sulfoxide (DMSO). Nicotinamide adenine dinucleotide phosphate (NADP) was purchased from Fisher Scientifi c Co. (Suwannee, GA). Sodium phosphate buffer was obtained from Moltox (Boone, NC). Glucose 6 phosphate and Tween 20 were received from Sigma Aldrich (St Louis, MO), and 4’ ,6- diamidino-2-phenylindole dihydrochloride (DAPI) was purchased from Sigma. The test substances:

OB and three Hydrillien 9 compounds (As shown in Table) labeled as A, B and C were products from Lipo Chemicals Inc. (Paterson, NJ).

5.2.2 Preparation of chemicals

The study was conducted under good laboratory practice conditions. Cyclophosphamide and EMS were used as positive controls to analyze the formation of micronuclei. Cyclophosphamide (1 g) was dissolved in 100 mL of water to give a concentration of 10 mg/mL, and 5 µL of this solution was added to a 5-ml volumetric volumetric flask and brought to volume with water to give the required final concentration of 10 µg/mL (47, 245). EMS is a liquid with a density of 1.15 g/mL at room temperature. EMS (0.1 mL) was diluted in 0.9 mL of DMSO, and 17.5 µL of this solution was added to a 5-ml flask and brought to volume with DMSO to give the final required concentration of 400 µg/mL (245).

The OB powder was dispersed at 10 mg/ml in DMSO. An amount of 50 mg of this suspension was added to 5 ml of DMSO, subjected to ultrasonification for 30 minutes, and centrifuged at 2000 rpm for 15 minutes. Volumes of 100 µL and 150 µL of the supernatant were added to flasks of 25 cm^2 base surface area containing 5 ml of media, to give final concentrations of 0.2 mg/ml and 0.3 mg/ml, respectively. These doses were selected in preliminary experiments based on the concentrations of DMSO that are nontoxic for the types of cells used.

Compounds A, B and C were soft granular gels that were soluble in water. A 5 mg amount of each of these compounds was dissolved in 10 mL of distilled water. This gave three stock solutionof 0.1% of A, B and C in water. Finally, 2.5 mL of each stock solution

was diluted with 2.5 mL of media to give a working solution of 0.05% concentration. The solution was clear and colourless.The pH of each solution was as follows: A(7.48), B(7.45) and C(7.43). The concentrations of preservatives in each solution were as follows:

• A 0.25% pentylene glycol and 0.01% ethylhexylglycerine;

• B 0.05% caprylyl glycol and 0.01% ethylhexylglycerine;

• C 0.015% caprylyl glycol and 0.01% phenoxyethanol.

To prepare the stock solution, 5 mg of 4', 6-diamidino-2-phenylindole dihydrochloride (DAPI) was dissolved in 1 mL of dimethyl formamide and allowed to stand until complete dissolution was obtained. For the working solution, 4 µL of the stock solution was added to 50 mL of Phosphate Buffer System (PBS) and stored at 4^{o}C protected from light before the time of staining.

5.2.3 Metabolic activation system

Inclusion of a metabolic activation system in the genotoxicity assay enables the detection of mutagenic activity for carcinogens and/or mutagens that require such transformation (i.e., cyclophosphamide). The metabolic activation system was prepared according to the method described in references (40, 246). Aroclor-1254-induced rat liver S9 fraction was purchased from Moltox (Boone, NC, U.S.A.). The following chemicals were added in the order listed to get a total volume of 3 ml of S9 mix: sterile double-distilled H2O (840 µL); sodium phosphate buffer (0.1 M), pH 7.4 (1.5 ml); 4 mM NADP (150 µL); 120 mM glucose-6-phosphate (22 µL); potassium magnesium salt solution, 8 mM–33 mM (60 µL); and rat liver fraction (3.00 µL) to give a final

concentration of 10% (v/v). The final concentration of the metabolic activator used for each test flask was 1% (v/v). In contrast to cyclophosphamide, EMS does not require metabolic activation and therefore the metabolic activation system was not used in the experiments involving EMS.

5.2.4 Cell line

Chinese hamster ovary (CHO-K1) cells were used as recommended in the OECD protocol (39) and were bought from American Type Culture Collection (ATCC, Manassas, VA). Cells were cultured in ATCC-formulated F-12K medium supplemented with 10% fetal bovine serum (Fisher Chemicals, Fairlawn, NJ) and penicillin-streptomycin (100 UI/ mL–100 µg/mL). Cells were grown at 37°C in a humidified atmosphere of 5% CO2 (v/v) in air. All experiments were performed on cells in the exponential growth phase.

5.2.5 Experimental series and condition

The experiments for OB and the Hydrillien 9 compounds were carried out separately. In each experiment, about 300,000 cells were cultured with the media in each 25-cm^2 flask and held 24 hours before treatment. For the series with metabolic activation, the cells were treated for three hours after which the media were replaced with fresh media and the cells were incubated for 24 hours. For the groups without S9 activation, the cells were incubated for 24 hours. All the cells were harvested at the end of 24 hours and stained to detect the presence of micronuclei. The following series of treatments was carried out for OB : (1) media only (negative control); (2) DMSO (negative control); (3) cyclophosphamide + S9 mix (10 µg /mL) (positive control); (4) ethyl methanesulfonate (400 µg /ml) (positive control); (5) OB (0.2 mg/ml); (6) OB (0.3 mg/ml); (7) OB (0.2

mg/ml) + S9 mix; and (8) OB (0.3 mg/ml) + S9 mix. They were incubated with the substances as indicated in **Fig 5.1 A**. For the experiments with Hydrillien 9 compounds (A, B and C) the series of treatments carried out were as follows: (1) Media only (negative control); (2) media with S9 (negative control); (3) cyclophosphamide + S9 mix (10 µg/mL) (positive control); (4) EMS (400 µg/mL) (positive control); (5) A (0.05%); (6) A (0.05%) + S9 mix; (7) B (0.05%); (8) B (0.05%) + S9 mix; (9) C (0.05%); (10) C (0.05%) + S9 mix. They were incubated with the substances as indicated in **Fig 5.1 B**. All the treatment groups were set up as duplicates; the determination of cellular toxicity was made in independent measurements. After the end of all treatments, the cells were harvested for staining.

5.2.6 Cell staining

After 24 h of incubation with the aforementioned substances, the media from all the flasks were removed. The cells were fixed by slowly adding a cold solution of 100% methanol and allowed to stand for 5 min. The methanol was removed, and the cells were washed with PBS two times for 2 min each. The cells' nuclei were then stained with 600 nM of DAPI for 8 min. This solution was removed, and all the flasks were washed with PBS containing 0.05% Tween 20. The cells were kept moist by adding PBS at the end. The cells were then observed under a microscope.

5.2.7 Counting of micronuclei

For each experimental series, the formation of micronuclei was determined as described (254) by counting the number of micronuclei per 1000 cells using light and a fluorescent microscope (Olympus I×71, New York).

5.2.8 Cellular viability and proliferation

A modified MTT (3-(4, 5-dimethylthiazol-2-yl)-2,5-diphenyltetrazolium bromide) assay was used to assess the cytotoxicity of studied substances as previously described (255). This method is utilized for the determination of the highest non-cytotoxic concentration because the aim of this study is to assess the potential genotoxic effect at this concentration. To measure cytotoxicity, cells were separately incubated in a microtitre plate with each studied substances. Control cells received an equivalent volume of fresh medium with or without S9 activation. The duration of incubation was 24 h. Based on these measurements, cellular viability was calculated for each substance. A decrease in cellular viability indicated an increase in toxicity of the test substance.

Cell proliferation was conducted using a Hemacytometer (Veeder-Root, Elizabeth Town, NC, U.S.A.) and light microscope (Zeiss, NewYork, NY, U.S.A.). For the OB compound and Hydrillien 9 compounds (A,B and C), 4.0×10^4 cells and 3×10^4 were seeded in each well of a 6-well plate respectively along with the treatment conditions described previously. At the end of 48 h, the contents from each well were removed. The cells were washed with Dulbecco's Phosphate Buffered Saline (DPBS) once for 1 min. DPBS was removed, and 1 mL of trypsin was added to each well. The plates were then placed in an incubator at 37^0C for 2 min. The plates were gently shaken, and the cells were detached with a cell scrapper. A 20 µL sample of this mixture was added to a hemacytometer. Cells were

counted in each of the four grids and the average count was recorded. The final number represents the average number x 104 cells per ml (SIGMA).

5.2.9 Statistical analysis

Data obtained were analyzed using descriptive statistics and single factor analysis of variance (ANOVA), and were presented as mean value ± S.D.

5.3 Results

5.3.1 Micronuclei formation

The in vitro micronucleus assay is a mutagen test system for the detection of the chemically induced formation of small membrane-bound DNA fragments, i.e., micronuclei in the cytoplasm of cells (43, 254). These micronuclei may originate from acentric fragments (chromosome fragments lacking a centromere) or whole chromosomes that are unable to migrate with the rest of the chromosomes during the anaphase of cell division. The micronucleus assay is widely used for monitoring genetic damage caused by different substances. Typical images of cells with stained nuclei populations and quantitative analysis for OB are represented in **Figs 5.2 and 5.3** respectively whereas Hydrillien 9 compounds (A, B and C) are presented in **Figs 5.4 and 5.5 respectively.** It can be clearly seen that both positive controls induced substantial genetic damage leading to the formation of 140–170 micronuclei per 1000 cells. In contrast, cellular nuclei appeared intact after the incubation with OB as well as Hydrillien 9 compounds (A, B and C) at the tested non-cytotoxic concentrations and the average number of micronuclei per 1000 cells was close to that of the control cells.

5.3.2 Cell viability and proliferation

A cell that had gone through mutational changes can either go into senescence or apoptosis, or it may survive. If it survives and mutations are not corrected by DNA repair enzymes, these mutations can possibly lead to unregulated cell division and the creation of cancerous tissue. Cancerous cells, therefore, do not obey the normal apoptotic paths that are typical of normal cells. In fact, in cancer cells activation of biochemical substances such as cytokines and other mediators may enhance cell proliferation and viability markers may increase as the cell becomes more sensitive in response to promoters that are involved in the induction of cell division. In addition, in these cells metabolic activity may be accelerated. The MTT ((3-(4,5-dimethylthiazol-2-yl)-2,5-diphenyltetrazolium bromide, a tetrazole) test detects the activity of mitochondrial enzymes in viable cells and is an indication of cell viability (256). We tested cell viability in an attempt to draw additional data that will further validate our findings related to chromosomal changes. It was previously shown that a positive cell viability assay response has a strong probability of predicting carcinogenicity in vivo (257). In other words, if a compound (such as the positive controls in this study) is generating both micronuclei formation and accelerating cell proliferation and/or metabolism, there are two related pieces of evidence that point to its potential of being a carcinogen. The cell-counting studies also show that the proliferation of the cells incubated with the studied compound are similar to the proliferation of the cells incubated with fresh media. The cellular viability and proliferation data for OB and Hydrillien 9 compounds are presented in **Figs 5.6 and 5.7** respectively.

5.4 Discussion

5.4.1 Optical brighteners

Cosmetic and personal care products are used on a daily basis, either in the forms of a "wash off," such as soaps and shampoos, or a "leave on," such as creams, lotions, and makeup preparations. Over a lifetime, a person living in the Western world is expected to be exposed to thousands of different chemicals repeatedly. While most of these chemicals will not penetrate healthy intact skin, depending on their chemical and physical properties, numerous compounds can partition into the skin and either accumulate in its viable layers or further penetrate to the blood circulation. If these compounds carry toxic potential, their accumulation can lead to diseases and disorders. Moreover, our skin and our internal organs contain metabolic systems that can convert an inert compound into a toxic substance.

Since, unlike pharmaceutical grade compounds, the production of a cosmetic ingredient does not require strict conditions such as GMP, the residuals and the impurities that these ingredients may contain are of major concern. For example, it was shown that polyethylene glycol (PEG) molecules with a molecular weight of around 200 Da can induce a genotoxic effect in Chinese Hamster Ovarian (CHO) cells after metabolic activation with S9 following chromosome aberration study protocols (258). The researchers also concluded that their findings may reflect a potential mutagenic risk of PEG derivatives with similar molecular sizes. Another example is sodium benzoate, which is used extensively as a preservative in cosmetic formulations. In a report issued

by the EU Commission Scientific Committee, the SCCNFP, in 2002 (259), the Committee reviewed genotoxicity data generated on sodium benzoate. This compound demonstrated positive results for genotoxicity in a CHO cell line without metabolic activation. Although chromosomal aberrations were not induced when tested *in vivo* in rats, a dominant lethal assay with sodium benzoate in rats did show a genotoxic effect. Based on these data, the committee concluded that sodium benzoate carries a potential genotoxic risk and called for the generation of additional studies to either confirm these observations or rule them out. Structural aberrations may be of the chromosome or chromatid type. The induction of generation of two or more homologous sets of chromosomes, called polyploidy, may be an indication that a substance carries the potential to induce numerous aberrations that can lead to the initiation of mutations that transform the cells to the cancerous stage. The identification of aberrations in this study is normally conducted by observational assessment of the morphological changes in the nucleus. It therefore requires an experienced individual who is capable of differentiating between a state that is unusual and a state wherein the cell was arrested in the course of normal division. Therefore, we also added quantification of the data to corroborate the microscope observations.

5.4.2 Hydrillien Compounds

A review of studies conducted to assess the safety of preservatives used in cosmetics revealed that compounds that release formaldehyde, such as dimethylol urea (DMU) and diazolidinyl urea (DZU), raise safety concerns (260). When tested in vitro, both induced genotoxic effects that led to the conclusion that further risk assessment

evaluation is required. Both compounds induced the formation of micronuclei. However, DMU showed a relatively weaker effect in the absence of metabolizing enzymes. DZU yielded significant increases of micronuclei formation both in the absence and in the presence of S9 enzymatic activation. Both compounds also showed cytotoxic effects, suggesting possible breakage of chromosomes that lead to cell death (clastogenic effect), and DZU also induced the formation of large nuclei, suggesting an effect on cell division (aneugenic effect).

Because the events leading to an observable genotoxic effect in cell culture are complicated, the effect of a combination of ingredients may be different from the effect of each individual component. Moreover, although a compound itself can result in a negative effect, a derivative can lead to a mutagenic effect. Examples of such compounds are sorbic acid and potassium sorbate in comparison with sodium sorbate (261). Sorbic acid did not induce DNA repair in cultured human A549 cells in the unscheduled DNA synthesis assay. In vitro incubation of cells with potassium sorbate in the absence and presence of enzymatic activation did not result in the formation of DNA single-strand breaks. However, in contrast to these observations, sodium sorbate is sensitive to oxidative degradation, producing 4,5-oxohexenoate, an oxidation product that showed a mutagenic effect when tested in the Ames test.

A review of the literature on the toxic effects of the compounds described previously revealed that the only alert is related to the phenoxyethanol included in the compound

C mixture. However, delving into details, it appears that the toxic effects were observed only in concentrations that are far higher than the concentrations one would be exposed the normal use of this product. For example, it only showed cell-induced apoptosis and necrosis when introduced to HL60 cell cultures at 0.01–0.5% and 1%, respectively (262). These are concentrations that are approximately 100 times higher than the ones used in this current study. Another effect of phenoxyethanol that was observed at high levels is teratogenicity in rabbits (263). Pregnant rabbits were fed 1000, 600 or 300 mg phenoxyethanol/kg/day on days 6 through 18 of gestation. The two high concentrations resulted in the death of a significant number of the animals. In one animal that survived, although no mutations were observed in the fetuses, maternal toxicity such as intravascular hemolysis was observed. With respect to metabolicvconversion, phenoxyethanol was shown to undergo dermal metabolic oxidation that potentially leads to the generation of oxidation products such as aldehydes and alkoxyacetic acids (264). These are known to potentially lead to localized or systemic toxicity, including skin sensitization and irritancy, reproductive, developmental and hematological effects. The Environmental Protection Agency (EPA) has published a table summarizing the effect of exposure to phenoxyethanol (http://www.epa.gov/opptintr/chemtest/pubs/phenox.pdf. EPA Publication accessed on October 19, 2010). This document summarizes a few observations:

• Dermal exposure in rabbits resulted in the following effects: Maternal toxicity expressed by weight loss and death at high concentrations, no effects at the No Observable Effect Level

(Systemic toxicity, 500 ng/kg per day) or below;

• Dermal exposure in humans: Repetitive exposure to an occlusive patch containing 0.3 mL of 10% solution with rest periods showed no evidence of cumulative irritation or delayed sensitization. When tested in vitro on CHO cells at concentrations ranging from 62.2 to 5000 µg /mL, no significant mutation frequencies were noted in the presence or absence of exogenous metabolic activation. These data correlate with the findings of our study because the final concentration of the phenoxyethanol we used is 0.01% (100 µg/mL).

5.5 Conclusion

Under the conditions of the study, the test substance, OB, did not show promotion of the generation of micronuclei with and without enzymatic activation. The measurements of cellular viability showed that cyclosphosphamide + S9 mix (10 µg/ml), ethyl methanesulfonate (EMS, 400 µg/ml), or OB (0.2 mg/ml and 0.3 mg/ml) alone or in combination with S9 did not inhibit the growth of cells (Figure 4) at the concentrations used. This study also demonstrates a way to test a compound that is not fully solubilized in the media. Stages of introduction of the OB to the cell culture included dissolution in DMSO (which had no effect on the cells when tested alone), sonication, centrifugation, and drawing the supernatant. This is to mimic real-life exposure wherein the particle

does not penetrate healthy intact skin, but its impurities and residuals can dissolve in skin fluids.

The results from the study of Hydrillien 9 compounds also clearly demonstrate similar results. At the tested concentrations, none of the compounds (A,B and C) demonstrated cytotoxic or genotoxic effects either alone or when undergoing enzymatic metabolism. This was shown both quantitatively and quantitatively under microscopic observation. Nevertheless, the fact that no toxic effects were observed in this study does not exclude the possibility that under extreme and/or cumulative exposure conditions, a potential toxic effect will be generated as in the known case of phenoxyethanol. When using compounds to be applied as cosmetics, we assume that they are interacting with healthy intact skin, mostly in a non-occlusive manner, and therefore, penetration is negligible. If, however, the formulation is designed to be applied to a disrupted barrier such as in shaving formulations or diseased skin, extra precautions should be taken and exposure should be carefully evaluated.

Consequently, we conclude that all tested substances do not promote cell death at the concentrations used and that the positive controls may have generated a shift in cellular function that led to enhanced proliferation. It is also important to note that when testing a raw material for safety, specific attention should be paid to the compounds used as additives, such as preservatives and antioxidants. These compounds can change the safety profile of a the product, a new battery of studies should be conducted to ensure consumer safety

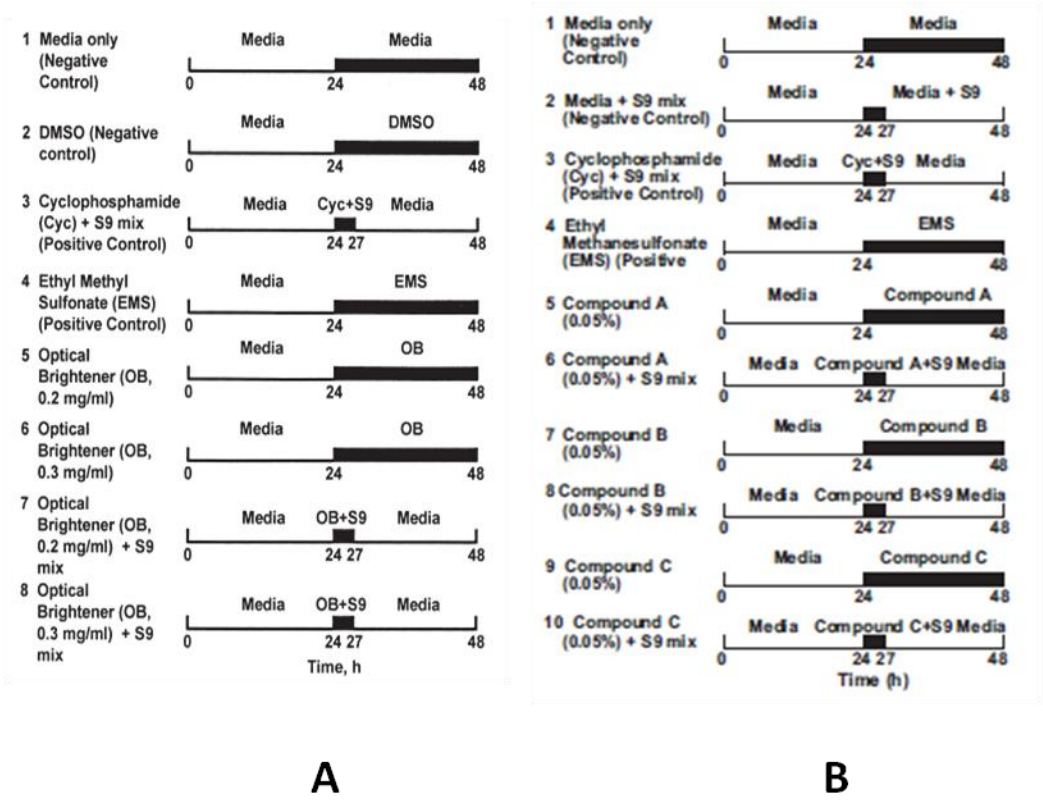

Figure 5.1: Treatments used in the study along with the incubation times. A) OB : (1) media only (negative control); (2) DMSO (negative control); (3) cyclophosphamide + S9 mix (10 µg /mL) (positive control); (4) ethyl methanesulfonate (400 µg /ml) (positive control); (5) OB (0.2 mg/ml); (6) OB (0.3 mg/ml); (7) OB (0.2 mg/ml) + S9 mix; and (8) OB (0.3 mg/ml) + S9 mix. B) Hydrillien 9 compounds (A, B and C): (1) Media only (negative control); (2) media with S9 (negative control); (3) cyclophosphamide + S9 mix (10 µg/mL) (positive control); (4) EMS (400 µg/mL) (positive control); (5) A (0.05%); (6) A (0.05%) + S9 mix; (7) B (0.05%); (8) B (0.05%) + S9 mix; (9) C (0.05%); (10) C (0.05%) + S9 mix. The shaded areas represent the treatments employed. The treatments without S9 activation were incubated for 24 h before harvesting. The treatments with S9 activation were incubated for 3 h. At the end of 3 h, the contents were replaced with media and allowed to incubate for 21 h before harvesting.

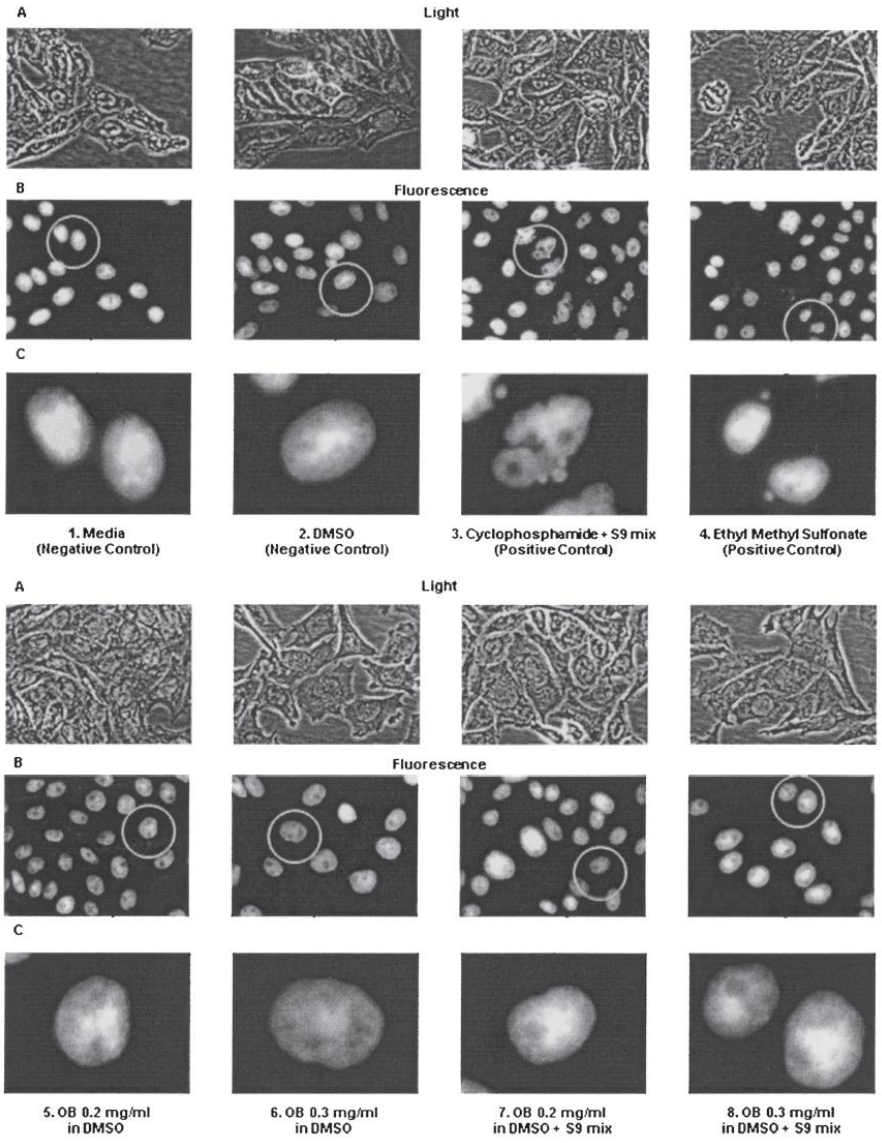

Figure 5.2: Typical light and fluorescent images of CHO-K1 cells incubated for 24 hours with the OB as follows: (1) Media (negative control); (2) DMSO (negative control); (3) Cyclosphosphamide + S9 mix (positive control); (4) Ethyl methyl sulfonate (positive control); (5) OB, 0.2 mg/ml in DMSO; (6) OB, 0.3 mg/ml in DMSO; (7) OB, 0.2 mg/ml in DMSO + S9 mix; and (8) OB, 0.3 mg/ml in DMSO + S9 mix. The cells were stained with DAPI nuclear dye.

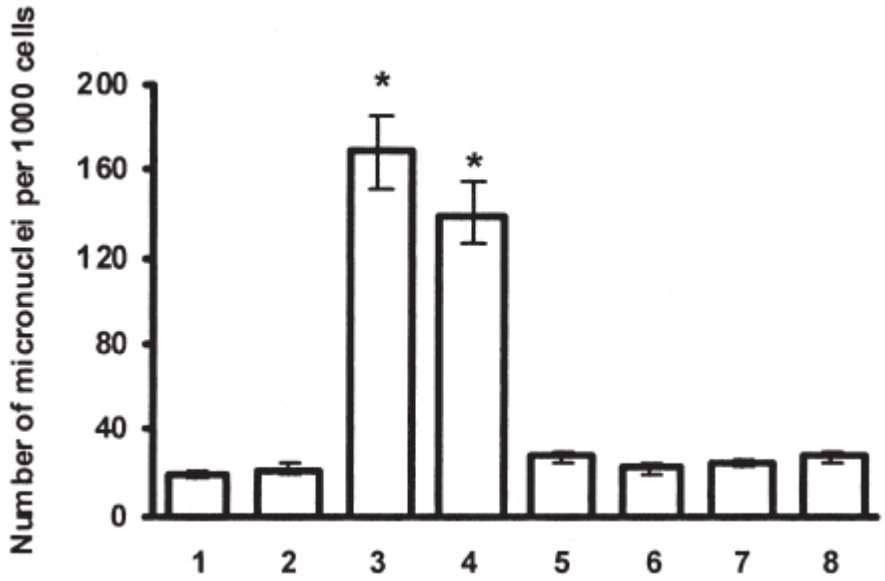

Figure 5.3: Number of micronuclei per 1000 cells for OB. CHO-K1 cells were incubated for 24 hours with the following substances: (1) Media (negative control); (2) DMSO (negative control); (3) Cyclosphosphamide + S9 mix (positive control); (4) Ethyl methanesulfonate (positive control); (5) OB, 0.2 mg/ml in DMSO; (6) OB, 0.3 mg/ml in DMSO; (7) OB, 0.2 mg/ml in DMSO + S9 mix; and (8) OB, 0.3 mg/ml in DMSO + S9 mix. Means ± S.D. are shown. *$P<0.05$ when compared with negative control.

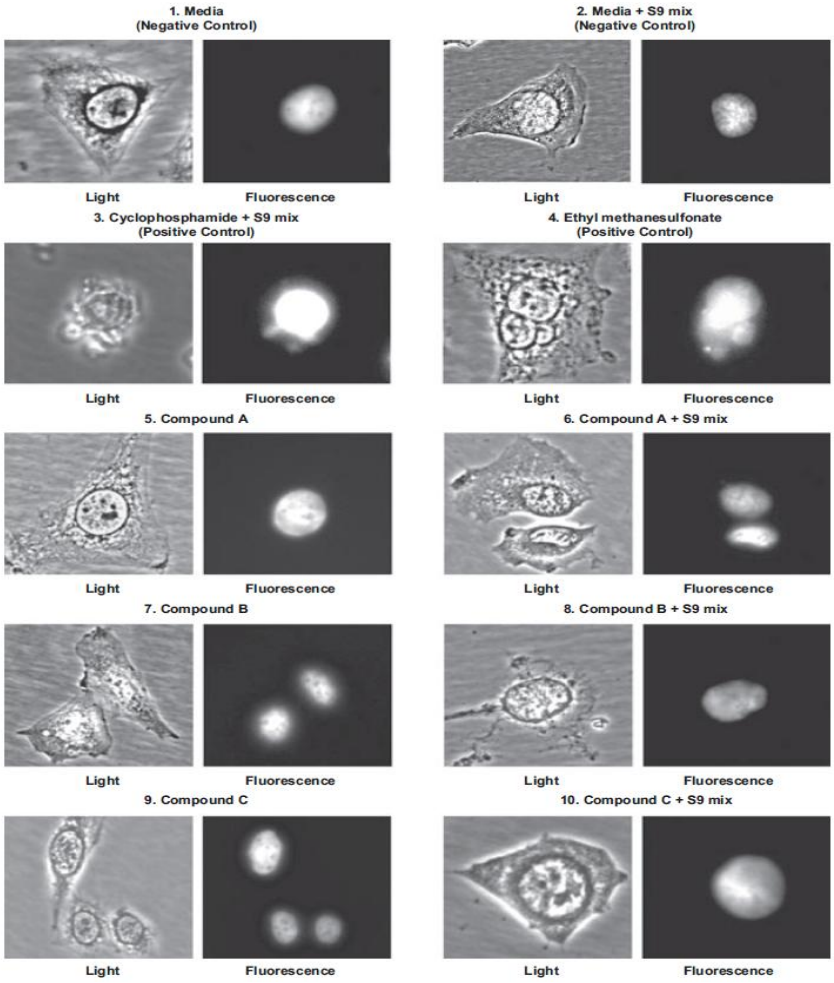

Figure 5.4: Typical light and fluorescent images of Chinese Hamster Ovary-K1 cells incubated for 24 h with Hydrillien 9 compounds as follows: 1 – media (negative control); 2 – media (negative control) + S9 mix; 3 – cyclophosphamide + S9 mix (positive control); 4 – ethyl methanesulfonate (positive control); 5 – compound A (0.05%); 6 -compound A (0.05%) + S9 mix; 7 – compound B (0.05%); 8 – compound B (0.05%) + S9 mix; 9 – compound C (0.05%); 10 – compound C (0.05%) + S9 mix. The cells were stained with 6-diamidino-2-phenylindole dihydrochloride nuclear dye.

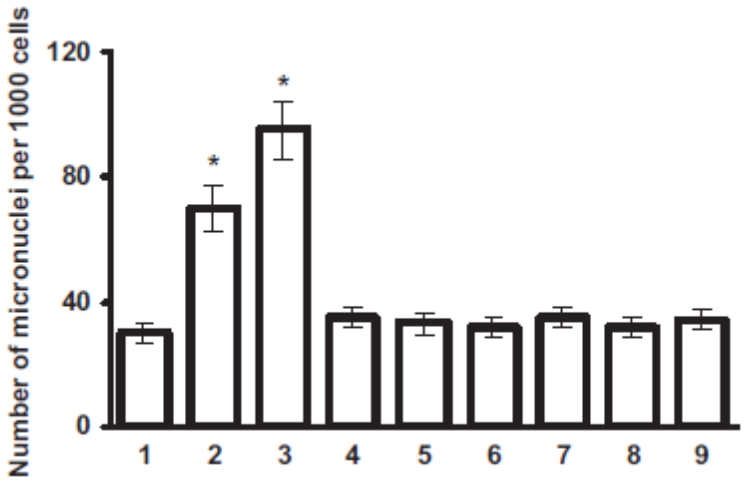

Figure 5.5: Number of micronuclei per 1000 cells for Hydrillien compounds. Chinese Hamster Ovary-K1 cells were incubated for 24 h with the following substances: 1 – media (negative control); 2 – cyclophosphamide + S9 mix (positive control); 3 – ethyl methanesulfonate (positive control); 4 – compound A (0.05%); 5 – compound A (0.05%) + S9 mix; 6 – compound B (0.05%); 7 – compound B (0.05%) + S9 mix; 8 – compound C (0.05%); 9 – compound C (0.05%) + S9 mix. Means ± SD are shown. *P < 0.05 when compared with negative control.

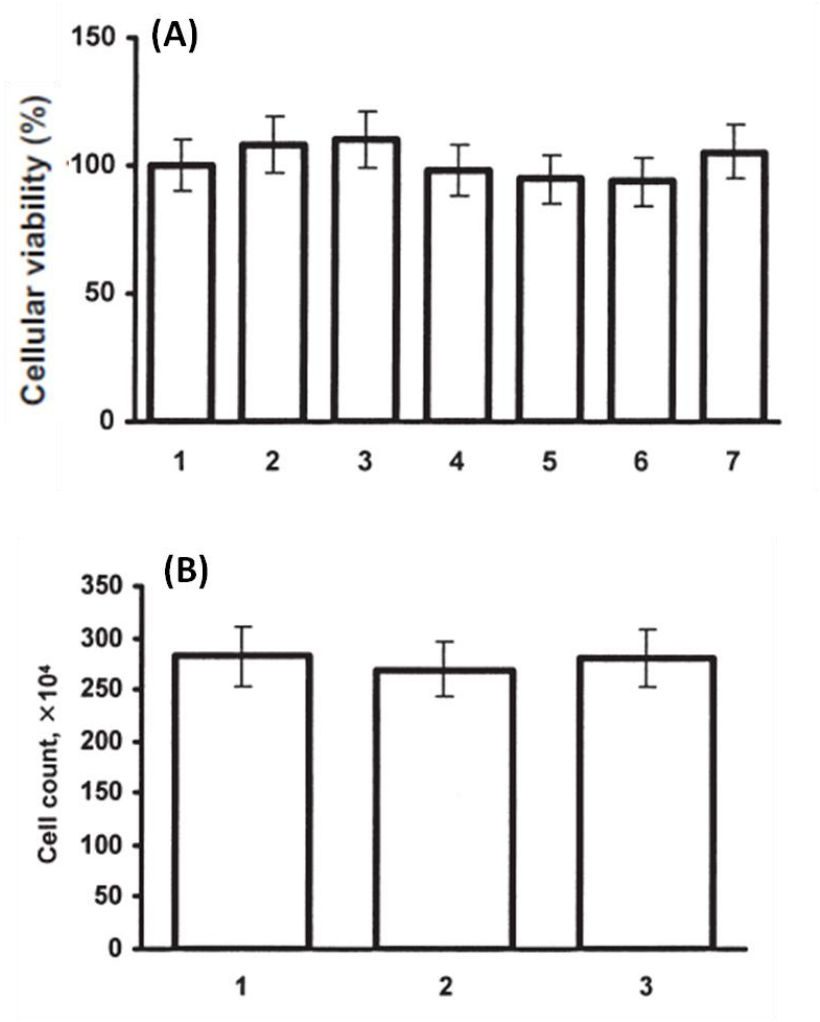

Figure 5.6: (A) Cellular viability. CHO-K1 cells were incubated for 24 hours with the following substances: (1) DMSO (negative control); (2) Cyclophosphamide + S9 mix (positive control); (3) Ethyl methanesulfonate (positive control); (4) OB, 0.2 mg/ml in DMSO; (5) OB, 0.3 mg/ml in DMSO; (6) OB, 0.2 mg/ml in DMSO + S9 mix; and (7) OB, 0.3 mg/ml in DMSO + S9 mix. Means ± S.D. are shown. (B) Influence of test substances on cellular proliferation. The same number of cells (3 × 104) were seeded in the flask and incubated with media (1) and a test substance in two concentrations: 0.2 mg/ml (2) and 0.3 mg/ml (3). Cells were counted 48 h after the addition of the test substances. Means ± S.D. are shown from four independent measurements.

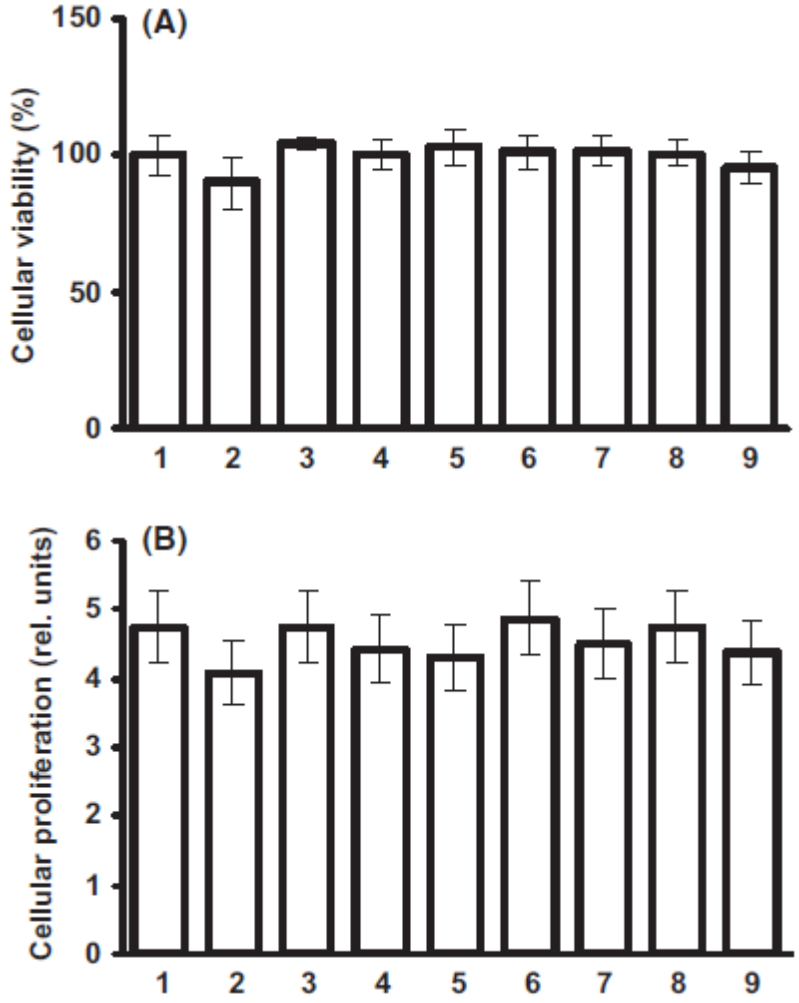

Figure 5.7: Cellular viability (A) and proliferation (B). Chinese Hamster Ovary-K1 cells were incubated for 24 h with the following substances: 1 – media (negative control); 2 – cyclophosphamide + S9 mix (positive control); 3 – ethyl methanesulfonate (positive control); 4 – compound A (0.05%); 5 - compound A (0.05%) + S9 mix; 6 – compound B (0.05%); 7 – compound B (0.05%) + S9 mix; 8 – compound C (0.05%); 9 – compound C (0.05%) + S9 mix. For (B), cellular proliferation was calculated as the ratio of the cell count 48 h after incubation to the initial cell count seeded on the plate. Means ± SD are shown.

6 TARGETED NANOMEDICINE FOR SIMULTANEOUS SUPPRESSION OF CD44 PROTEIN AND CELL DEATH INDUCTION

6.1 Introduction

Ovarian cancer is the fifth leading cause of cancer-related deaths in women and the most lethal of all gynecologic cancers in the United States. In 2011, an estimated 21,990 new cases of ovarian cancer were registered out of which 15,460 cases were considered deadly (2). In 75% of the cases, the disease is dispersed throughout the intraperitoneal cavity (Stage III and higher) at diagnosis (19). Although the initial chemotherapy has responded well by ovarian cancer, the five year survival rates for patients with advanced Stage IIIC disease are extremely low at approximately 30% (19). Consequently, novel approaches to chemotherapy of advanced spread ovarian cancer is very important in order to increase the survival rate.

CD44 is a cell surface glycoprotein involved in cell-cell interactions, cell adhesion, and migration (32). It is considered as a major cell surface marker for metastasis and progression in certain types of cancers, including ovarian carcinoma. CD44 is a receptor for hyaluronic acid (265, 266). Hyaluronic acid is the principal glycosaminoglycan found in extracellular matrices. It is a major component of the peritoneum which is considered as the most important site for ovarian cancer metastases (168, 265). CD44 interacts with hyaluronic acid to activate Nanog-Stat-3 and ankyrin based signaling pathways. Activation of these signaling pathways is considered to be responsible for conferring the tumor stem cell specific behavior like transcriptional activation, tumor cell growth, and

multidrug resistance in ovarian and breast cancers (33). It was shown that CD44 is not expressed in normal cells and certain non-invasive established cell lines(267-270). It was also found that interactions of CD44 with tumor stroma and tumor microenvironment are closely related to the metastatic growth of cancer (29, 269). Based on the aforementioned findings, we hypothesized that suppression of CD44 protein could enhance the efficiency of chemotherapy and prevent the development of metastases. In order to verify the hypothesis, in the present study, we constructed a multifunctional nanocarrier-based (dendrimer) system that is capable of simultaneous delivering of an anticancer drug (paclitaxel) and siRNA targeted to CD44 mRNA specifically to ovarian cancer cells. This system was tested in vitro in experiments on cells isolated from malignant intraperitoneal ascites obtained from patients with advanced ovarian carcinoma and also on murine xenograft model of human ovarian carcinoma initiated by subcutaneous injection of these cells to nude mice.

6.2 Materials and Methods

6.2.1 Materials

Dimethyl-3-3'-dithiobispropionimidate-HCl (DTBP) was obtained from Thermo Fisher Scientific Inc. (Rockford, IL). Polypropylenimine (PPI) tetrahexacontaamine dendrimer was obtained from Symo Chem (Eindhoven, the Netherlands), O-[2-(N-succinimidyloxycarbonyl)-ethyl]-O'-methylpolyethylene glycol 5000 (NHS-PEG(5000)OCH3) was obtained from Sigma-Aldrich (Milwaukee, WI), α-maleimide-ω-N-hydroxysuccinimide ester poly(ethylene glycol) (MAL–PEG–NHS, MW 5000 Da) was

purchased from NOF Corporation (White Plains, NY). Synthetic analog of luteinizing hormone-releasing hormone (LHRH) decapeptide (Gln-His-Trp-Ser-Tyr-DLys(D-Cys)-Leu-Arg-Pro) was synthesized according to our design by the American Peptide Company, Inc. (Sunnyvale, CA). Fluorescent RNA duplex, siRNA labeled with Pierce NuLight DY-547 fluorophores (siGLO Red Transfection Indicator, red fluorescence), was also obtained from Applied Biosystems (Ambion, Inc., Foster City, CA). The primary rat CD44 antibody against human was obtained from Developmental studies at hybridoma bank (University of Iowa, Iowa). The secondary anti-rat conjugated with Cy3® goat antibody was obtained from Invitrogen (Eugene, Oregon). CD44 siRNA with a sequence of sense 5'-UAUUCCACGUGGAGAAAAAtt-3' and antisense 5'-UUUUUCUCCACGUGGAAUAca-3' was obtained from Applied Biosystems (Ambion, Inc., Foster City, CA). All other reagents were purchased from Sigma-Aldrich Co. LLC (St. Louis, MO) and used without modifications. Discarded anonymous pathological materials (primary solid gynecologic tumors and malignant ascites) were provided by the Cancer Institute of New Jersey. The samples did not allow identifying patient information.

6.2.2 Synthesis of Paclitaxel - Succinic Acid Conjugate

Succinic acid as a bis(carboxylic acid moiety) was conjugated with the hydroxyl group in paclitaxel (1 equiv.), leaving another carboxylic group free for further modifications. The flask was charged with paclitaxel (250.0 mg), succinic acid (SA, 34.58 mg) and 4-Dimethylaminopyridine (DMAP, 10.0 mg) in 5.0 mL of anhydrous dimethyl sulfoxide (DMSO) and 20.0 mL of anhydrous CH2Cl2. The reaction mixture was stirred for 30 min

at room temperature and finally N-(3-dimethylaminopropyl)-N-ethylcarbodiimide HCl (EDC·HCl, 57.51 mg) was added. The reaction was carried out with continuous stirring for 24 h at room temperature. The resulting reaction mixture turned light yellow due to the formation of dicyclohexylurea (DCU) as a byproduct. Paclitaxel-succinic acid conjugate (paclitaxel-SA) was precipitated using diethyl ether and dried under vacuum. To remove unreacted paclitaxel, the crude was purified by gel column chromatography.

6.2.3 Synthesis of Paclitaxel – PPI Conjugate

Reaction was performed in a similar condition as the synthesis of paclitaxel - succinic acid conjugate. Paclitaxel was conjugated to PPI dendrimer at 1:1 molar ratio as previously described (248, 271). Briefly, the flask was charged with paclitaxel-SA (15.3 mg), PPI (115.1 mg) and DMAP (1.0 mg) in 1.0 mL of anhydrous DMSO and 7.0 mL of anhydrous CH2Cl2. The reaction mixture was stirred for 30 min at room temperature and finally 3.1 mg of EDC·HCl were added. The reaction was carried out with continuous stirring for 24 h at room temperature. The resulting reaction mixture turned light yellow due to the formation of DCU as a byproduct. The reaction mixture (cloudy) was filtered to remove DCU. Paclitaxel-SA-PPI conjugate was precipitated using diethyl ether and dried under vacuum. To remove unreacted paclitaxel-SA, the crude was purified by dialysis membrane. The final product was characterized and confirmed by proton NMR and MALDI.

6.2.4 Modification of Paclitaxel – PPI Conjugate with MAL–PEG–NHS and LHRH

Paclitaxel – PPI conjugates dissolved in 5 mM HEPES (4-(2-hydroxyethyl)-1-piperazineethanesulfonic acid) buffer (pH=7.2) at the concentration 5 µM was mixed with α -Maleimide-ω-N-hydroxysuccinimide ester Poly(ethylene glycol) (MAL-PEG-NHS) with PEG: NH2 ratio equal to 2 rel. units. The NHS groups on the distal end of PEG reacted with amine groups on the periphery of Paclitaxel – PPI conjugate. After the reaction within 1 h at room temperature, LHRH peptide was added to the solution to covalently conjugate the peptide on the distal end of the PEG layer through the maleimide groups on the PEG and the thiol groups in LHRH (LHRH : PEG = 2). After 12 h of the reaction, the modified complexes were then purified by dialysis (MW cut-off 5 kDa) against water for 24 h and used for further studies.

6.2.5 Preparation of PPI – siRNA complexes

PPI-siRNA complexes have been prepared and modified according to our previously developed procedure (248). Briefly, the siRNA complexes were prepared at an amine/phosphate (N/P) ratio of 2.4 in 5 mM HEPES buffer (pH 8.0) by adding stock solution of PPI dendrimer into a pre-prepared siRNA solution. The final concentrations of siRNA and PPI in the solution were 28.6 µM and 45 µM, respectively. The samples were vortexed briefly, and the solutions were then incubated at room temperature for 30 min to ensure complex formation. In order to cross-link individual complexes, DTBP dissolved in 5 mM HEPES buffer was added to the above-formulated PPI –siRNA complexes solution at DTBP:NH2=3.2 cross-linking ratio (ratio between DTBP and total amino groups of PPI available after being complexed with siRNAs). After 3 h of reaction,

pH of the solution was adjusted to 7.2, followed by the addition of MAL–PEG–NHS (PEG: NH2= 2). The NHS groups on the distal end of PEG reacted with amine groups on the periphery of PPI –siRNA complex. After the reaction within 1 h at room temperature, LHRH peptide was added to the solution to covalently conjugate the peptide on the distal end of the PEG layer through the maleimide groups on the PEG and the thiol groups in LHRH (LHRH : PEG = 2). After 12 h of the reaction, the modified complexes were then purified by dialysis (MW cut-off 10 kDa) against water for 24 h and used for further studies.

6.2.6 Study of Complex Formation Between siRNA and Dendrimers

In order to evaluate the formation of complexes between siRNA and PPI dendrimers, ethidium bromide (EtBr), and agarose gel retardation assays were used. Various solutions of siRNA with dendrimers were prepared. The N/P ratios in the solutions were 0, 0.25, 0.5, 0.75, 1, 1.25, 1.5, 1.75, 2, 2.25, 2.5, 2.75 and 3. The concentration of siRNA was kept constant at 0.4 µM while the concentration of dendrimer was increased to achieve the aforementioned N/P ratios. EtBr was added to all solutions in the concentration of 126 µM. After 30 min reaction, the fluorescence intensity at excitation wavelength of 526 nm and emission at 592 nm was measured using Hitachi F 7000 Fluorescence Spectrophotometer (Tokyo, Japan). Reduced fluorescence (Ft/F0) was determined for each sample where Ft was the fluorescence of the dendrimer and siRNA complexes and F0 was the fluorescence of the siRNA alone (37). Agarose gel retardation assay of the above samples were also carried out. 15 µl of the complex solution was

mixed with 3 µl of gel loading dye (New England Biolabs, Ipswich, MA). These mixtures were then loaded on 4% Nu Sieve Agarose gel (Lonza, Rockland, ME) and allowed to run 1.5 h at 96V.

6.2.7 MALDI TOF Mass Spectroscopy

PPI-Paclitaxel conjugates were analyzed to determine their molecular masses by Matrix-assisted laser desorption/ionization time-of-flight (MALDI TOF) mass spectrometer (Applied Biosystems Voyager STR, Life Technologies, Grand Island, NY) by utilizing 2',4',6'-Trihydroxyacetophenone monohydrate (THAP) as matrix. Approximately 1 mg/mL of sample was mixed with the matrix at a ratio of 1:1 (v/v). 1 µl of mixture was spotted on a stainless steel plate and analyzed according to manufacturer instructions.

6.2.8 Atomic Force Microscopy

Atomic force microscopy (AFM) of the resulting nanoparticles was performed as previously described (271). Briefly, 5 µL aliquots of siRNA-dendrimer solutions were deposited on a freshly cleaved mica surface. After 5 min of incubation, the surface was rinsed with several drops of nanopure water (distilled water filtered through an ion filter with organic compounds also has been removed using a carbon filter resulting in analytical grade water), and dried under a flow of dry nitrogen. AFM images were obtained using Nanoscope IIIA AFM (Digital Instruments, Santa Barbara, CA) in tapping mode, operating in an ambient atmosphere.

6.2.9 Stability of the Complexes in Serum

Serum stability of naked siRNA and siRNA complexated with PPI dendrimer and protected by DTBP caging were investigated by incubating siRNA or PPI-siRNA complex in 50% human serum at 37 ºC. The concentration of siRNA in the final mixture was 4 µM. At each predetermined time interval (0, 5, 15, 30 min,1, 2, 3, 4, 5, 6, 7, 24 and 48 h), 50 µL of the mixture were withdrawn and stored at −20 ºC until gel electrophoresis was performed. In order to release siRNA from the complexes for gel electrophoresis, each sample was treated with 25 mM of reduced glutathione and 100 µM of poly(methacrylic acid) (PMAA). The aliquots from different incubation time periods were loaded onto 4% NuSieve 3:1 Reliant agarose gels (Lonza, Rockland, ME) in 1×TBE buffer (0.089 M Tris/Borate, 0.002 M EDTA, pH 8.3; Research Organic Inc., Cleveland, OH) and subjected to submarine electrophoresis. The gels were stained with ethidium bromide, digitally photographed, and scanned using Gel Documentation System 920 (NucleoTech, San Mateo, CA).

6.2.10 Cancer Cells and Animal Model

The ascitic fluid with cancer cells was obtained from the peritoneum area of the patients with ovarian cancer provided by the Cancer Institute of New Jersey. The samples were centrifuged for 20 min at 2000 g; the supernatant was discarded and cell pellets were consequently resuspended. The resuspended cells were cultured in RPMI 1640 media with L-glutamine (Lonza, Walkersvile, MD) supplemented with 15% fetal bovine serum (Invitrogen, Carlsbad, CA), 2.5 µg/ml insulin (Sigma, St. Louis, MO) and 1.2 mL/100 mL penicillin-streptomycin (Gibco, Grand Island, NY). Cells were grown at 37 °C in a

humidified atmosphere of 5% CO2 (v/v) in air. All of the experiments were performed on the cells in exponential growth phase. An animal model of human ovarian carcinoma xenografts was created as previously described (272-274). Briefly, human ascitic cells (2x106) were subcutaneously transplanted into the flanks of female athymic nu/nu mice. When the tumors reached a size of about 0.4 cm3 (15-20 days after transplantation), mice were treated intraperitoneally with saline (control) and different formulations: Dendrimer (PPI), LHRH, PPI-Scrambled siRNA, Paclitaxel (TAX), PPI-CD44 siRNA, PPI-TAX, LHRH-CD44 siRNA, LHRH-PPI-TAX, LHRH-PPI-TAX + LHRH-PPI-CD44 siRNA. The dose of TAX (2.5 mg/kg) in all drug-containing formulations corresponded to the maximum tolerated dose of this drug estimated in separate experiments as previously described (34, 273, 274). The animals were treated twice per week seven times within four weeks and tumor size was measured by a caliper. The weight of tumors was also measured at the end of the experiment after euthanizing the animals. Animal weight was evaluated every day during the treatment period. Changes in tumor size were used as an overall marker for antitumor activity. All animal experiments were carried out according to the approved protocol and Institutional guidance.

6.2.11 Cellular Internalization

Cellular internalization of fluorophore-labeled siRNA (siGLO Red, red fluorescence) and FITC labeled PPI (green fluorescence) complexes were analyzed by fluorescence (Olympus America Inc., Melville, NY) and laser scanning spectral confocal (Leica Miscrosystems Inc., Bannockburn, IL) microscopes. Prior to visualization, 9,000 cells

were plated in a 4 well-chambered slide (Nalge Nunc, Naperville, IL) and treated with the siRNA or PPI siRNA samples for 24 hours. The concentration of siRNA and PPI were 0.25 µM and 0.4 µM, respectively. After the treatment, the cells were washed with DPBS+0.05% tween 20 and fixed with 4% formaldehyde solution. DPBS (500 µL) was added to each chamber and slides were analyzed by a fluorescent or confocal microscope. To assess intracellular distribution of the particles and siRNA, eight optical sections, known as z series, were scanned sequentially along the vertical (z) axis from the top to the bottom of the cell.

6.2.12 Cell Invasion Assay

The cell invasion assay was performed using Corning 96 well HTS Transwell® permeable supports (Corning, Corning, NY). Briefly, the transwells were first coated with 0.2x Basal Membrane Extract (BME) (Trevigen, Gaithersburg, MD). 1·105 untreated cells and cells treated with tested substances were seeded in each well of the transwell plate for 24 hours. Some receiver plates were setup with serum-free 1640 RPMI medium while the remaining wells were setup with 1640 RPMI medium plus 15% fetal bovine serum (chemoattractant). The cultures were incubated for 24 hours. After 24 hours, the medium from the transwell inserts and the receiver plates were aspirated. 1x Calcein AM (Invitrogen, Molecular probes, Eugene, OR) solution prepared in Cell Dissociation Solution (Trevigen, Gaithersburg, MD) was added to each receiver plate. Transwell inserts were placed on the receiver plates and incubated for 1 hour in dark at room temperature. The transwell inserts were discarded and the receiver plates were read

using fluorescent plate reader with a 485 nm excitation and 520 nm emission wavelengths. Percent of cell invasion was calculated using a standard curve for different cell numbers.

6.2.13 *In Vitro* Cytotoxicity

A modified MTT (3-(4,5-dimethylthiazol-2-yl)-2,5-diphenyl tertrazolium bromide) assay was utilized to evaluate the cytotoxicity of the nanoparticles as previously described (255, 275) (19, 20). To measure the cytotoxicity, cells were separately incubated in a 96 well microtiter plate with serial dilutions of the tested formulations. Control cells received an equivalent volume of fresh medium. The duration of incubation was 24 hours. On the basis of the absorbance measurement, the cellular viability for each treatment was calculated. A decrease in cellular viability indicated an increase in cellular toxicity of the formulation.

6.2.14 LHRH Expression

The expression of genes encoding luteinizing hormone releasing hormone receptors (LHRHR) and β2-microglobulin (β2-m, internal standard) in cell and tissue homogenates was measured by Reverse Transcriptase-Polymerase Chain Reaction (RT-PCR) as previously described (34). The following pairs of primers were used: LHRHR – GAC CTT GTC TGG AAA GAT CC (sense), CAG GCT GAT CAC CAC CAT CA (antisense); β2-m – ACC CCC ACT GAA AAA GAT GA (sense), ATC TTC AAA CCT CCA TGA TG (antisense). Gene expression was calculated as the ratio of analyzed RT-PCR product to the internal

standard (β2-m). The expression of LHRHR gene was measured in human ovarian (primary solid tumor and malignant ascites), fallopian and endometrial tumors and different healthy visceral human organs (liver, kidney, spleen, heart, lung, brain, thymus and skeletal muscle). cDNA isolated from human organs was purchased from Clontech Laboratories, Inc (Mountain View, CA).

6.2.15 CD44 Expression

The expression of CD44 mRNA and protein was measured by Quantitative Reverse Transcriptase-Polymerase Chain Reaction (QRT-PCR) and immunocytochemistry, respectively. β-actin (internal standard) was also measured by QRT-PCR. RNA was isolated using an RNeasy kit (Qiagen, Valencia, CA) for in vitro and in vivo studies. First-strand cDNA was synthesized using High Capacity RNA-to-cDNA kit (Applied biosystems, Carlsbad, CA) using Veriti 96 well thermal cycler (Applied Biosystems, Carlsbad, CA). After synthesis, the reaction mixture was subjected to quantitative PCR, which was carried out by Step One Plus Real time PCR system (Applied Biosystems, Carlsbad, CA). The pairs of primers for CD44 (Hs_01075861) and β-actin (Hs_99999903) were obtained from Applied Biosystems (Carlsbad, CA). The PCR regimen was: 94°C/30 s, 55°C/1 min, 72°C/1 min for 30 cycles. A modified immunocytochemistry method (276) was used to analyze the expression of CD44 protein. Briefly, 1·105 cells were seeded to a 4 well chambered glass slide and allowed to incubate overnight with analyzed substances. Control cells received fresh media alone. The cells were then fixed with 4 % formaldehyde solution for 45 min. The fixed cells were washed thrice with PBS and then

incubated with 5% bovine serum albumin (BSA) in PBS for 20 min to suppress nonspecific binding of IgG. After another washing with PBS, the cells were incubated with anti-CD44 antibodies (570 ng/mL, Hermes, University of Iowa, Iowa City, IA) in 5% BSA in PBS for 1 h followed by 45 min incubation with Cy3®-conjugated secondary antibody (2.5 µg/mL, Goat, Invitrogen, Eugene,OR) in PBS with 5% BSA. The labeled cells were analyzed by a fluorescence microscope (Olympus America Inc., Melville, NY).

6.2.16 Immunohistochemistry

To visualize the expression of CD44 protein in vitro in tumor tissues after various treatments, immunohistochemical staining was conducted on paraffin-embedded slides. At the end of the experiments, the animals were euthanized, tumors were extracted, immediately fixed in 10% phosphate-buffered formalin. Samples were subsequently dehydrated and embedded in Paraplast®. Slides (5 µm) were deparaffiized in xylene for 5 min followed by progressive rehydration in 100%, 95%, 70%, and 50% ethanol for 3 min during each step. The slides were subjected to 10 mM citrate buffer, pH 6.0 for 5 minutes in a microwave at a power of 300 watt, washed twice with PBS and then incubated with 5% Bovine Serum Albumin (BSA) in PBS for 20 minutes to suppress nonspecific binding of IgG. Tissue slides were washed twice with PBS for 5 minutes. The cells and tissue slides were incubated with anti-CD44 (570 ng/mL, Hermes, University of Iowa, Iowa City, IA) in 5% BSA in PBS for 1 h followed by 45 minute incubation with Cy3® fluorophore- conjugated secondary antibody (2.5 µg/mL, Goat, Invitrogen, Eugene, OR) in PBS with 5% BSA. The nuclei were stained with 600 nM of 4, 6 diamidino-2-

phenylindole (DAPI) for 8 minutes. The labeled slides were analyzed by a fluorescence microscope (Olympus America Inc., Melville, NY). Red color represented CD44 protein; blue color represented cell nuclei.

6.2.17 Apoptosis Detection

Apoptosis induction in the tumor and other organs (liver, kidney, spleen, heart, lung and brain) was measured using the Cell Death Plus ELISA and TUNEL kits (F. Hoffmann-La Roche Ltd, Nutley, NJ) as previously described (223, 241, 277). For TUNEL assay, tissue slides were subjected to deparaffinzation, rehydration, peroxidase blocking and antigen retrieval as described above. TUNEL reaction mixture (50 µL) was added to the sections. The slides were incubated in the dark for 60 min at 37 ºC in a humidified atmosphere, washed with PBS, and mounted with cover slip using fluoromount mounting medium (Sigma, St Louis, MO). The sections were then analyzed using a fluorescence microscope (Olympus America Inc., Melville, NY). Another method of apoptosis detection - the Cell Death ELISA assay is based on the measurement of the enrichment of histone-associated DNA fragments (mononucleosomes and oligonucleosomes). Tumor and other tissues were homogenized and anti-histone and anti-DNA antibodies were used according to manufacturer instructions.

6.2.18 Statistical Analysis

Data were analyzed using descriptive statistics and single-factor ANOVA, and are presented as a mean ± SD from five to ten independent measurements. Five to ten

animals were used in each experimental group. We analyzed data sets for significance with Student's t test and considered P values of less than 0.05 as statistically significant.

6.3 Results

6.3.1 Synthesis and Characterization of Cytotoxic Tumor Targeted siRNA Nanocomplexes

In order to synthesize a cytotoxic tumor-targeted nanocarrier, an anticancer drug (cytotoxic agent), TAX, was conjugated to the dendrimer via biodegradable succinic acid spacer while a cancer targeting moiety, LHRH peptide, was bound to the distal end of non-biodegradable PEG polymer that surrounds the DTBP-caged dendrimer **(Fig. 1A)**. The MALDI TOF mass spectrometry confirmed that TAX was really conjugated to the dendrimer with 8099 of mass/charge (m/z) ratio resulting in the strong peak of the subsequent complex with at 8122 m/z **(Fig. 1C)**. The complex formation between the synthesized cytotoxic cancer targeted PPI carriers and siRNA were studied by ethidium bromide (EtBr) and agarose gel retardation assays **(Fig.1B and D)**. It was found that when the N/P ratio exceeded 0.75 related units, all used siRNA was completely conjugated to the carrier(s) resulting in disappearing of a small band of naked siRNA on gel electrophoresis **(Fig. 1B)**. At the same time, binding of siRNA to the dendrimer carrier at N/P>0.5 led to the quenching of EtBr fluorescence **(Fig. 1B)**. AFM data **(Fig. 1E)** showed that synthesized carrier condensated siRNA into stable compact nanoparticles with average diameter of 100 - 200 nm. Incubation of naked siRNA and PPI-siRNA complexes in 50% human serum at 37 ºC demonstrated that the condensation of siRNA and dendrimers into

nanoparticles, caging and PEGylation significantly increased the stability of siRNA. We found that the band of naked siRNA on the agarose gel almost completely disappeared after 6-7 h of incubation reflecting the degradation of siRNA. In contrast, the siRNA-PPI band did not decrease its intensity even after 48 h of incubation. These data indicate an increase in the stability of siRNA after conjugation of PPI dendrimer carriers.

6.3.2 Expression of CD44 and LHRH in Cancer Cells

It was found that CD44 mRNA and protein were overexpressed in primary and metastatic tumor tissues isolated from patients with different types of gynecological cancers and in cancer cells isolated from malignant ascites **(Fig. 2A and B)**. Moreover, the expression was significantly higher in metastatic tissues when compared with primary tumors (**Fig. 2A**, $P < 0.05$). Staining with anti-CD44 antibodies followed by a fluorescence microscopy analysis showed that the overexpressed CD44 proteins were localized predominately in the plasma membrane and partially in the cytoplasm of cancer cells **(Fig. 3)**. It was also found that endometrial, fallopian, ovarian (primary and metastatic) tumors overexpressed LHRH receptors; in contrast, in the healthy liver, kidney, spleen, heart and lung tissues, detectable levels of LHRHR was not registered **(Fig. 2C)**. Ovarian cancer metastatic cells isolated from malignant ascites obtained from patients with advanced ovarian carcinoma were treated with non-targeted and LHRH receptor-targeted PPI-siRNA complexes. It was found that naked siRNA as well as PPI complexes with siRNA with scrambled sequence did not change the expression of CD44 mRNA **(Fig. 2B)**. In contrast, incubation of cells with PPI-siRNA complexes significantly (P

< 0.05) decreased the overexpression. Furthermore, LHRH tumor-targeted PPI-siRNA complexes reduced the expression much more efficiently (P < 0.05) when compared with non-targeted system (PPI-CD44 siRNA). In fact, the expression of CD44 mRNA in ascitic cells treated with PPI-siRNA decreased down to 53.5% when compared with control cells **(Fig. 2B)**. Targeting of the complex specifically to ovarian cancer cells by LHRH peptide significantly decreased the overexpression (down to 18.6% of control). In other words, the overexpression of CD44 in cells treated with cancer-targeted complexes was almost three fold lower when compared with cells treated with non-targeted complexes. A high efficiency of LHRH-PPI-siRNA in suppression of targeted protein was confirmed by direct measurement of the expression of CD44 protein **(Fig. 3)**.

6.3.3 Cytotoxicity and Cell Invasiveness

Data obtained show that tumor targeted LHRH-PPI-siRNA conjugate significantly suppressed the invasiveness of cancer cells isolated from malignant ascites **(Fig. 4A)**. It should be stressed that similar effect was registered in the cells incubated both with fresh media alone and with media supplemented with a chemoattractant. In both cases, the percentage of cell invasion was 6-7–fold inhibited. The incubation of ascitic cells with naked siRNA targeted to CD44 mRNA and with siRNA with a scrambled sequence delivered by PPI dendrimer did not demonstrate toxicity in maximum available concentrations **(Fig. 4B)**. Free non-bound TAX in concentration of 55 µM led to the death of around 50-60% of cells. Therefore, this concentration of TAX was close to its

IC50 dose in ascitic cells. Conjugation of TAX to non-targeted PPI dendrimer enhanced its cytotoxic effect leading to the 1.6-fold decrease in cellular viability under the same drug concentration. PPI-siRNA conjugates induced a cell death comparable with that originated by PPI-TAX. Combination of siRNA and TAX in one dendrimer-based delivery system substantially increased the cytotoxicity of TAX leading to the further decrease in cellular viability down to 2.5-fold when compared with free non-bound TAX in the same concentration. Finally, the use of LHRH peptide to enhance cellular internalization of the LHRH-PPI-TAX-siRNA complex specifically by cancer cells enhanced the cytotoxicity of the conjugate. The viability of ascitic cells in this case was decreased almost 10-fold when compared with control cells, more than 5-fold when compared with free TAX and more than 2-fold when compared with non-targeted PPI-TAX-siRNA complex **(Fig. 4B)**.

6.3.4 Cellular Internalization of siRNA

An increase in the cytotoxicity and efficiency of the suppression of targeted mRNA/protein by CD44 siRNA delivered by PPI dendrimer was attributed to its higher internalization by cancer cells. Analysis of cellular internalization and distribution of naked and conjugated siRNA **(Fig. 5)** showed that naked siRNA poorly penetrate cancer cells leading to high red fluorescence of labeled siRNA in the medium and very low fluorescence inside the cell **(Fig. 5A)**. In contrast, high level of both green (PPI dendrimer labeled by FITC) and red fluorescence (siRNA) was registered in cellular cytoplasm when siRNA was conjugated with the dendrimer. This fact indicates that (1) PPI dendrimer substantially enhanced cellular internalization of siRNA and (2) siRNA delivered by

dendrimer was separated (released) from the carrier and accumulated predominately in the cytoplasm. Serial confocal microscope images (z-series) showed that distribution of siRNA was uniform from the top to the bottom of the cell **(Fig. 5C)**. These data clearly show the high efficiency of cellular penetration of siRNA delivered by PPI dendrimer and also successful release of siRNA from the complex inside the cells.

6.3.5 *In Vivo* Antitumor Activity

In order to support in vitro findings and analyze the antitumor efficiency of the synthesized complexes, the following in vivo experiments were carried out in mice bearing xenografts of human cancer cells isolated from malignant ascites from patients with advanced ovarian carcinoma. Mice were treated seven times twice per week within four weeks starting from day 0 when tumor volume reached 0.4 cm^3. Expression of CD44 protein and apoptosis induction in tumor tissues isolated at the end of the experiments as well as tumor volume was measured. The animals were treated with the proposed formulations. Corresponding controls were used. The concentration of TAX in all drug-containing formulations was equal to 2.5 mg/kg. The experiments were terminated if tumor size reached the maximum allowed by the Institutional Animal Care and Use Committee approved animal protocol (~2 cm^3 that corresponded to approximately 10% of body mass). The data showed that either LHRH-PPI dendrimer (without drug and siRNA), or free TAX, or PPI-TAX or LHRH-PPI-TAX did not change significantly the expression of CD44 protein **(Fig. 6)**. At the same time, complexes of CD44 siRNA with tumor-targeted dendrimers containing TAX (LHRH-PPI-CD44 siRNA +

LHRH-PPI-TAX) almost completely inhibited the expression of targeted protein (**Fig. 6**, lower panel). Analysis of cell death induction by two independent methods showed that in agreement with the in vitro data conjugation of TAX to PPI dendrimer significantly enhanced drug antitumor activity (**Fig. 7A and B**). Further enhancement was achieved by employing LHRH peptide as a tumor-targeting moiety. Finally, suppression of CD44 protein by siRNA delivered by PPI dendrimer dramatically enhanced cell death inducing ability of the proposed complexes. Consequently, such enhancements led to the more effective suppression of tumor growth by the tested formulations **(Fig. 8)**. The data obtained show that tumors in control animals (treated with saline) as well as those treated with PPI dendrimer alone, LHRH, PPI-siRNA with a scrambled sequence reached maximum allowed by the institutional policy size around 10 days after beginning of the treatment (**Fig. 8**, curves 1-4). As expected, free unbound TAX limited tumor growth and the maximal tumor size was reached at day 17 (**Fig. 8**, curve 5). PPI-siRNA complexes and PPI-TAX conjugates showed more pronounced antitumor effect when compared with free TAX (**Fig. 8**, curves 6 and 7) and slow down tumor growth (maximum tumor size was reached on day 24). Consistently with in vitro data, targeting of PPI complexes to ovarian tumor by LHRH peptide significantly enhanced antitumor activity of TAX and CD44 siRNA (**Fig. 8**, curves 8 and 9, respectively). Finally, the combination of the anticancer drug (TAX), siRNA targeted to CD44 mRNA, and tumor-specific targeting agent (LHRH peptide) delivered by the nanocarrier (PPI dendrimer) led to the almost complete shrinkage of the tumor within the 28 day studied period (**Fig. 8**, curve 10).

6.4 Discussion

In the present investigation, we discovered several interesting facts and proposed new approaches for the treatment of ovarian carcinoma. We found that a marker for so called “cancer stem cells” - CD44 mRNA and protein is overexpressed in the plasma membrane of cancer cells isolated from patients with gynecological malignancies. Moreover, this overexpression is more pronounced in metastatic cells when compared with the cells from primary tumor. One can hypothesize that CD44 is involved in the development of resistance and invasiveness of cancer cells. Several facts support these suggestions. Previously, we found that the expression of CD44 correlates with the expression of the main drug efflux pump – P-glycoprotein and resistance to chemotherapy (268, 269, 276). Moreover, current in vitro and in vivo data showed that the suppression of CD44 protein enhances the activity of the anticancer drug – paclitaxel, initiates and promotes cell death by apoptosis and led to the tumor shrinkage. This finding also indicates that CD44 might be involved in the development of metastases and its expression correlates with cell invasiveness. Present data obtained using cell invasion assay support this suggestion and show that the suppression of CD44 protein dramatically decreases the invasiveness of malignant cells. Consequently, it is understandable that CD44 protein may represent an attractive target for chemotherapy both as a primary target for cell death induction and also and most probably as an enhancer of the specific anticancer activity of the main anticancer drugs. In order to validate the hypothesis, we constructed a novel dendrimer-based delivery system that is

capable of simultaneously inducing cell death and suppressing cellular resistance specifically in tumor cells.

The proposed multifunctional and multicomponent delivery system includes PPI dendrimer as a carrier, paclitaxel as an anticancer drug/cell death inducer, LHRH peptide as a cancer-specific targeting moiety, and siRNA targeted to CD44 mRNA as an ovarian cancer stem cells cell death enhancer. In order to increase the stability of the proposed drug-siRNA combination, complexes of siRNA with dendrimers were protected from the harsh extracellular environment by caging with DTBP. We previously used such caging of PPI dendrimer-siRNA complexes and showed its high efficiency in increasing the stability of complexated siRNA in plasma (248). Detailed characterization of resulting complexes showed that indeed siRNA and the carrier were condensed into spherical nanoparticles with an increased stability.

Previously, we revealed that similar dendrimer-based system effectively delivered and released inside the cells different anticancer drugs including Paclitaxel (271, 278). Present data showed that siRNA was also effectively delivered into the cytoplasm of cancer cells by the proposed nanosystem and separated (released) from the carrier in the cytoplasm. This separation was possible due in part to lower pH in the cytoplasm and cellular organelles that transporting internalized system which decreased positive charge of the carrier and released electrostatically bound siRNA. So called proton sponge effect (279) might also be responsible in part for the effective release of siRNA into the cytoplasm. Moreover, the distribution of siRNA in the cytoplasm was

homogenous in all directions including so-called z-section from the top to the bottom of the cells. Our present data show that delivered and released siRNA possessed its specific activity and effectively suppressed the targeted CD44 mRNA and protein. We found that the suppression of CD44 protein significantly enhanced the ability of TAX of inducing cell death and the proposed complex delivery system demonstrated high antitumor efficiency in vitro and in vivo.

6.5 Conclusion

In summary, we were able to verify the hypothesis and show that suppression of CD44 protein decreases the invasiveness of cancer cells and enhances the efficiency of cell induction activity of the anticancer drug in cancer cells isolated from malignant ascites from patients with advanced ovarian carcinoma. It seems that the proposed cancer targeted complex chemotherapy approach and multifunctional nanocarrier-based delivery system especially designed to effectively suppress invasiveness and kill cancer stem cells may substantially enhance efficiency of therapy of ovarian cancer and possibly other gynecologic malignancies, limiting at the same time adverse side effect of chemotherapy on healthy tissues.

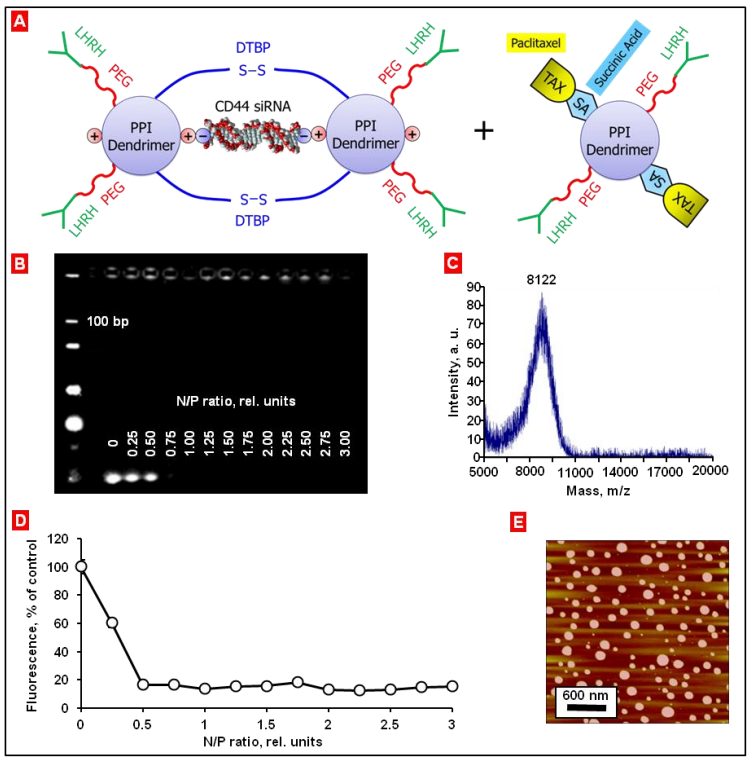

Fig.6.1 Complex cancer targeted drug delivery system. **A**, Schema of the delivery system containing poly(propylenimine) (PPI) dendrimer as a carrier; paclitaxel (TAX) as an anticancer drug, conjugated to the dendrimer via succinic acid (SA) spacer; luteinizing-hormone-releasing hormone (LHRH) as a cancer targeting moiety, conjugated to the dendrimer via poly(ethylene glycol) (PEG) spacer; siRNA targeted to CD44 mRNA and caged by DTPB. **B**, Representative gel electrophoresis image of siRNA complexated with PPI dendrimer at different nitrogen to phosphate (N/P) ratios from 0 (no PPI dendrimer) to 3.00. **C**, representative image of matrix-assisted laser desorption/ionisation-time of flight (MALDI-TOF) mass spectrometry analysis of PPI-TAX conjugate. The most abundant peak [M+Na] was observed at mass M=8122 indicating that paclitaxel was conjugated with the PPI G5 dendrimer (M=7162). **D**, Quantitative analysis of ethidium bromide displacement assay for PPI dendrimer-siRNA complexes. The complexes were synthesized with 0.4 µM siRNA and 126 µM ethidium bromide. The concentration of PPI dendrimer was increased to obtain N/P ratios from 0 (no PPI dendrimer) to 3. A decrease in fluorescence indicates binding of siRNA to PPI dendrimer. **E**, AFM images of nanoparticles resulted from the complex formation between the carrier and siRNA.

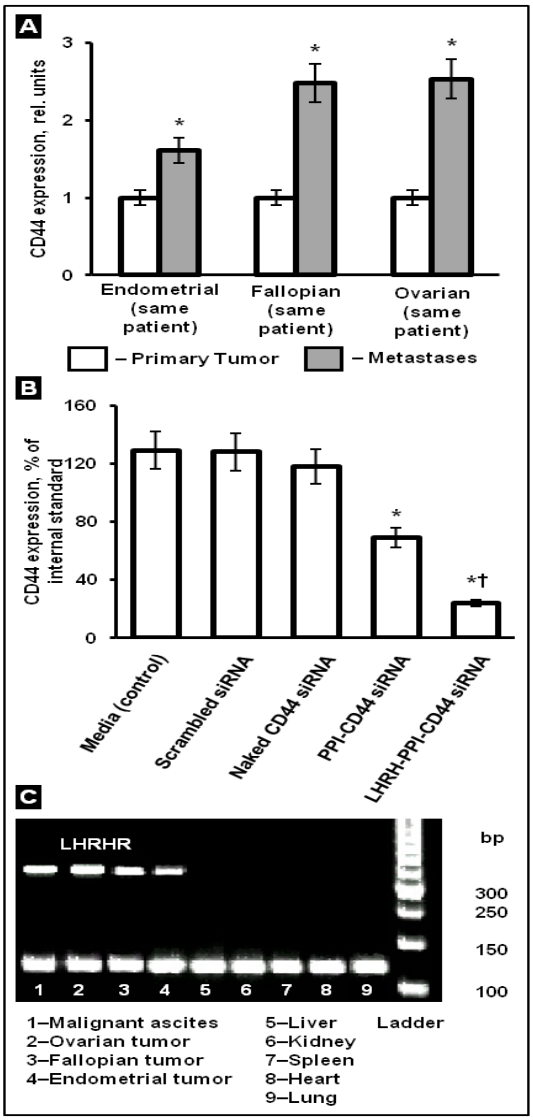

Fig.6.2: Expression of CD44 and LHRHR mRNA. A, Expression of CD44 mRNA in tissues isolated from primary tumor and metastases in same patients with different types of gynecological cancers. Means ± SD are shown. *P < 0.05 when compared with primary tumor. B, Expression of CD44 mRNA in cancer cells isolated from malignant ascites obtained from patients with advanced ovarian carcinoma. Cells were incubated with substances indicated. Means ± SD are shown. *P < 0.05 when compared with control (cells incubated with fresh media); †P < 0.05 when compared with non-targeted complexes. C, Expression of LHRH receptors in gynecological tumors and healthy tissues.

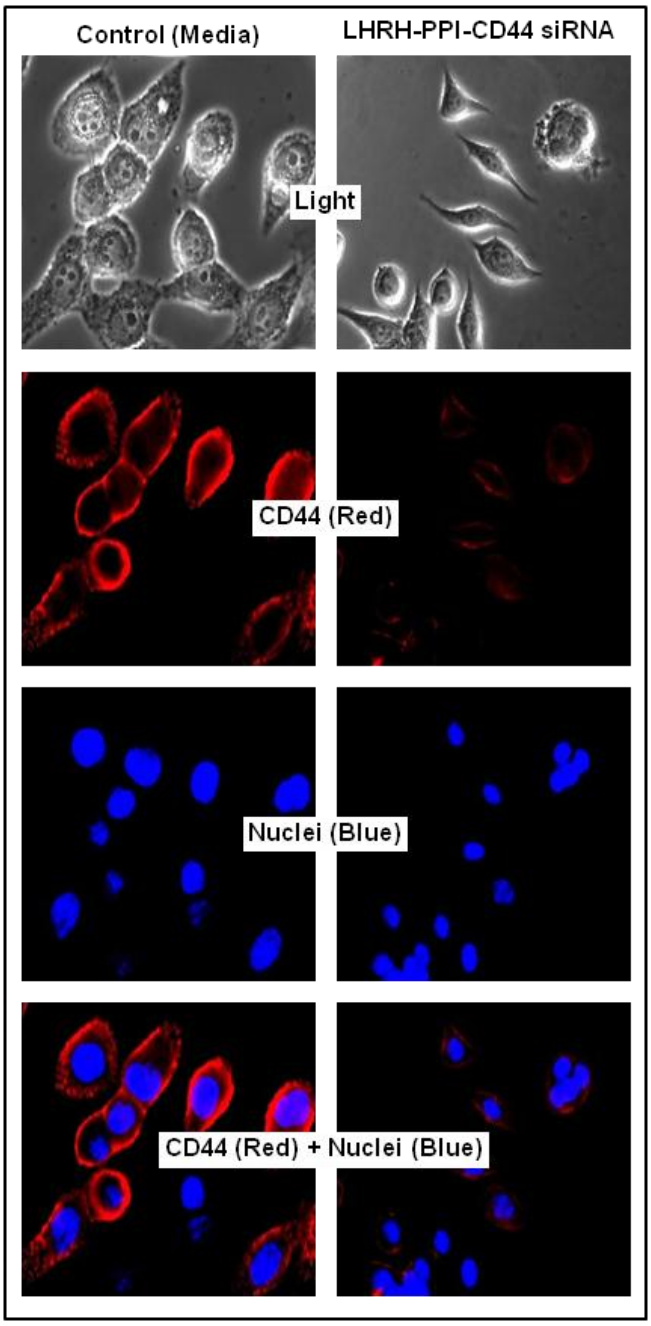

Fig.6.3: Expression of CD44 protein (immunocytochemistry) in human cancer cells isolated from malignant ascites from patient with advanced ovarian carcinoma. Cells were treated with PPi-siRNA-LHRH nanocomplex. Untreated cells received media alone. Representative light and fluorescence microscope images. CD44 protein was stained using primary anti-CD44 antibody and secondary antibody conjugated with Cy3® fluorofor. Nuclei were stained with DAPI nuclear dye. Red color represents CD44 protein; blue color represents cell nuclei.

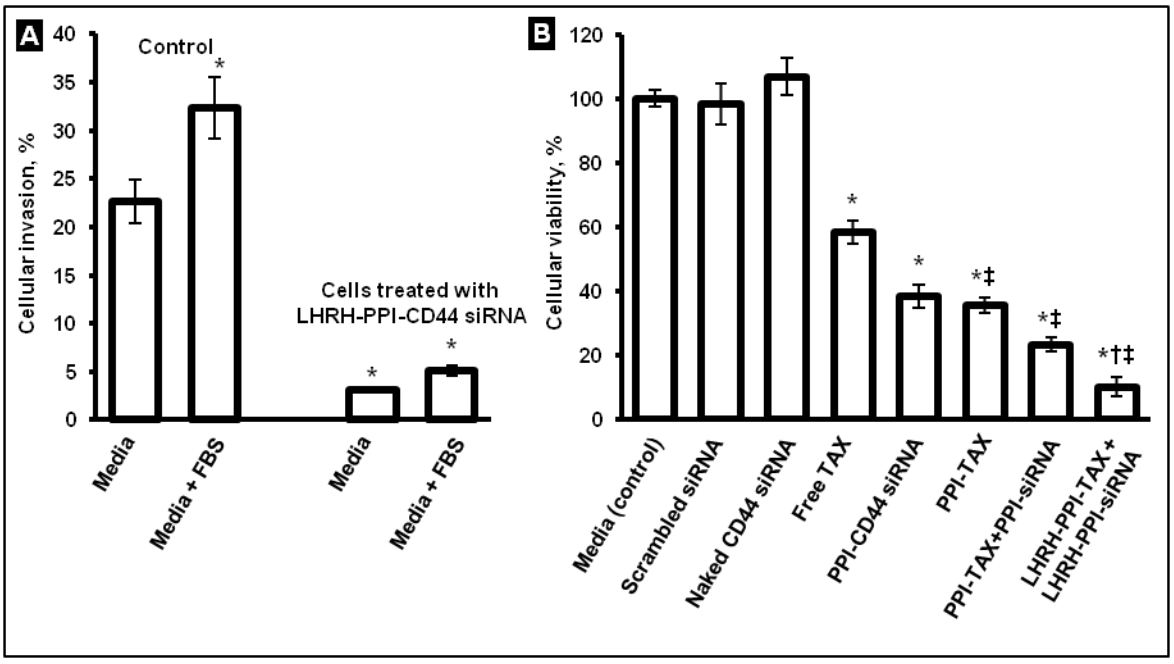

Fig. 6.4: Invasion and viability of cancer cells isolated from malignant ascites obtained from patients with advanced ovarian carcinoma. A, Cell invasion was measured in the cells growing with media alone or media containing 15% fetal bovine serum (FBS, chemoattractant) and treated with LHRH -PPI-CD44 siRNA. B, Influence of different substances on cellular viability. Cells were incubated with substances indicated. Means ± SD are shown. *P < 0.05 when compared with control (cells incubated with fresh media); †P < 0.05 when compared with non-targeted complexes; ‡P < 0.05 when compared with free non-bound TAX.

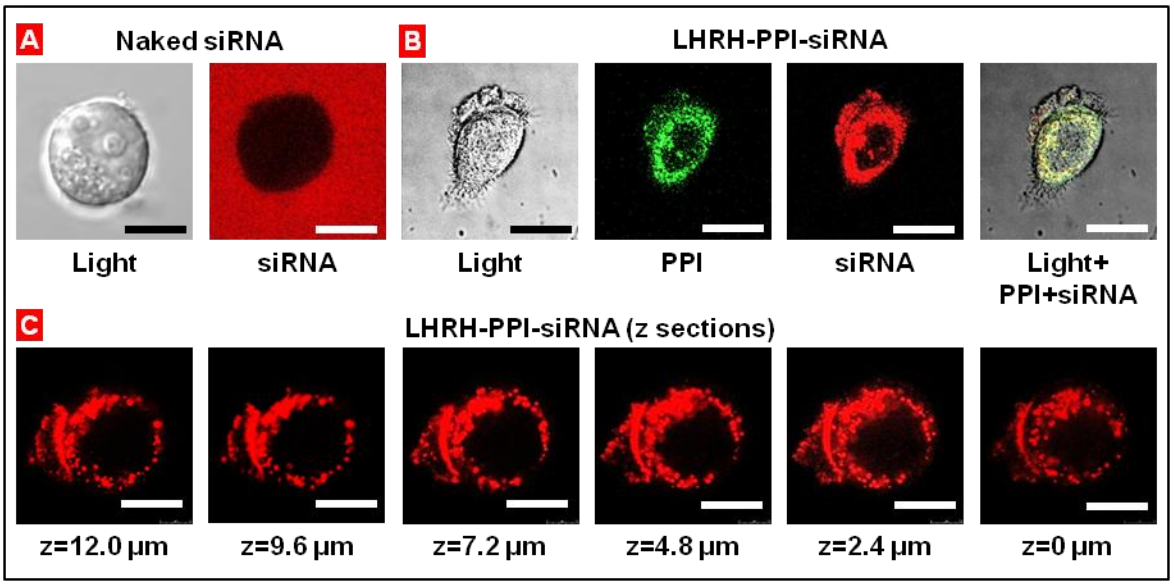

Fig.6.5: Cellular internalization of naked siRNA and siRNA delivered by cancer targeted delivery system. A, representative images of naked fluorophore-labeled siRNA (siGLO Red, red fluorescence) incubated with ovarian cancer cells. B, representative images of ovarian cancer cells incubated with fluorescently labeled siRNA (siGLO Red, red fluorescence) conjugated to cancer targeted PPI dendrimer labeled with FITC (green fluorescence). Superimposition of red (siRNA) and green (dendrimer) fluorescence images gives yellow color. C, Representative confocal microscopy images of ovarian cancer cells incubated with LHRH-PPI-siRNA (z-series, from the top of the cell to the bottom). Red color represents siRNA. Scale bar – 15 µm.

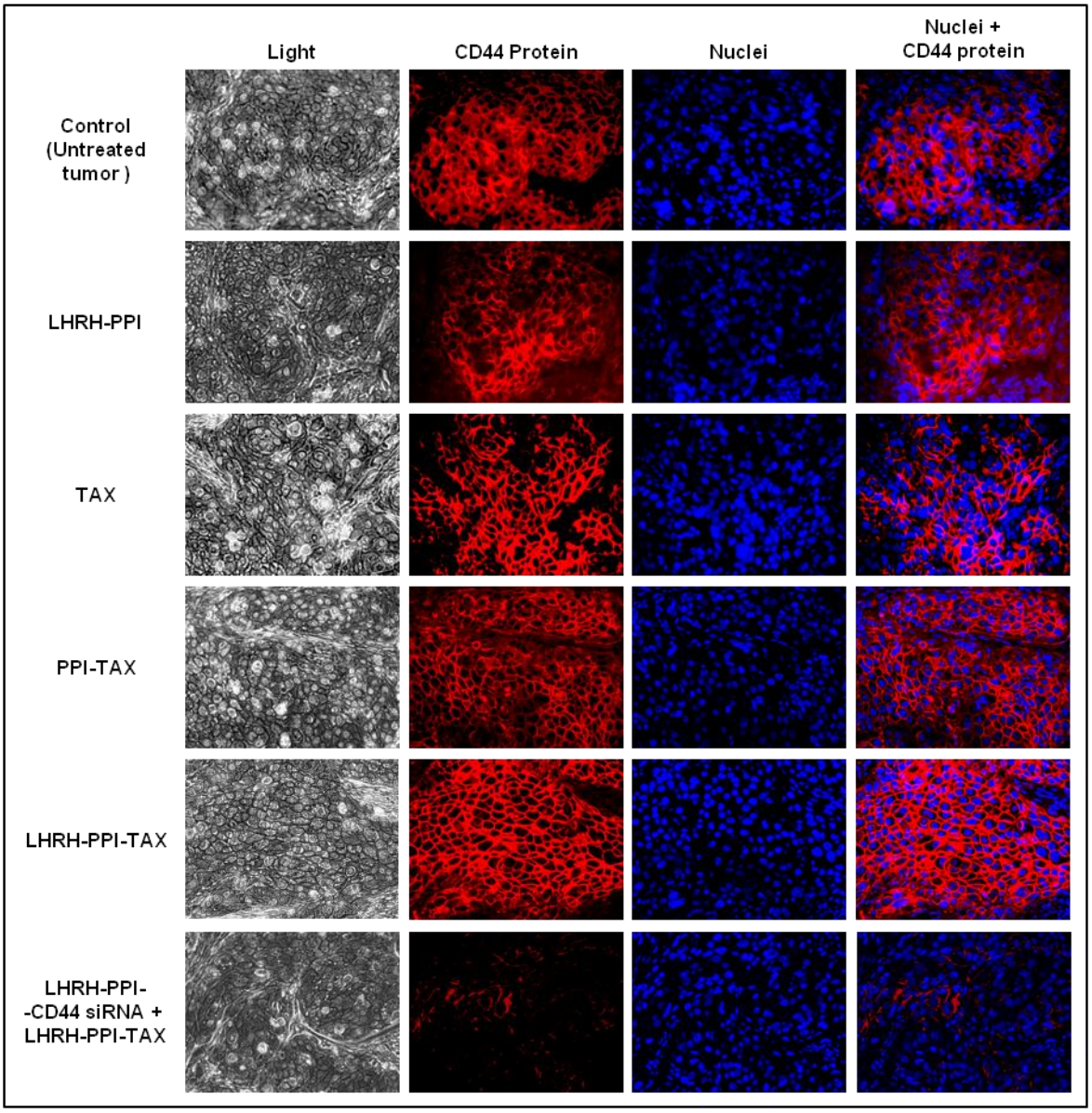

Fig.6.6: Expression of CD44 protein (immunohistochemistry) in tumor tissues form mice bearing xenografts of human cancer cells isolated from malignant ascites from patient with advanced ovarian carcinoma. Mice were treated seven times twice per week within four weeks starting from the day 0 with the indicated formulations. Representative fluorescence images are shown.

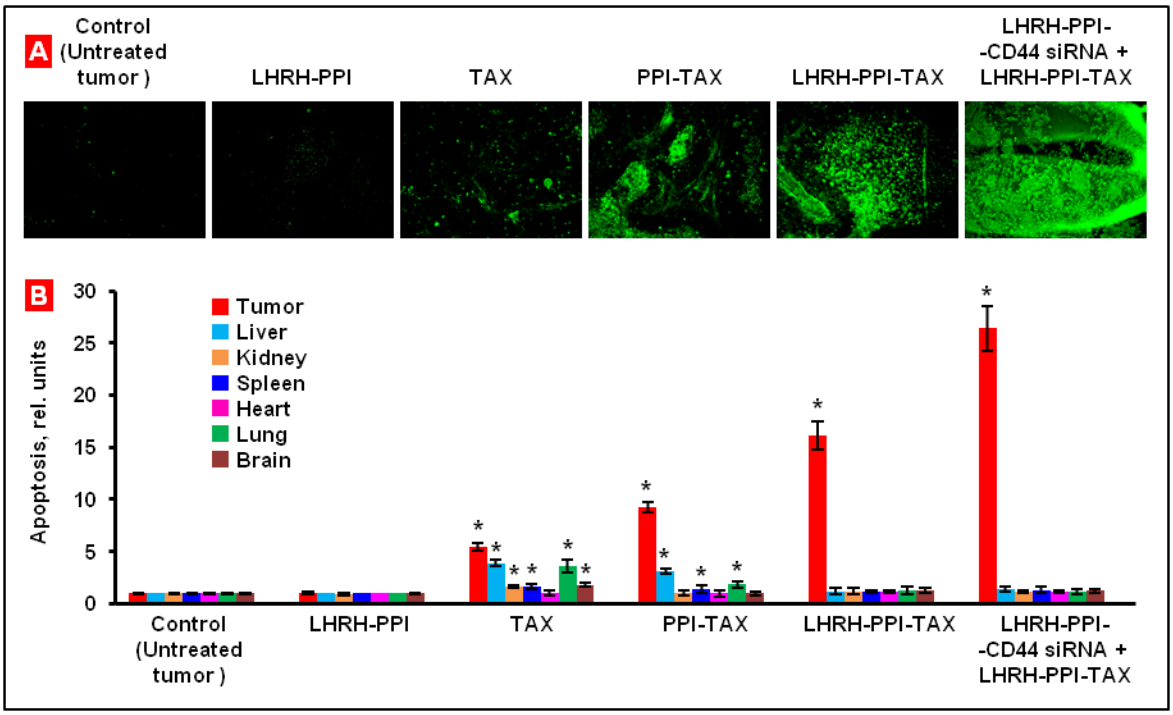

Fig.6.7: Apoptosis induction in tumor and other organs at the end of the experiments (day 28 of the treatment) of mice bearing xenografts of human cancer cells isolated from malignant ascites from patient with advanced ovarian carcinoma. Mice were treated seven times twice per week within four weeks starting from the day 0 with the indicated formulations. A, Representative fluorescence microscopy images of tumor tissue slides labeled by TUNEL. B, The enrichment of histone-associated DNA fragments (mono- and oligonucleosomes) per gram tissue in the tumor and different organs. Values in control animals were set to unit 1, and the degree of apoptosis was expressed in relative units. Means ± SD are shown. *P < 0.05 when compared with control.

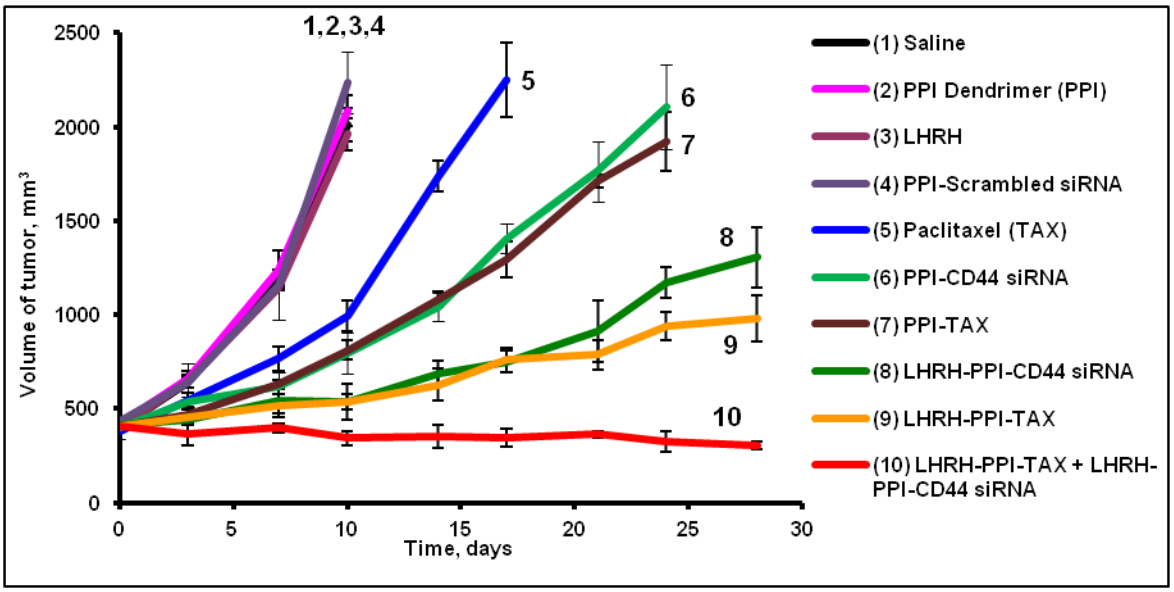

Fig.6.8: Tumor volume in mice bearing xenografts of human cancer cells isolated from malignant ascites from patient with advanced ovarian carcinoma. Mice were treated seven times twice per week within four weeks starting from the day 0 with the indicated formulations. Means ± SD are shown.

7 REFERENCES

1. Stewart BW, Kleihues P. World cancer report world cancer report. World Health Organization Press, Geneva,. . (2003).

2. Siegel R, Ward E, Brawley O, Jemal A. Cancer statistics, 2011: The impact of eliminating socioeconomic and racial disparities on premature cancer deaths. CA Cancer J Clin. 2011 Jul-Aug;61(4):212-36.

3. Sinha R, Kim GJ, Nie S, Shin DM. Nanotechnology in cancer therapeutics: Bioconjugated nanoparticles for drug delivery. Mol Cancer Ther. 2006 Aug;5(8):1909-17.

4. Cho K, Wang X, Nie S, Chen ZG, Shin DM. Therapeutic nanoparticles for drug delivery in cancer. Clin Cancer Res. 2008 Mar 1;14(5):1310-6.

5. Maeda H. The enhanced permeability and retention (EPR) effect in tumor vasculature: The key role of tumor-selective macromolecular drug targeting. Adv Enzyme Regul. 2001;41:189-207.

6. Larsen AK, Escargueil AE, Skladanowski A. Resistance mechanisms associated with altered intracellular distribution of anticancer agents. Pharmacol Ther. 2000 Mar;85(3):217-29.

7. Royal society and royal academy of engineering report. nanoscience andnanotechnologies: Opportunities and uncertainties [Internet].; 2004. Available from: http:// www.nanotec.org.uk/finalReport.htm.

8. Ng CT, Li JJ, Bay BH, Yung LY. Current studies into the genotoxic effects of nanomaterials. J Nucleic Acids. 2010 Sep 21;2010:947859.

9. Norppa H, Catalan J, Falck G, Hannukainen K, Siivola K, Savolainen K. Nano-specific genotoxic effects. J Biomed Nanotechnol. 2011 Feb;7(1):19.

10. Shah V, Taratula O, Garbuzenko OB, Patil ML, Savla R, Zhang M, et al. Genotoxicity of different nanocarriers: Possible modifications for the delivery of nucleic acids. Curr Drug Discov Technol. 2012 May 4.

11. Singh N, Manshian B, Jenkins GJ, Griffiths SM, Williams PM, Maffeis TG, et al. NanoGenotoxicology: The DNA damaging potential of engineered nanomaterials. Biomaterials. 2009 Aug;30(23-24):3891-914.

12. Stone V, Johnston H, Schins RP. Development of in vitro systems for nanotoxicology: Methodological considerations. Crit Rev Toxicol. 2009;39(7):613-26.

13. Garbuzenko OB, Saad M, Betigeri S, Zhang M, Vetcher AA, Soldatenkov VA, et al. Intratracheal versus intravenous liposomal delivery of siRNA, antisense oligonucleotides and anticancer drug. Pharm Res. 2009 Feb;26(2):382-94.

14. Huang Y, Gao H, Gou M, Ye H, Liu Y, Gao Y, et al. Acute toxicity and genotoxicity studies on poly(epsilon-caprolactone)-poly(ethylene glycol)-poly(epsilon-caprolactone) nanomaterials. Mutat Res. 2010 Feb;696(2):101-6.

15. Moreira S, Silva NB, Almeida-Lima J, Rocha HA, Medeiros SR, Alves C,Jr, et al. BC nanofibres: In vitro study of genotoxicity and cell proliferation. Toxicol Lett. 2009 Sep 28;189(3):235-41.

16. Yang H, Liu C, Yang D, Zhang H, Xi Z. Comparative study of cytotoxicity, oxidative stress and genotoxicity induced by four typical nanomaterials: The role of particle size, shape and composition. J Appl Toxicol. 2009 Jan;29(1):69-78.

17. Dayan N, Shah V, Minko T. Genotoxic potential evaluation of a cosmetic insoluble substance by the micronuclei assay. J Cosmet Sci. 2011 Jan-Feb;62(1):29-39.

18. [Internet]. Available from: http://www.ovariancancer.org/about-ovarian-cancer/statistics/.

19. Cannistra SA. Cancer of the ovary. N Engl J Med. 2004 Dec 9;351(24):2519-29.

20. Lane D, Matte I, Rancourt C, Piche A. The prosurvival activity of ascites against TRAIL is associated with a shorter disease-free interval in patients with ovarian cancer. J Ovarian Res. 2010 Jan 18;3:1.

21. Berkenblit A, Cannistra SA. Advances in the management of epithelial ovarian cancer. J Reprod Med. 2005 Jun;50(6):426-38.

22. Masiakos PT, MacLaughlin DT, Maheswaran S, Teixeira J, Fuller AF,Jr, Shah PC, et al. Human ovarian cancer, cell lines, and primary ascites cells express the human mullerian inhibiting substance (MIS) type II receptor, bind, and are responsive to MIS. Clin Cancer Res. 1999 Nov;5(11):3488-99.

23. Mills GB, May C, Hill M, Campbell S, Shaw P, Marks A. Ascitic fluid from human ovarian cancer patients contains growth factors necessary for intraperitoneal growth of human ovarian adenocarcinoma cells. J Clin Invest. 1990 Sep;86(3):851-5.

24. Mills GB, May C, McGill M, Roifman CM, Mellors A. A putative new growth factor in ascitic fluid from ovarian cancer patients: Identification, characterization, and mechanism of action. Cancer Res. 1988 Mar 1;48(5):1066-71.

25. Xu Y, Gaudette DC, Boynton JD, Frankel A, Fang XJ, Sharma A, et al. Characterization of an ovarian cancer activating factor in ascites from ovarian cancer patients. Clin Cancer Res. 1995 Oct;1(10):1223-32.

26. Abdollahi T, Robertson NM, Abdollahi A, Litwack G. Identification of interleukin 8 as an inhibitor of tumor necrosis factor-related apoptosis-inducing ligand-induced apoptosis in the ovarian carcinoma cell line OVCAR3. Cancer Res. 2003 Aug 1;63(15):4521-6.

27. Radke J, Schmidt D, Bohme M, Schmidt U, Weise W, Morenz J. -Cytokine level in malignant ascites and peripheral blood of patients with advanced ovarian carcinoma-. Geburtshilfe Frauenheilkd. 1996 Feb;56(2):83-7.

28. Ahmed N, Riley C, Oliva K, Rice G, Quinn M. Ascites induces modulation of alpha6beta1 integrin and urokinase plasminogen activator receptor expression and associated functions in ovarian carcinoma. Br J Cancer. 2005 Apr 25;92(8):1475-85.

29. Stadlmann S, Raffeiner R, Amberger A, Margreiter R, Zeimet AG, Abendstein B, et al. Disruption of the integrity of human peritoneal mesothelium by interleukin-1beta and tumor necrosis factor-alpha. Virchows Arch. 2003 Nov;443(5):678-85.

30. Singla AK, Garg A, Aggarwal D. Paclitaxel and its formulations. Int J Pharm. 2002 Mar 20;235(1-2):179-92.

31. de Fougerolles A, Vornlocher HP, Maraganore J, Lieberman J. Interfering with disease: A progress report on siRNA-based therapeutics. Nat Rev Drug Discov. 2007 Jun;6(6):443-53.

32. Naor D, Sionov RV, Ish-Shalom D. CD44: Structure, function, and association with the malignant process. Adv Cancer Res. 1997;71:241-319.

33. Bourguignon LY, Peyrollier K, Xia W, Gilad E. Hyaluronan-CD44 interaction activates stem cell marker nanog, stat-3-mediated MDR1 gene expression, and ankyrin-regulated multidrug efflux in breast and ovarian tumor cells. J Biol Chem. 2008 Jun 20;283(25):17635-51.

34. Dharap SS, Wang Y, Chandna P, Khandare JJ, Qiu B, Gunaseelan S, et al. Tumor-specific targeting of an anticancer drug delivery system by LHRH peptide. Proc Natl Acad Sci U S A. 2005 Sep 6;102(36):12962-7.

35. Maurici D, Aardema M, Corvi R, Kleber M, Krul C, Laurent C, et al. Genotoxicty and mutagenicity. Altern Lab Anim. 2005 Jul;33 Suppl 1:117-30.

36. Genotoxicity [Internet].; June 20, 2011. Available from: http://alttox.org/ttrc/toxicity-tests/genotoxicity/.

37. U.S. Department of Health and Human Services Food and Drug Administration. S2(R1) genotoxicity testing and data interpretation for pharmaceuticals intended for human use. June 2012.

38. Corvi R, Albertini S, Hartung T, Hoffmann S, Maurici D, Pfuhler S, et al. ECVAM retrospective validation of in vitro micronucleus test (MNT). Mutagenesis. 2008 Jul;23(4):271-83.

39. OECD guideline for the testing of chemical. draft proposal for a new guideline 487: In vitro mammalian cell micronucleus test (MNvit). . November 2009.

40. Fenech M. The in vitro micronucleus technique. Mutat Res. 2000 Nov 20;455(1-2):81-95.

41. Kirsch-Volders M. Towards a validation of the micronucleus test. Mutat Res. 1997 Aug 1;392(1-2):1-4.

42. Parry JM, Sors A. The detection and assessment of the aneugenic potential of environmental chemicals: The european community aneuploidy project. Mutat Res. 1993 May;287(1):3-15.

43. Fenech M, Morley AA. Cytokinesis-block micronucleus method in human lymphocytes: Effect of in vivo ageing and low dose X-irradiation. Mutat Res. 1986 Jul;161(2):193-8.

44. Farooqi Z, Darroudi F, Natarajan AT. The use of fluorescence in situ hybridization for the detection of aneugens in cytokinesis-blocked mouse splenocytes. Mutagenesis. 1993 Jul;8(4):329-34.

45. Eastmond DA, Tucker JD. Identification of aneuploidy-inducing agents using cytokinesis-blocked human lymphocytes and an antikinetochore antibody. Environ Mol Mutagen. 1989;13(1):34-43.

46. Eastmond DA, Pinkel D. Detection of aneuploidy and aneuploidy-inducing agents in human lymphocytes using fluorescence in situ hybridization with chromosome-specific DNA probes. Mutat Res. 1990 Oct;234(5):303-18.

47. Miller BM, Zitzelsberger HF, Weier HU, Adler ID. Classification of micronuclei in murine erythrocytes: Immunofluorescent staining using CREST antibodies compared to in situ hybridization with biotinylated gamma satellite DNA. Mutagenesis. 1991 Jul;6(4):297-302.

48. Maron DM, Ames BN. Revised methods for the salmonella mutagenicity test. Mutat Res. 1983 May;113(3-4):173-215.

49. Ong T, Mukhtar M, Wolf CR, Zeiger E. Differential effects of cytochrome P450-inducers on promutagen activation capabilities and enzymatic activities of S-9 from rat liver. J Environ Pathol Toxicol. 1980 Aug;4(1):55-65.

50. Morpurgo M, Monfardini C, Hofland LJ, Sergi M, Orsolini P, Dumont JM, et al. Selective alkylation and acylation of alpha and epsilon amino groups with PEG in a somatostatin analogue: Tailored chemistry for optimized bioconjugates. Bioconjug Chem. 2002 Nov-Dec;13(6):1238-43.

51. Harris JM, Chess RB. Effect of pegylation on pharmaceuticals. Nat Rev Drug Discov. 2003 Mar;2(3):214-21.

52. Davis F, Abuchowski A, Van Es T, Palczuk N, Chen R, Savoca K, et al. Enzyme polyethylene glycol adducts:Modified enzymes with unique properties. Enzyme Eng. 1978(4):169-173.

53. Kozlowski A, Harris JM. Improvements in protein PEGylation: Pegylated interferons for treatment of hepatitis C. J Control Release. 2001 May 14;72(1-3):217-24.

54. Kopecek J, Kopeckova P, Minko T, Lu Z. HPMA copolymer-anticancer drug conjugates: Design, activity, and mechanism of action. Eur J Pharm Biopharm. 2000 Jul;50(1):61-81.

55. Monfardini C, Schiavon O, Caliceti P, Morpurgo M, Harris JM, Veronese FM. A branched monomethoxypoly(ethylene glycol) for protein modification. Bioconjug Chem. 1995 Jan-Feb;6(1):62-9.

56. Okamoto CT. Endocytosis and transcytosis. Adv Drug Deliv Rev. 1998 Feb 2;29(3):215-28.

57. Takakura Y, Mahato RI, Hashida M. Extravasation of macromolecules. Adv Drug Deliv Rev. 1998 Oct 5;34(1):93-108.

58. Allen TM. Ligand-targeted therapeutics in anticancer therapy. Nat Rev Cancer. 2002 Oct;2(10):750-63.

59. Pasut G, Veronese F. PEGylation of proteins as tailored chemistry for optimized bioconjugates. Adv polym sci. 2006(192):95.

60. Levy Y, Hershfield MS, Fernandez-Mejia C, Polmar SH, Scudiery D, Berger M, et al. Adenosine deaminase deficiency with late onset of recurrent infections: Response to treatment with polyethylene glycol-modified adenosine deaminase. J Pediatr. 1988 Aug;113(2):312-7.

61. Graham ML. Pegaspargase: A review of clinical studies. Adv Drug Deliv Rev. 2003 Sep 26;55(10):1293-302.

62. Wang YS, Youngster S, Grace M, Bausch J, Bordens R, Wyss DF. Structural and biological characterization of pegylated recombinant interferon alpha-2b and its therapeutic implications. Adv Drug Deliv Rev. 2002 Jun 17;54(4):547-70.

63. Bailon P, Palleroni A, Schaffer CA, Spence CL, Fung WJ, Porter JE, et al. Rational design of a potent, long-lasting form of interferon: A 40 kDa branched polyethylene glycol-conjugated interferon alpha-2a for the treatment of hepatitis C. Bioconjug Chem. 2001 Mar-Apr;12(2):195-202.

64. Rajender Reddy K, Modi MW, Pedder S. Use of peginterferon alfa-2a (40 KD) (pegasys) for the treatment of hepatitis C. Adv Drug Deliv Rev. 2002 Jun 17;54(4):571-86.

65. Trainer PJ, Drake WM, Katznelson L, Freda PU, Herman-Bonert V, van der Lely AJ, et al. Treatment of acromegaly with the growth hormone-receptor antagonist pegvisomant. N Engl J Med. 2000 Apr 20;342(16):1171-7.

66. Gordon AN, Fleagle JT, Guthrie D, Parkin DE, Gore ME, Lacave AJ. Recurrent epithelial ovarian carcinoma: A randomized phase III study of pegylated liposomal doxorubicin versus topotecan. J Clin Oncol. 2001 Jul 15;19(14):3312-22.

67. Park JW. Liposome-based drug delivery in breast cancer treatment. Breast Cancer Res. 2002;4(3):95-9.

68. Smith AM, Duan H, Mohs AM, Nie S. Bioconjugated quantum dots for in vivo molecular and cellular imaging. Adv Drug Deliv Rev. 2008 Aug 17;60(11):1226-40.

69. Ekimov A, Onushchenko A. Quantum size effect in the optical-spectra of semiconductor microcrystals. Sov Phys Semicond. 1982(16):775-778.

70. Efros A. Interband absorption of light in a semiconductor sphere. . Sov Phys Semicond. 1982(16):772-775.

71. Murray C, Norris D, Bawendi M. Synthesis and characterization of nearly monodisperse CdE(E = S, se, te) semiconductor nanocrystallites. J Am Chem Soc. 1993;115:8706-8715.

72. Tanaka N, Yamasaki J, Fuchi S, Takeda Y. First observation of in(x)ga(1-x)as quantum dots in GaP by spherical-aberration-corrected HRTEM in comparison with ADF-STEM and conventional HRTEM. Microsc Microanal. 2004 Feb;10(1):139-45.

73. Zhong X, Feng Y, Knoll W, Han M. Alloyed zn(x)cd(1-x)S nanocrystals with highly narrow luminescence spectral width. J Am Chem Soc. 2003 Nov 5;125(44):13559-63.

74. Bailey RE, Nie S. Alloyed semiconductor quantum dots: Tuning the optical properties without changing the particle size. J Am Chem Soc. 2003 Jun 11;125(23):7100-6.

75. Pietryga JM, Schaller RD, Werder D, Stewart MH, Klimov VI, Hollingsworth JA. Pushing the band gap envelope: Mid-infrared emitting colloidal PbSe quantum dots. J Am Chem Soc. 2004 Sep 29;126(38):11752-3.

76. Bagalkot V, Zhang L, Levy-Nissenbaum E, Jon S, Kantoff PW, Langer R, et al. Quantum dot-aptamer conjugates for synchronous cancer imaging, therapy, and sensing of drug delivery based on bi-fluorescence resonance energy transfer. Nano Lett. 2007 Oct;7(10):3065-70.

77. Savla R, Taratula O, Garbuzenko O, Minko T. Tumor targeted quantum dot-mucin 1 aptamer-doxorubicin conjugate for imaging and treatment of cancer. J Control Release. 2011 Jul 15;153(1):16-22.

78. Juzenas P, Chen W, Sun YP, Coelho MA, Generalov R, Generalova N, et al. Quantum dots and nanoparticles for photodynamic and radiation therapies of cancer. Adv Drug Deliv Rev. 2008 Dec 14;60(15):1600-14.

79. Maurer N, Fenske DB, Cullis PR. Developments in liposomal drug delivery systems. Expert Opin Biol Ther. 2001 Nov;1(6):923-47.

80. Pattnaik P, Ray T. Improving liposome integrity and easing bottlenecks to production. PHARMACEUTICAL TECHNOLOGY EUROPE. 2009;22(6).

81. Bangham A. Development of the liposome concept. in: Gregoridiadis G, allison A C (eds). Liposomes in biological systems John Wiley & Sons, Chichester,. 1980:1-24.

82. Samad A, Sultana Y, Aqil M. Liposomal drug delivery systems: An update review. Curr Drug Deliv. 2007 Oct;4(4):297-305.

83. Sessa G, Weissmann G. Incorporation of lysozyme into liposomes. A model for structure-linked latency. J Biol Chem. 1970 Jul 10;245(13):3295-301.

84. Gregoriadis G. Enzyme entrapment in liposomes. Methods Enzymol. 1976;44:218-27.

85. GENNIS R. Interactions of small molecules with membranes: Partitioning, permeability, and electrical effects in biomembranes. . Molecular Structure and Function. 1989:235-269.

86. Senior J, Delgado C, Fisher D, Tilcock C, Gregoriadis G. Influence of surface hydrophilicity of liposomes on their interaction with plasma protein and clearance from the circulation: Studies with poly(ethylene glycol)-coated vesicles. Biochim Biophys Acta. 1991 Feb 11;1062(1):77-82.

87. Zhang M, Garbuzenko OB, Reuhl KR, Rodriguez-Rodriguez L, Minko T. Two-in-one: Combined targeted chemo and gene therapy for tumor suppression and prevention of metastases. Nanomedicine (Lond). 2012 Feb;7(2):185-97.

88. Gabizon A, Papahadjopoulos D. The role of surface charge and hydrophilic groups on liposome clearance in vivo. Biochim Biophys Acta. 1992 Jan 10;1103(1):94-100.

89. Cullis PR, Chonn A, Semple SC. Interactions of liposomes and lipid-based carrier systems with blood proteins: Relation to clearance behaviour in vivo. Adv Drug Deliv Rev. 1998 Jun 8;32(1-2):3-17.

90. Gabizon A, Papahadjopoulos D. Liposome formulations with prolonged circulation time in blood and enhanced uptake by tumors. Proc Natl Acad Sci U S A. 1988 Sep;85(18):6949-53.

91. Webb MS, Harasym TO, Masin D, Bally MB, Mayer LD. Sphingomyelin-cholesterol liposomes significantly enhance the pharmacokinetic and therapeutic properties of vincristine in murine and human tumour models. Br J Cancer. 1995 Oct;72(4):896-904.

92. Zhang M, Garbuzenko OB, Reuhl KR, Rodriguez-Rodriguez L, Minko T. Two-in-one: Combined targeted chemo and gene therapy for tumor suppression and prevention of metastases. Nanomedicine (Lond). 2012 Feb;7(2):185-97.

93. Tack F, Bakker A, Maes S, Dekeyser N, Bruining M, Elissen-Roman C, et al. Modified poly(propylene imine) dendrimers as effective transfection agents for catalytic DNA enzymes (DNAzymes). J Drug Target. 2006 Feb;14(2):69-86.

94. Buhleier E, Wehner W, Vögtle F. 'Cascade'- and 'Nonskid-chain-like' syntheses of molecular cavity topologies. Synthesis. 1978:155-158.

95. Tomalia D, Naylor A, Goddard W. Starburst dendrimers—molecular-level control of size, shape, surface-chemistry, topology, and flexibility from atoms to macroscopic matter. Angew Chem, Int Ed Engl. 1990;29:138-175.

96. Archut A, Vögtle F. Functional cascade molecules. Chem Soc Rev. 1998;27:233-240.

97. Cheng Y, Xu Z, Ma M, Xu T. Dendrimers as drug carriers: Applications in different routes of drug administration. J Pharm Sci. 2008 Jan;97(1):123-43.

98. Sakthivel T, Florence AT. Adsorption of amphipathic dendrons on polystyrene nanoparticles. Int J Pharm. 2003 Mar 18;254(1):23-6.

99. Hari BN, Kalaimagal K, Porkodi R, Gajula P, Ajay J. Dendrimer: Globular nanostructured materials for drug delivery. International Journal of PharmTech Research. 2012;4(1):432-451.

100. Jain NK, Khopade AJ. Dendrimers as potential delivery systems for bioactives. N.K.jain, editor,

. Advances in controlled and novel drug delivery,. 2001:361-380.

101. Klajnert B, Bryszewska M. Dendrimers: Properties and applications. Acta Biochim Pol. 2001;48(1):199-208.

102. Frechet JM. Functional polymers and dendrimers: Reactivity, molecular architecture, and interfacial energy. Science. 1994 Mar 25;263(5154):1710-5.

103. Tomalia DA, Dewald JR, Hall MR, Martin SJ, Smith PB. Preprints of the 1st SPSJ international polymer conference. Society of Polymer Science Japan. 1984:65.

104. [Internet]. Available from: http://bme240.eng.uci.edu/students/06s/katherjl/.

105. Haensler J, Szoka FC,Jr. Polyamidoamine cascade polymers mediate efficient transfection of cells in culture. Bioconjug Chem. 1993 Sep-Oct;4(5):372-9.

106. Bielinska A, Kukowska-Latallo JF, Johnson J, Tomalia DA, Baker JR,Jr. Regulation of in vitro gene expression using antisense oligonucleotides or antisense expression plasmids transfected using starburst PAMAM dendrimers. Nucleic Acids Res. 1996 Jun 1;24(11):2176-82.

107. Patil ML, Zhang M, Minko T. Multifunctional triblock nanocarrier (PAMAM-PEG-PLL) for the efficient intracellular siRNA delivery and gene silencing. ACS Nano. 2011 Mar 22;5(3):1877-87.

108. Zhuo RX, Du B, Lu ZR. In vitro release of 5-fluorouracil with cyclic core dendritic polymer. J Control Release. 1999 Feb 22;57(3):249-57.

109. Wiener EC, Brechbiel MW, Brothers H, Magin RL, Gansow OA, Tomalia DA, et al. Dendrimer-based metal chelates: A new class of magnetic resonance imaging contrast agents. Magn Reson Med. 1994 Jan;31(1):1-8.

110. Malik N, Wiwattanapatapee R, Klopsch R, Lorenz K, Frey H, Weener JW, et al. Dendrimers: Relationship between structure and biocompatibility in vitro, and preliminary studies on the biodistribution of 125I-labelled polyamidoamine dendrimers in vivo. J Control Release. 2000 Mar 1;65(1-2):133-48.

111. Chen HT, Neerman MF, Parrish AR, Simanek EE. Cytotoxicity, hemolysis, and acute in vivo toxicity of dendrimers based on melamine, candidate vehicles for drug delivery. J Am Chem Soc. 2004 Aug 18;126(32):10044-8.

112. Lee JH, Lim YB, Choi JS, Lee Y, Kim TI, Kim HJ, et al. Polyplexes assembled with internally quaternized PAMAM-OH dendrimer and plasmid DNA have a neutral surface and gene delivery potency. Bioconjug Chem. 2003 Nov-Dec;14(6):1214-21.

113. Patil ML, Zhang M, Taratula O, Garbuzenko OB, He H, Minko T. Internally cationic polyamidoamine PAMAM-OH dendrimers for siRNA delivery: Effect of the degree of quaternization and cancer targeting. Biomacromolecules. 2009 Feb 9;10(2):258-66.

114. Berg DB, Meijer EW. Poly(propyleneimine) dendrimers: Large scale synthesis by heterogenously catalyzed hydrogenations.
. Angew Chem Int Ed Engl. 1993;32:1308–1311.

115. Chen AM, Santhakumaran LM, Nair SK, Amenta PS, Thomas T, He H. Oligodeoxynucleotide nanostructure formation in the presence of polypropyleneimine dendrimers and their uptake in breast cancer cells. Nanotechnology. 2006;17:5449-60.

116. Hollins AJ, Benboubetra M, Omidi Y, Zinselmeyer BH, Schatzlein AG, Uchegbu IF, et al. Evaluation of generation 2 and 3 poly(propylenimine) dendrimers for the potential cellular delivery of antisense oligonucleotides targeting the epidermal growth factor receptor. Pharm Res. 2004 Mar;21(3):458-66.

117. Schatzlein AG, Zinselmeyer BH, Elouzi A, Dufes C, Chim YT, Roberts CJ, et al. Preferential liver gene expression with polypropylenimine dendrimers. J Control Release. 2005 Jan 3;101(1-3):247-58.

118. Zinselmeyer BH, Mackay SP, Schatzlein AG, Uchegbu IF. The lower-generation polypropylenimine dendrimers are effective gene-transfer agents. Pharm Res. 2002 Jul;19(7):960-7.

119. Lim YB, Kim T, Lee JW, Kim SM, Kim HJ, Kim K, et al. Self-assembled ternary complex of cationic dendrimer, cucurbituril, and DNA: Noncovalent strategy in developing a gene delivery carrier. Bioconjug Chem. 2002 Nov-Dec;13(6):1181-5.

120. Agashe HB, Dutta T, Garg M, Jain NK. Investigations on the toxicological profile of functionalized fifth-generation poly (propylene imine) dendrimer. J Pharm Pharmacol. 2006 Nov;58(11):1491-8.

121. Taratula O, Garbuzenko OB, Kirkpatrick P, Pandya I, Savla R, Pozharov VP, et al. Surface-engineered targeted PPI dendrimer for efficient intracellular and intratumoral siRNA delivery. J Controlled Release. 2009 12/16;140(3):284-93.

122. Tartaj P, Morales M, Veintemillas-Verdaguer S, Gonzalez-Carreno T, Serna C. The preparation of magnetic nanoparticles for applications in biomedicine. J Phys D: Appl Phys. 2003;36:R182-R197.

123. Lu AH, Salabas EL, Schuth F. Magnetic nanoparticles: Synthesis, protection, functionalization, and application. Angew Chem Int Ed Engl. 2007;46(8):1222-44.

124. Akbarzadeh A, Samiei M, Davaran S. Magnetic nanoparticles: Preparation, physical properties, and applications in biomedicine. Nanoscale Res Lett. 2012 Feb 21;7(1):144.

125. GILCHRIST RK, MEDAL R, SHOREY WD, HANSELMAN RC, PARROTT JC, TAYLOR CB. Selective inductive heating of lymph nodes. Ann Surg. 1957 Oct;146(4):596-606.

126. Kwon SG, Piao Y, Park J, Angappane S, Jo Y, Hwang NM, et al. Kinetics of monodisperse iron oxide nanocrystal formation by "heating-up" process. J Am Chem Soc. 2007 Oct 17;129(41):12571-84.

127. Torney F, Trewyn BG, Lin VS, Wang K. Mesoporous silica nanoparticles deliver DNA and chemicals into plants. Nat Nanotechnol. 2007 May;2(5):295-300.

128. Wu SH, Hung Y, Mou CY. Mesoporous silica nanoparticles as nanocarriers. Chem Commun (Camb). 2011 Sep 28;47(36):9972-85.

129. Cai Q, Luo Z, Pang W, Fan W, Chen X, Cui F. Dilute solution routes to various controllable morphologies of MCM-41 silica with a basic medium. Chem Mater. 2001;13:258-263.

130. Suzuki K, Ikari K, Imai H. Synthesis of silica nanoparticles having a well-ordered mesostructure using a double surfactant system. J Am Chem Soc. 2004 Jan 21;126(2):462-3.

131. Urata C, Aoyama Y, Tonegawa A, Yamauchi Y, Kuroda K. Dialysis process for the removal of surfactants to form colloidal mesoporous silica nanoparticles. Chem Commun (Camb). 2009 Sep 14;(34)(34):5094-6.

132. Lim MH, Stein A. Comparative studies of grafting and direct syntheses of inorganic-organic hybrid mesoporous materials. Chem Mater. 1999;11:3285-3295.

133. Li Z, Barnes JC, Bosoy A, Stoddart JF, Zink JI. Mesoporous silica nanoparticles in biomedical applications. Chem Soc Rev. 2012 Apr 7;41(7):2590-605.

134. Liong M, Lu J, Kovochich M, Xia T, Ruehm SG, Nel AE, et al. Multifunctional inorganic nanoparticles for imaging, targeting, and drug delivery. ACS Nano. 2008 May;2(5):889-96.

135. Lu J, Liong M, Zink JI, Tamanoi F. Mesoporous silica nanoparticles as a delivery system for hydrophobic anticancer drugs. Small. 2007 Aug;3(8):1341-6.

136. Slowing I, Trewyn BG, Lin VS. Effect of surface functionalization of MCM-41-type mesoporous silica nanoparticles on the endocytosis by human cancer cells. J Am Chem Soc. 2006 Nov 22;128(46):14792-3.

137. Rosenholm JM, Meinander A, Peuhu E, Niemi R, Eriksson JE, Sahlgren C, et al. Targeting of porous hybrid silica nanoparticles to cancer cells. ACS Nano. 2009 Jan 27;3(1):197-206.

138. Ferris DP, Lu J, Gothard C, Yanes R, Thomas CR, Olsen JC, et al. Synthesis of biomolecule-modified mesoporous silica nanoparticles for targeted hydrophobic drug delivery to cancer cells. Small. 2011 Jul 4;7(13):1816-26.

139. Meng H, Liong M, Xia T, Li Z, Ji Z, Zink JI, et al. Engineered design of mesoporous silica nanoparticles to deliver doxorubicin and P-glycoprotein siRNA to overcome drug resistance in a cancer cell line. ACS Nano. 2010 Aug 24;4(8):4539-50.

140. [Internet].; December,2011. Available from: http://www.ncbi.nlm.nih.gov/pubmedhealth/PMH0001891/.

141. Ovarian cancer. 11 January, 2012.

142. Auersperg N, Ota T, Mitchell GW. Early events in ovarian epithelial carcinogenesis: Progress and problems in experimental approaches. Int J Gynecol Cancer. 2002 Nov-Dec;12(6):691-703.

143. Reya T, Morrison SJ, Clarke MF, Weissman IL. Stem cells, cancer, and cancer stem cells. Nature. 2001 Nov 1;414(6859):105-11.

144. Weissman IL. Stem cells: Units of development, units of regeneration, and units in evolution. Cell. 2000 Jan 7;100(1):157-68.

145. Beltrami AP, Barlucchi L, Torella D, Baker M, Limana F, Chimenti S, et al. Adult cardiac stem cells are multipotent and support myocardial regeneration. Cell. 2003 Sep 19;114(6):763-76.

146. Kim CF, Jackson EL, Woolfenden AE, Lawrence S, Babar I, Vogel S, et al. Identification of bronchioalveolar stem cells in normal lung and lung cancer. Cell. 2005 Jun 17;121(6):823-35.

147. Shackleton M, Vaillant F, Simpson KJ, Stingl J, Smyth GK, Asselin-Labat ML, et al. Generation of a functional mammary gland from a single stem cell. Nature. 2006 Jan 5;439(7072):84-8.

148. Cheng T, Rodrigues N, Shen H, Yang Y, Dombkowski D, Sykes M, et al. Hematopoietic stem cell quiescence maintained by p21cip1/waf1. Science. 2000 Mar 10;287(5459):1804-8.

149. McCulloch EA, Till JE. Perspectives on the properties of stem cells. Nat Med. 2005 Oct;11(10):1026-8.

150. Gat U, DasGupta R, Degenstein L, Fuchs E. De novo hair follicle morphogenesis and hair tumors in mice expressing a truncated beta-catenin in skin. Cell. 1998 Nov 25;95(5):605-14.

151. Kuhnert F, Davis CR, Wang HT, Chu P, Lee M, Yuan J, et al. Essential requirement for wnt signaling in proliferation of adult small intestine and colon revealed by adenoviral expression of dickkopf-1. Proc Natl Acad Sci U S A. 2004 Jan 6;101(1):266-71.

152. Reya T, Duncan AW, Ailles L, Domen J, Scherer DC, Willert K, et al. A role for wnt signalling in self-renewal of haematopoietic stem cells. Nature. 2003 May 22;423(6938):409-14.

153. Varnum-Finney B, Xu L, Brashem-Stein C, Nourigat C, Flowers D, Bakkour S, et al. Pluripotent, cytokine-dependent, hematopoietic stem cells are immortalized by constitutive Notch1 signaling. Nat Med. 2000 Nov;6(11):1278-81.

154. Al-Hajj M, Clarke MF. Self-renewal and solid tumor stem cells. Oncogene. 2004 Sep 20;23(43):7274-82.

155. Li F, Tiede B, Massague J, Kang Y. Beyond tumorigenesis: Cancer stem cells in metastasis. Cell Res. 2007 Jan;17(1):3-14.

156. Clarke MF, Dick JE, Dirks PB, Eaves CJ, Jamieson CH, Jones DL, et al. Cancer stem cells--perspectives on current status and future directions: AACR workshop on cancer stem cells. Cancer Res. 2006 Oct 1;66(19):9339-44.

157. Bonnet D, Dick JE. Human acute myeloid leukemia is organized as a hierarchy that originates from a primitive hematopoietic cell. Nat Med. 1997 Jul;3(7):730-7.

158. Al-Hajj M, Wicha MS, Benito-Hernandez A, Morrison SJ, Clarke MF. Prospective identification of tumorigenic breast cancer cells. Proc Natl Acad Sci U S A. 2003 Apr 1;100(7):3983-8.

159. Singh SK, Clarke ID, Terasaki M, Bonn VE, Hawkins C, Squire J, et al. Identification of a cancer stem cell in human brain tumors. Cancer Res. 2003 Sep 15;63(18):5821-8.

160. Fang D, Nguyen TK, Leishear K, Finko R, Kulp AN, Hotz S, et al. A tumorigenic subpopulation with stem cell properties in melanomas. Cancer Res. 2005 Oct 15;65(20):9328-37.

161. Collins AT, Berry PA, Hyde C, Stower MJ, Maitland NJ. Prospective identification of tumorigenic prostate cancer stem cells. Cancer Res. 2005 Dec 1;65(23):10946-51.

162. Muthukumaran N, Miletti-Gonzalez KE, Ravindranath AK, Rodriguez-Rodriguez L. Tumor necrosis factor-alpha differentially modulates CD44 expression in ovarian cancer cells. Mol Cancer Res. 2006 Aug;4(8):511-20.

163. Mimeault M, Hauke R, Mehta PP, Batra SK. Recent advances in cancer stem/progenitor cell research: Therapeutic implications for overcoming resistance to the most aggressive cancers. J Cell Mol Med. 2007 Sep-Oct;11(5):981-1011.

164. Screaton GR, Bell MV, Jackson DG, Cornelis FB, Gerth U, Bell JI. Genomic structure of DNA encoding the lymphocyte homing receptor CD44 reveals at least 12 alternatively spliced exons. Proc Natl Acad Sci U S A. 1992 Dec 15;89(24):12160-4.

165. Hughes EN, Colombatti A, August JT. Murine cell surface glycoproteins. purification of the polymorphic pgp-1 antigen and analysis of its expression on macrophages and other myeloid cells. J Biol Chem. 1983 Jan 25;258(2):1014-21.

166. Jalkanen ST, Bargatze RF, Herron LR, Butcher EC. A lymphoid cell surface glycoprotein involved in endothelial cell recognition and lymphocyte homing in man. Eur J Immunol. 1986 Oct;16(10):1195-202.

167. Naor D, Nedvetzki S, Golan I, Melnik L, Faitelson Y. CD44 in cancer. Crit Rev Clin Lab Sci. 2002 Nov;39(6):527-79.

168. Aruffo A, Stamenkovic I, Melnick M, Underhill CB, Seed B. CD44 is the principal cell surface receptor for hyaluronate. Cell. 1990 Jun 29;61(7):1303-13.

169. Ponta H, Sherman L, Herrlich PA. CD44: From adhesion molecules to signalling regulators. Nat Rev Mol Cell Biol. 2003 Jan;4(1):33-45.

170. Toole BP. Hyaluronan: From extracellular glue to pericellular cue. Nat Rev Cancer. 2004 Jul;4(7):528-39.

171. Kosaki R, Watanabe K, Yamaguchi Y. Overproduction of hyaluronan by expression of the hyaluronan synthase Has2 enhances anchorage-independent growth and tumorigenicity. Cancer Res. 1999 Mar 1;59(5):1141-5.

172. Itano N, Sawai T, Atsumi F, Miyaishi O, Taniguchi S, Kannagi R, et al. Selective expression and functional characteristics of three mammalian hyaluronan synthases in oncogenic malignant transformation. J Biol Chem. 2004 Apr 30;279(18):18679-87.

173. Li Y, Heldin P. Hyaluronan production increases the malignant properties of mesothelioma cells. Br J Cancer. 2001 Aug 17;85(4):600-7.

174. Zoltan-Jones A, Huang L, Ghatak S, Toole BP. Elevated hyaluronan production induces mesenchymal and transformed properties in epithelial cells. J Biol Chem. 2003 Nov 14;278(46):45801-10.

175. Peterson RM, Yu Q, Stamenkovic I, Toole BP. Perturbation of hyaluronan interactions by soluble CD44 inhibits growth of murine mammary carcinoma cells in ascites. Am J Pathol. 2000 Jun;156(6):2159-67.

176. Sohara Y, Ishiguro N, Machida K, Kurata H, Thant AA, Senga T, et al. Hyaluronan activates cell motility of v-src-transformed cells via ras-mitogen-activated protein kinase and phosphoinositide 3-kinase-akt in a tumor-specific manner. Mol Biol Cell. 2001 Jun;12(6):1859-68.

177. Itano N, Atsumi F, Sawai T, Yamada Y, Miyaishi O, Senga T, et al. Abnormal accumulation of hyaluronan matrix diminishes contact inhibition of cell growth and promotes cell migration. Proc Natl Acad Sci U S A. 2002 Mar 19;99(6):3609-14.

178. Misra S, Ghatak S, Zoltan-Jones A, Toole BP. Regulation of multidrug resistance in cancer cells by hyaluronan. J Biol Chem. 2003 Jul 11;278(28):25285-8.

179. Misra S, Ujhazy P, Varticovski L, Arias IM. Phosphoinositide 3-kinase lipid products regulate ATP-dependent transport by sister of P-glycoprotein and multidrug resistance associated protein 2 in bile canalicular membrane vesicles. Proc Natl Acad Sci U S A. 1999 May 11;96(10):5814-9.

180. Chambers AF, Matrisian LM. Changing views of the role of matrix metalloproteinases in metastasis. J Natl Cancer Inst. 1997 Sep 3;89(17):1260-70.

181. Egeblad M, Werb Z. New functions for the matrix metalloproteinases in cancer progression. Nat Rev Cancer. 2002 Mar;2(3):161-74.

182. Park MJ, Kim MS, Park IC, Kang HS, Yoo H, Park SH, et al. PTEN suppresses hyaluronic acid-induced matrix metalloproteinase-9 expression in U87MG glioblastoma cells through focal adhesion kinase dephosphorylation. Cancer Res. 2002 Nov 1;62(21):6318-22.

183. Zhang Y, Thant AA, Machida K, Ichigotani Y, Naito Y, Hiraiwa Y, et al. Hyaluronan-CD44s signaling regulates matrix metalloproteinase-2 secretion in a human lung carcinoma cell line QG90. Cancer Res. 2002 Jul 15;62(14):3962-5.

184. Yu Q, Stamenkovic I. Cell surface-localized matrix metalloproteinase-9 proteolytically activates TGF-beta and promotes tumor invasion and angiogenesis. Genes Dev. 2000 Jan 15;14(2):163-76.

185. Bourguignon LY, Gunja-Smith Z, Iida N, Zhu HB, Young LJ, Muller WJ, et al. CD44v(3,8-10) is involved in cytoskeleton-mediated tumor cell migration and matrix metalloproteinase (MMP-9) association in metastatic breast cancer cells. J Cell Physiol. 1998 Jul;176(1):206-15.

186. Mori H, Tomari T, Koshikawa N, Kajita M, Itoh Y, Sato H, et al. CD44 directs membrane-type 1 matrix metalloproteinase to lamellipodia by associating with its hemopexin-like domain. EMBO J. 2002 Aug 1;21(15):3949-59.

187. Okamoto I, Kawano Y, Tsuiki H, Sasaki J, Nakao M, Matsumoto M, et al. CD44 cleavage induced by a membrane-associated metalloprotease plays a critical role in tumor cell migration. Oncogene. 1999 Feb 18;18(7):1435-46.

188. Bourguignon LY, Singleton PA, Diedrich F, Stern R, Gilad E. CD44 interaction with na+-H+ exchanger (NHE1) creates acidic microenvironments leading to hyaluronidase-2 and cathepsin B activation and breast tumor cell invasion. J Biol Chem. 2004 Jun 25;279(26):26991-7007.

189. Zhu D, Bourguignon LY. Interaction between CD44 and the repeat domain of ankyrin promotes hyaluronic acid-mediated ovarian tumor cell migration. J Cell Physiol. 2000 May;183(2):182-95.

190. Legg JW, Lewis CA, Parsons M, Ng T, Isacke CM. A novel PKC-regulated mechanism controls CD44 ezrin association and directional cell motility. Nat Cell Biol. 2002 Jun;4(6):399-407.

191. Weber GF, Bronson RT, Ilagan J, Cantor H, Schmits R, Mak TW. Absence of the CD44 gene prevents sarcoma metastasis. Cancer Res. 2002 Apr 15;62(8):2281-6.

192. Mitsui K, Tokuzawa Y, Itoh H, Segawa K, Murakami M, Takahashi K, et al. The homeoprotein nanog is required for maintenance of pluripotency in mouse epiblast and ES cells. Cell. 2003 May 30;113(5):631-42.

193. Kuroda T, Tada M, Kubota H, Kimura H, Hatano SY, Suemori H, et al. Octamer and sox elements are required for transcriptional cis regulation of nanog gene expression. Mol Cell Biol. 2005 Mar;25(6):2475-85.

194. Rodda DJ, Chew JL, Lim LH, Loh YH, Wang B, Ng HH, et al. Transcriptional regulation of nanog by OCT4 and SOX2. J Biol Chem. 2005 Jul 1;280(26):24731-7.

195. Lin T, Chao C, Saito S, Mazur SJ, Murphy ME, Appella E, et al. p53 induces differentiation of mouse embryonic stem cells by suppressing nanog expression. Nat Cell Biol. 2005 Feb;7(2):165-71.

196. Levy DE, Lee CK. What does Stat3 do? J Clin Invest. 2002 May;109(9):1143-8.

197. Sato N, Meijer L, Skaltsounis L, Greengard P, Brivanlou AH. Maintenance of pluripotency in human and mouse embryonic stem cells through activation of wnt signaling by a pharmacological GSK-3-specific inhibitor. Nat Med. 2004 Jan;10(1):55-63.

198. Bourguignon LY, Peyrollier K, Xia W, Gilad E. Hyaluronan-CD44 interaction activates stem cell marker nanog, stat-3-mediated MDR1 gene expression, and ankyrin-regulated multidrug efflux in breast and ovarian tumor cells. J Biol Chem. 2008 Jun 20;283(25):17635-51.

199. Bennett V, Baines AJ. Spectrin and ankyrin-based pathways: Metazoan inventions for integrating cells into tissues. Physiol Rev. 2001 Jul;81(3):1353-92.

200. Fire A, Xu S, Montgomery MK, Kostas SA, Driver SE, Mello CC. Potent and specific genetic interference by double-stranded RNA in caenorhabditis elegans. Nature. 1998 Feb 19;391(6669):806-11.

201. Montgomery MK, Xu S, Fire A. RNA as a target of double-stranded RNA-mediated genetic interference in caenorhabditis elegans. Proc Natl Acad Sci U S A. 1998 Dec 22;95(26):15502-7.

202. Kennerdell JR, Carthew RW. Use of dsRNA-mediated genetic interference to demonstrate that frizzled and frizzled 2 act in the wingless pathway. Cell. 1998 Dec 23;95(7):1017-26.

203. Ngo H, Tschudi C, Gull K, Ullu E. Double-stranded RNA induces mRNA degradation in trypanosoma brucei. Proc Natl Acad Sci U S A. 1998 Dec 8;95(25):14687-92.

204. Sanchez Alvarado A, Newmark PA. Double-stranded RNA specifically disrupts gene expression during planarian regeneration. Proc Natl Acad Sci U S A. 1999 Apr 27;96(9):5049-54.

205. Lohmann JU, Endl I, Bosch TC. Silencing of developmental genes in hydra. Dev Biol. 1999 Oct 1;214(1):211-4.

206. Hamilton AJ, Baulcombe DC. A species of small antisense RNA in posttranscriptional gene silencing in plants. Science. 1999 Oct 29;286(5441):950-2.

207. Elbashir SM, Harborth J, Lendeckel W, Yalcin A, Weber K, Tuschl T. Duplexes of 21-nucleotide RNAs mediate RNA interference in cultured mammalian cells. Nature. 2001 May 24;411(6836):494-8.

208.
[Internet]. Available from: http://www.alnylam.com/rnai_primer/rna-interference-pg5.htm.

209. Bernstein E, Caudy AA, Hammond SM, Hannon GJ. Role for a bidentate ribonuclease in the initiation step of RNA interference. Nature. 2001 Jan 18;409(6818):363-6.

210. Tuschl T. RNA interference and small interfering RNAs. Chembiochem. 2001 Apr 2;2(4):239-45.

211. Matranga C, Tomari Y, Shin C, Bartel DP, Zamore PD. Passenger-strand cleavage facilitates assembly of siRNA into Ago2-containing RNAi enzyme complexes. Cell. 2005 Nov 18;123(4):607-20.

212. Hammond SM, Bernstein E, Beach D, Hannon GJ. An RNA-directed nuclease mediates post-transcriptional gene silencing in drosophila cells. Nature. 2000 Mar 16;404(6775):293-6.

213. Hutvagner G, Zamore PD. A microRNA in a multiple-turnover RNAi enzyme complex. Science. 2002 Sep 20;297(5589):2056-60.

214. Chiu YL, Ali A, Chu CY, Cao H, Rana TM. Visualizing a correlation between siRNA localization, cellular uptake, and RNAi in living cells. Chem Biol. 2004 Aug;11(8):1165-75.

215. Choung S, Kim YJ, Kim S, Park HO, Choi YC. Chemical modification of siRNAs to improve serum stability without loss of efficacy. Biochem Biophys Res Commun. 2006 Apr 14;342(3):919-27.

216. Layzer JM, McCaffrey AP, Tanner AK, Huang Z, Kay MA, Sullenger BA. In vivo activity of nuclease-resistant siRNAs. RNA. 2004 May;10(5):766-71.

217. Dykxhoorn DM, Lieberman J. The silent revolution: RNA interference as basic biology, research tool, and therapeutic. Annu Rev Med. 2005;56:401-23.

218. Elbashir SM, Martinez J, Patkaniowska A, Lendeckel W, Tuschl T. Functional anatomy of siRNAs for mediating efficient RNAi in drosophila melanogaster embryo lysate. EMBO J. 2001 Dec 3;20(23):6877-88.

219. Han S, Mahato RI, Sung YK, Kim SW. Development of biomaterials for gene therapy. Mol Ther. 2000 Oct;2(4):302-17.

220. Schally AV. Hypothalamic hormones: From neuroendocrinology to cancer therapy. Anticancer Drugs. 1994 Apr;5(2):115-30.

221. Grundker C, Gunthert AR, Westphalen S, Emons G. Biology of the gonadotropin-releasing hormone system in gynecological cancers. Eur J Endocrinol. 2002 Jan;146(1):1-14.

222. Dharap SS, Chandna P, Wang Y, Khandare JJ, Qiu B, Stein S, et al. Molecular targeting of BCL2 and BCLXL proteins by synthetic BCL2 homology 3 domain peptide enhances the efficacy of chemotherapy. J Pharmacol Exp Ther. 2006 Mar;316(3):992-8.

223. Dharap SS, Minko T. Targeted proapoptotic LHRH-BH3 peptide. Pharm Res. 2003 Jun;20(6):889-96.

224. Grundker C, Volker P, Griesinger F, Ramaswamy A, Nagy A, Schally AV, et al. Antitumor effects of the cytotoxic luteinizing hormone-releasing hormone analog AN-152 on human endometrial and ovarian cancers xenografted into nude mice. Am J Obstet Gynecol. 2002 Sep;187(3):528-37.

225. Emons G, Sindermann H, Engel J, Schally AV, Grundker C. Luteinizing hormone-releasing hormone receptor-targeted chemotherapy using AN-152. Neuroendocrinology. 2009;90(1):15-8.

226. Zhang M, Garbuzenko OB, Reuhl KR, Rodriguez-Rodriguez L, Minko T. Two-in-one: Combined targeted chemo and gene therapy for tumor suppression and prevention of metastases. Nanomedicine (Lond). 2012 Feb;7(2):185-97.

227. Wani MC, Taylor HL, Wall ME, Coggon P, McPhail AT. Plant antitumor agents. VI. the isolation and structure of taxol, a novel antileukemic and antitumor agent from taxus brevifolia. J Am Chem Soc. 1971 May 5;93(9):2325-7.

228. Kumar S, Mahdi H, Bryant C, Shah JP, Garg G, Munkarah A. Clinical trials and progress with paclitaxel in ovarian cancer. Int J Womens Health. 2010 Nov 19;2:411-27.

229. 2012 antineoplastics [Internet].; 2012. Available from: http://www.d.umn.edu/~jfitzake/Lectures/DMED/Antineoplastics/Antimitotics/PaclitaxelMechanism.html.

230. Downing KH. Structural basis for the interaction of tubulin with proteins and drugs that affect microtubule dynamics. Annu Rev Cell Dev Biol. 2000;16:89-111.

231. Jordan A, Hadfield JA, Lawrence NJ, McGown AT. Tubulin as a target for anticancer drugs: Agents which interact with the mitotic spindle. Med Res Rev. 1998 Jul;18(4):259-96.

232. McGuire WP, Hoskins WJ, Brady MF, Kucera PR, Partridge EE, Look KY, et al. Cyclophosphamide and cisplatin compared with paclitaxel and cisplatin in patients with stage III and stage IV ovarian cancer. N Engl J Med. 1996 Jan 4;334(1):1-6.

233. Piccart MJ, Bertelsen K, James K, Cassidy J, Mangioni C, Simonsen E, et al. Randomized intergroup trial of cisplatin-paclitaxel versus cisplatin-cyclophosphamide in women with advanced epithelial ovarian cancer: Three-year results. J Natl Cancer Inst. 2000 May 3;92(9):699-708.

234. Vega-Villa KR, Takemoto JK, Yanez JA, Remsberg CM, Forrest ML, Davies NM. Clinical toxicities of nanocarrier systems. Adv Drug Deliv Rev. 2008 May 22;60(8):929-38.

235. Warheit DB, Donner EM. Rationale of genotoxicity testing of nanomaterials: Regulatory requirements and appropriateness of available OECD test guidelines. Nanotoxicology. 2010 Dec;4:409-13.

236. Norppa H, Catalan J, Falck G, Hannukainen K, Siivola K, Savolainen K. Nano-specific genotoxic effects. J Biomed Nanotechnol. 2011 Feb;7(1):19.

237. Singh N, Manshian B, Jenkins GJ, Griffiths SM, Williams PM, Maffeis TG, et al. NanoGenotoxicology: The DNA damaging potential of engineered nanomaterials. Biomaterials. 2009 Aug;30(23-24):3891-914.

238. Choi YJ, Kang SJ, Kim YJ, Lim YB, Chung HW. Comparative studies on the genotoxicity and cytotoxicity of polymeric gene carriers polyethylenimine (PEI) and

polyamidoamine (PAMAM) dendrimer in jurkat T-cells. Drug Chem Toxicol. 2010 Oct;33(4):357-66.

239. Yin L, Zhao X, Cui L, Ding J, He M, Tang C, et al. Cytotoxicity and genotoxicity of superporous hydrogel containing interpenetrating polymer networks. Food Chem Toxicol. 2009 Jun;47(6):1139-45.

240. Zuzana M, Alessandra R, Lise F, Maria D. Safety assessment of nanoparticles cytotoxicity and genotoxicity of metal nanoparticles in vitro. J Biomed Nanotechnol. 2011 Feb;7(1):20-1.

241. Betigeri S, Zhang M, Garbuzenko O, Minko T. Non-viral systemic delivery of siRNA or antisense oligonucleotides targeted to jun N-terminal kinase 1 prevents cellular hypoxic damage. Drug Deliv Transl Res. 2011 Feb;1(1):13-24.

242. Garbuzenko O, Zalipsky S, Qazen M, Barenholz Y. Electrostatics of PEGylated micelles and liposomes containing charged and neutral lipopolymers. Langmuir. 2005 Mar 15;21(6):2560-8.

243. Taratula O, Garbuzenko O, Savla R, Wang YA, He H, Minko T. Multifunctional nanomedicine platform for cancer specific delivery of siRNA by superparamagnetic iron oxide nanoparticles-dendrimer complexes. Curr Drug Deliv. 2011 Jan;8(1):59-69.

244. Patil ML, Zhang M, Betigeri S, Taratula O, He H, Minko T. Surface-modified and internally cationic polyamidoamine dendrimers for efficient siRNA delivery. Bioconjug Chem. 2008 Jul;19(7):1396-403.

245. Miller B, Potter-Locher F, Seelbach A, Stopper H, Utesch D, Madle S. Evaluation of the in vitro micronucleus test as an alternative to the in vitro chromosomal aberration assay: Position of the GUM working group on the in vitro micronucleus test. gesellschaft fur umwelt-mutations-forschung. Mutat Res. 1998 Feb;410(1):81-116.

246. The micronucleus assay. *LPI/CCP protocol for in vitro micronucleus assay using CHO-K1 cells* [Internet].; 2009. Available from: http://lpi.oregonstate.edu/CCP/micronucleus.html.

247. Pakunlu RI, Wang Y, Tsao W, Pozharov V, Cook TJ, Minko T. Enhancement of the efficacy of chemotherapy for lung cancer by simultaneous suppression of multidrug resistance and antiapoptotic cellular defense: Novel multicomponent delivery system. Cancer Res. 2004 Sep 1;64(17):6214-24.

248. Taratula O, Garbuzenko OB, Kirkpatrick P, Pandya I, Savla R, Pozharov VP, et al. Surface-engineered targeted PPI dendrimer for efficient intracellular and intratumoral siRNA delivery. J Control Release. 2009 Dec 16;140(3):284-93.

249. Arvizo RR, Miranda OR, Thompson MA, Pabelick CM, Bhattacharya R, Robertson JD, et al. Effect of nanoparticle surface charge at the plasma membrane and beyond. Nano Lett. 2010 Jul 14;10(7):2543-8.

250. Asati A, Santra S, Kaittanis C, Perez JM. Surface-charge-dependent cell localization and cytotoxicity of cerium oxide nanoparticles. ACS Nano. 2010 Sep 28;4(9):5321-31.

251. Bhattacharjee S, de Haan LH, Evers NM, Jiang X, Marcelis AT, Zuilhof H, et al. Role of surface charge and oxidative stress in cytotoxicity of organic monolayer-coated silicon nanoparticles towards macrophage NR8383 cells. Part Fibre Toxicol. 2010 Sep 11;7:25.

252. Nabeshi H, Yoshikawa T, Arimori A, Yoshida T, Tochigi S, Hirai T, et al. Effect of surface properties of silica nanoparticles on their cytotoxicity and cellular distribution in murine macrophages. Nanoscale Res Lett. 2011 Jan 18;6(1):93.

253. Optical brighteners [Internet]. Available from: http://en.wikipedia.org/wiki/Optical_brightener.

254. Countryman PI, Heddle JA. The production of micronuclei from chromosome aberrations in irradiated cultures of human lymphocytes. Mutat Res. 1976 Dec;41(2-3):321-32.

255. Pakunlu RI, Wang Y, Tsao W, Pozharov V, Cook TJ, Minko T. Enhancement of the efficacy of chemotherapy for lung cancer by simultaneous suppression of multidrug resistance and antiapoptotic cellular defense: Novel multicomponent delivery system. Cancer research. 2004;64(17):6214-24.

256. Green LM, Reade JL, Ware CF. Rapid colorimetric assay for cell viability: Application to the quantitation of cytotoxic and growth inhibitory lymphokines. J Immunol Methods. 1984 May 25;70(2):257-68.

257. Ahu H, Rusyn I, Richard A, Tropsha A. Use of cell viability assay data improves the prediction accuracy of conventional quantitative structure activity relationship models of animal carcinogenicity. Environ Health Perspect ,. 2008;116(4):506-513.

258. Biondi O, Motta S, Mosesso P. Low molecular weight polyethylene glycol induces chromosome aberrations in chinese hamster cells cultured in vitro. Mutagenesis. 2002 May;17(3):261-4.

259. SCCNFP/0532/01. Final opinion of the scientifi c committee on cosmetic products and non-food productsintended for consumers concerning benzoic acid and sodium benzoate June, 2002.

260. Pfuhler S, Wolf HU. Effects of the formaldehyde releasing preservatives dimethylol urea and diazolidinyl urea in several short-term genotoxicity tests. Mutat Res. 2002 Feb 15;514(1-2):133-46.

261. Jung R, Cojocel C, Muller W, Bottger D, Luck E. Evaluation of the genotoxic potential of sorbic acid and potassium sorbate. Food Chem Toxicol. 1992 Jan;30(1):1-7.

262. Anselmi C, Ettorre A, Andreassi M, Centini M, Neri P, Di Stefano A. In vitro induction of apoptosis vs. necrosis by widely used preservatives: 2-phenoxyethanol, a mixture of isothiazolinones, imidazolidinyl urea and 1,2-pentanediol. Biochem Pharmacol. 2002 Feb 1;63(3):437-53.

263. Scortichini BH, Quast JF, Rao KS. Teratologic evaluation of 2-phenoxyethanol in new zealand white rabbits following dermal exposure. Fundam Appl Toxicol. 1987 Feb;8(2):272-9.

264. Lockley DJ, Howes D, Williams FM. Cutaneous metabolism of glycol ethers. Arch Toxicol. 2005 Mar;79(3):160-8.

265. Bajorath J, Greenfield B, Munro SB, Day AJ, Aruffo A. Identification of CD44 residues important for hyaluronan binding and delineation of the binding site. J Biol Chem. 1998 Jan 2;273(1):338-43.

266. Screaton GR, Bell MV, Jackson DG, Cornelis FB, Gerth U, Bell JI. Genomic structure of DNA encoding the lymphocyte homing receptor CD44 reveals at least 12 alternatively spliced exons. Proc Natl Acad Sci U S A. 1992 Dec 15;89(24):12160-4.

267. Mackay CR, Terpe HJ, Stauder R, Marston WL, Stark H, Gunthert U. Expression and modulation of CD44 variant isoforms in humans. J Cell Biol. 1994 Jan;124(1-2):71-82.

268. Rodriguez-Rodriguez L, Sancho-Torres I, Leakey P, Gibbon DG, Comerci JT, Ludlow JW, et al. CD44 splice variant expression in clear cell carcinoma of the ovary. Gynecol Oncol. 1998 Nov;71(2):223-9.

269. Rodriguez-Rodriguez L, Sancho-Torres I, Mesonero C, Gibbon DG, Shih WJ, Zotalis G. The CD44 receptor is a molecular predictor of survival in ovarian cancer. Med Oncol. 2003;20(3):255-63.

270. Speiser P, Wanner C, Breitenecker G, Kohlberger P, Kainz C. CD-44 is not involved in the metastatic spread of ovarian cancer in vivo. Anticancer Res. 1995 Nov-Dec;15(6B):2767-9.

271. Taratula O, Savla R. Poly(propyleneimine) dendrimers as potential siRNA delivery nanocarrier: From structure to function. Int J Nanotechnol. 2011;8:36.

272. Chandna P, Khandare JJ, Ber E, Rodriguez-Rodriguez L, Minko T. Multifunctional tumor-targeted polymer-peptide-drug delivery system for treatment of primary and metastatic cancers. Pharm Res. 2010 Nov;27(11):2296-306.

273. Chandna P, Saad M, Wang Y, Ber E, Khandare J, Vetcher AA, et al. Targeted proapoptotic anticancer drug delivery system. Mol Pharm. 2007 Sep-Oct;4(5):668-78.

274. Zhang M, Garbuzenko OB, Reuhl KR, Rodriguez-Rodriguez L, Minko T. Two-in-one: Combined targeted chemo and gene therapy for tumor suppression and prevention of metastases. Nanomedicine (Lond). 2012 Feb;7(2):185-97.

275. Jayant S, Khandare J, Wang Y, Singh A, Vorsa N, Minko T. Targeted sialic Acid–Doxorubicin prodrugs for intracellular delivery and cancer treatment. Pharmaceutical Research. 2007;24(11):2120-30.

276. Miletti-Gonzalez KE, Chen S, Muthukumaran N, Saglimbeni GN, Wu X, Yang J, et al. The CD44 receptor interacts with P-glycoprotein to promote cell migration and invasion in cancer. Cancer Res. 2005 Aug 1;65(15):6660-7.

277. Garbuzenko OB, Saad M, Pozharov VP, Reuhl KR, Mainelis G, Minko T. Inhibition of lung tumor growth by complex pulmonary delivery of drugs with oligonucleotides as suppressors of cellular resistance. Proc Natl Acad Sci U S A. 2010 Jun 8;107(23):10737-42.

278. Khandare JJ, Jayant S, Singh A, Chandna P, Wang Y, Vorsa N, et al. Dendrimer versus linear conjugate: Influence of polymeric architecture on the delivery and anticancer effect of paclitaxel. Bioconjug Chem. 2006 Nov-Dec;17(6):1464-72.

279. Benjaminsen RV, Mattebjerg MA, Henriksen JR, Moghimi SM, Andresen TL. The possible "proton sponge " effect of polyethylenimine (PEI) does not include change in lysosomal pH. Mol Ther. 2012 Oct 2.